THE UNIVERSITY OF MANITOBA

A POTENTIAL FLOW REPRESENTATION OF THE TWO-DIMENSIONAL AUGMENTOR WING WITH FINITE JET THICKNESS

by

Vinh Quyen Tang

A THESIS

SUBMITTED TO THE UNIVERSITY OF MANITOBA

IN PARTIAL FULFILLMENT OF THE REQUIREMENTS FOR THE DEGREE

OF DOCTOR OF PHILOSOPHY

DEPARTMENT OF MECHANICAL ENGINEERING

WINNIPEG, MANITOBA

March 1979

A POTENTIAL FLOW REPRESENTATION OF THE TWO-DIMENSIONAL AUGMENTOR WING WITH FINITE JET THICKNESS

BY

VINH QUYEN TANG

A dissertation submitted to the Faculty of Graduate Studies of the University of Manitoba in partial fulfillment of the requirements of the degree of

DOCTOR OF PHILOSOPHY

ABSTRACT

A method of potential flow solution for a simplified two dimensional augmentor wing with a thick uniform jet is presented. Also, a solution for the non-uniform jet is attempted.

In order to concentrate on the effect of the jet thickness and velocity profiles, the augmentor wing is simplified by assuming that the aerofoil is a flat plate and the augmentor has zero length. Thus, the thick jet starts at (and above) the trailing edge, inclined at an angle to the chord line.

For the uniform jet solution, the method replaces the aerofoil by a vortex distribution and uses source and vortex distributions at the jet origin and boundaries to represent the augmented jet. The source strength is related to the primary jet momentum coefficient. The problem is formulated by dividing the vortex distributions into line segments of linear and logarithmic strengths. The vortex strengths and the jet trajectory are determined by an iterative numerical method which requires the flow to be tangential to the aerofoil and jet boundaries, and the jet shape to be in equilibrium under the pressure loading.

When the jet has a thickness of only 0.5% of the chord, the solutions are in close agreement with linear theory and appropriate experiments. Solutions for a range of jet thickness (up to 9% of the chord) indicate that the lift coefficient and the jet trajectory are not affected very much by the jet thickness provided that the primary jet momentum coefficient is kept constant.

The solution for the non-uniform jet is formulated by approximating the jet by several uniform layers. Results are obtained for the special case of two equal thickness layers. It is found that, for a constant total primary jet momentum coefficient, a higher lift is developed when the lower part of the jet has a higher velocity than the upper part.

ACKNOWLEDGEMENTS

I would like to thank Dr. J. Tinkler for his invaluable help as a teacher and a research adviser. I greatly appreciate the long and late hours that Dr. Tinkler has spent generously to give me guidance, instruction, and assistance. Also, I would like to thank him for his concern and understanding of my personal difficulties.

I wish to thank Drs. D.J. Marsden, D.W. Trim and A. Trupp for their review of the thesis.

I wish to express my appreciation to the staff of the Mechanical Engineering Department, and my thanks to Mrs. Paulette Giardino for her typing of this manuscript and to Mr. P. Mitra and H. Weiss for their preparations of some of the drawings.

The grants from the Defence Research Board and National Research Council to support this work are acknowledged.

TABLE OF CONTENTS

LIST OF SYMBOLS

[A]	Coefficient matrix
A_1, A_2, A_3, A_4	Vortex segment end points
[B]	Column matrix
c	Chord length
C_1, C_2, C_3	Constants
C_J	Augmented jet momentum coefficient
$C_{J'}$	Primary jet momentum coefficient
C_L	Lift coefficient
C_M	Pitching moment coefficient (about the leading edge)
D	Function occurring in Equation 78
E	Function occurring in Equation 79
F	Function occurring in Equation 41
G	Slope of the jet center line
H	Function occurring in Equation 42
J	Augmented jet momentum
J'	Primary jet momentum
K	Coefficient in the expressions for singular vortex distributions
L	Lift
L	Function occurring in Equation 48
M	Function occurring in Equation 49
N	Total number of vortex segments
O	Origin of the x, y coordinates
O'	Origin of the ξ, η coordinates

P	Arbitrary point in the flow field
q	Source strength per unit length
R	Radius of curvature
S	Function occurring in Equation 68
T	Function occurring in Equation 69
u	x-component of the induced velocity
u'	ξ-component of the induced velocity
v	y-component of the induced velocity
v'	η-component of the induced velocity
U	Free stream velocity
U_u, U_e	Free stream velocities at upper and lower jet boundaries respectively
V	Augmented jet velocity
V_u, V_e	Augmented jet velocities at upper and lower jet boundaries respectively
W	Function occurring in Equation 64
x	Horizontal coordinate
y	Vertical coordinate
Z	Function occurring in Equation 65
α	Angle of attack
γ	Vortex strength per unit length
Γ	Circulation
δ	Jet thickness
η	Normal axis to the vortex segment line
θ	Angle measured from the source segment line to the line connecting the segment end point to control point ($0 < \theta < 2\Pi$)
Θ	Angle used in Equation 18

ξ	Tangential axis to the vortex segment line
ρ	Density
τ	Initial jet deflection angle
ϕ	Angle measured from the vortex segment line to the line connecting the segment end point to control point ($0 < \phi < 2\Pi$)
ψ	Tan ψ is the slope of the aerofoil and jet boundaries

LIST OF SUBSCRIPTS

a	average
A	of point A
B	of point B
c	of the chord
ct	center point of a segment
C	of point C
D	of point D
i	order of control points
i-j	(the induced velocity) at i^{th} control point due to j^{th} vortex element
j	order of vortex segments
k	constant
ℓ	linear
ℓ	of lower boundary
ℓd	linearly decreasing
ℓi	linearly increasing
N	number of vortex segments on the chord line and jet lower boundaries
N1	N + 1
N2	N + 2
N3	N + 3
NC	number of vortex segments on the chord line
NC1	NC + 1
NC2	NC + 2
NC3	NC + 3
oj	initial conditions of a vortex segment on the jet center line

P	of point P
P-s	(the induced velocity) at P due to a source distribution
P-γ	(the induced velocity) at P due to a vortex distribution
ps	peak strength
q	of the source distribution
u	of upper boundary
∞	at infinity (far upstream or downstream from the aerofoil)

LIST OF FIGURES

Figures | Page

CHAPTER I

INTRODUCTION

The development of high lift aerofoils is a step-by-step progress. Starting as early as 1920, methods of improving the aerofoil geometry to produce higher lift were studied. It was found, then, that the circulation around an aerofoil, which is directly proportional to the lift, could be improved by temporarily increasing the aerofoil camber and/or chord by means of mechanical flaps or slats. An example of a two dimensional aerofoil with a mechanical flap is presented in Fig. 1. In practice, there is a limit to the lift obtained by the modification of the aerofoil geometry because of the boundary layer separation which has an adverse effect on the circulation.

Means of controlling or retarding the flow separation were then tested. One method was the blowing of a high-speed jet sheet over the flap upper surface to suppress the separation. During the test of flow separation control in 1938, Hagedorn and Ruden (1) observed that the excess of the blown air originally used to control flow separation also resulted in a higher lift on the aerofoil.

Unfortunately the significance of this important observation was not recognized until more than a decade later, when the high-speed jet sheet was recognized as a solution to the high lift wings. In 1953, tests were done by Dimmock at the National Gas Turbine Establishment on the two dimensional elliptic aerofoil with a jet of air issuing from a slot near the trailing edge and at the lower surface of the aerofoil as seen in Fig. 2. The lift and pitching moment were measured by pressure plotting. The jet sheet behaved like an extended mechanical flap; thus, the name of the jet flap aerofoil was given.

The experimental results of the jet flap aerofoil by Dimmock and the empirical theory of Stratford were reported by M. Davidson in Ref. 2 showing that a very high lift coefficient could be obtained with the jet flap. Also another important result showed that the propulsive thrust was nearly equal to the momentum flux of the jet regardless of the jet deflection angle.

The first theoretical solution of a two dimensional jet flap was presented by Spence (3) in 1956. Spence's mathematical model of the jet-flap aerofoil consisted of a two dimensional flat plate aerofoil with an infinitesimally thin jet sheet issuing from the trailing edge. Ideal flow conditions were assumed, and the aerofoil and jet boundaries were replaced by vortex sheets whose distributed strengths were determined by satisfying the boundary conditions that the velocities on the aerofoil and jet boundaries must be tangential. An integro-differential equation for the vortex sheet strengths was formed. In order to obtain a less complex integro-differential equation, the jet sheet was assumed to be aligned with the aerofoil chord but the local slope of the jet streamline was that of the correct jet trajectory. Spence successfully solved this problem by approximating the distributed vortex strengths by the logarithmic functions, which satisfy the singularity behaviours of the velocity field at the leading and trailing edges, together with a Fourier series.

Spence's approximate solutions are applicable to a thin aerofoil at small angles of attack and small initial jet deflection angles, but the results are in good agreement with experimental findings even for an initial jet deflection angle of 50°. Spence's solutions have been regarded to be very reliable, however in recent years new methods of solutions for the jet flap were attempted.

Leamon and Plotkin (4) also used vortex sheets but allowed the boundary conditions to be satisfied on the real singular surfaces instead of the linearized ones. The distributed vortex strength on the chord and the jet center line trajectory were approximated by singular functions which satisfied the singular behaviours at the leading and trailing edges. The results deviate from the experimental and other theoretical results by 16 percent to 20 percent except for small jet momentum coefficients.

Sato (5) represented a circular cylinder with a jet flap with a number of discrete vortices located on the cylinder surface and along the jet. He then used conformal mapping to derive the flow about an elliptic aerofoil with a jet flap. Solutions of the effects of the jet flaps on an elliptic aerofoil section of 12.5% thickness chord ratio were found to be comparable to experimental results. Examples of calculations for other aerofoil sections were also presented.

At about the same time Herold (5) also presented a two dimensional, iterative solution for the jet flap. He also used the discrete vortex method but the thin aerofoil approximation was applied. His results agreed with those of Spence and experiment for low momentum coefficients, but in general, no marked improvement of the solutions by this method is noted.

Although no exact solution of the jet flap was found, efforts to improve the high lift system were never stopped in the laboratory. One of the practical difficulties of the jet flapped aerofoil was the control of the jet initial deflection angle. It was found that if the jet was ejected over a trailing edge flap (Fig. 3) instead of from the trailing edge, the jet would attach to the flap and leave the trailing edge at the same angle as the flap angle due to the Coanda effect. It was also recognized that this arrangement, known as the jet augmented flap, resulted in a remarkable improvement in lift. The first theoretical solution for the jet augmented flap was also presented by Spence (7) in 1958.

Almost a decade later, the jet-augmented flap arrangement was modified by adding a shroud to improve the thrust and lifting effectiveness. The latter arrangement is called an augmentor wing and is illustrated in Fig. 4. A jet issuing from a span-wise slot at the rear portion of an aerofoil emerges into a gap formed by the upper shroud and lower section of the flap, which directs the flow with a downward angle of deflection relative to the aerofoil chord. The flap is designed to allow mixing of the jet and the secondary induced air flow (Fig. 4) so that augmentation of momentum flux of the primary jet is obtained.

The arrangement of the augmentor wing contributes to high lift on two accounts: the presence of the jet induces an asymmetry in the main stream giving rise to a pressure lift on the aerofoil, and the reaction of the augmented jet momentum results in a contribution to lift (as well as a contribution to thrust). The augmented reaction lift is clearly an advantage over the jet flap arrangement.

Past augmentor wing investigations have been mainly laboratory experiments. In 1964, at the Fourth ICAS Conference in Paris, Whittley (8) presented a report on research progress which indicated the promise of the augmentor wing concept. Research work was then continued with tests on a large scale model in the NASA Ames 40 by 80 feet wind tunnel (9), and the results have shown a significant advantage of such a lifting system.

In 1969, Y.Y. Chan (10) contributed to the analytical solution of the augmentor wing by simplifying the model to that of a jet-augmented flap with the augmentor inlet suction represented by sinks at the hinge line on upper or lower surfaces. He showed that the lift coefficient could be improved by the augmentor wing arrangement. Later, Woolard in Ref. 11 tried to improve Chan's solution by redefining the sink strength.

Recently, Wilson et al (12) presented a new approach to the analysis of the augmentor wing, in which the restrictions of thin aerofoil and infinitesimally thin jet were avoided. The real two dimensional aerofoil and assumed-constant-thickness jet surfaces were used in the calculation of the potential flow field outside the jet. The solutions also allowed for the effects of the jet entrainment and the induced flow at the augmentor entrance by using source and sink distributions superimposed on the vortex sheets.

This thesis presents a theoretical model of the augmentor wing which, in the restrictive conditions of the ideal flow, represents a complete flow field around an augmentor wing including the jet flow. The object is to study the effects of the jet thickness and jet velocity or momentum distribution on the lift coefficient of the two dimensional augmentor wing.

CHAPTER II

MATHEMATICAL MODEL OF AUGMENTOR WING

II.1 Introduction

The velocity field induced by a distributed vortex is a very important concept in aerofoil theory as discussed, for example, in Chapter 12 of Reference 13. The flow about a two dimensional aerofoil can be represented by the flow resulting from the combination of a uniform stream with a distributed vortex, the actual strength distribution being determined by the shape of the aerofoil. The method provides a convenient means to determine not only the total lift but also the distribution of pressure on an aerofoil.

The problem of determining the aerodynamic coefficients of a given aerofoil profile is very difficult. However, as reported in Ref. 13, M. Munk introduced a method of approximation, known as the theory of thin aerofoil, which has proved to be very useful. The method replaces an aerofoil by its mean camber line which is assumed to deviate only slightly from the chord line.

Using the concept of vortex sheets and thin aerofoil theory, and based on Spence's solution for the jet flapped aerofoil, Chan (10) presented a theoretical model of the augmentor wing as shown in Fig. 5. The real augmentor wing was approximated by a flat plate aerofoil with a theoretical sink on the upper or lower surfaces of the aerofoil at the flap hinges. The sink was added to represent the suction flow at the flap hinge. The use of a sink, as in this case, or a distributed sink to represent the suction or entrainment is common. The strength of the sink was arbitrary, but in practice would be empirically determined. The jet thickness was assumed infinitesimal. The jet boundary conditions were satisfied on the linearized jet trajectory; i.e., on the extension of the chord line.

Woolard [11] interpreted Chan's suction coefficient as being based on the total mainstream flow into the augmentor and argued that it should have been based on the increase of flow (due to the jet entrainment), on the basis that no lift should be produced on a flat plate at zero angle of attack when the primary jet momentum is zero.

Another mathematical model of the two dimensional augmentor wing was presented by Wilson et al (12), based on the experimental model of the augmentor wing tested by Wang, Wright, and Mahal*. In Wilson's model, the aerofoil boundary was formed by connecting the front part of the real aerofoil boundary to the shroud and the flap chords by two planes, which were arbitrarily taken to represent the boundaries of the mixing zone of the primary jet and the secondary

---

*Wilson et al (12) incorrectly gave the reference as "Design Integration and Noise Studies for a Jet STOL Aircraft", Vol. IV, "Wind Tunnel Test Program", The Boeing Company, Commercial Airplane Group, Seattle, Washington, NASA CR-114286, May, 1972. Attempts to trace this report have been unsuccessful.

induced flow. The shroud and flap thickness were treated as negligible. The jet, whose thickness was constant and equal to the gap distance between the flap and the shroud, issued from the trailing edge. The aerofoil and the jet boundaries were divided into 200 segments of vortex and source-sink distributions. The segments were approximated by finite straight lines. The jet was truncated when it turned to within two degrees of the free stream. Then two end segments, having the same length as the adjacent segments, were added onto the jet.

II.2 Idealized Model of Augmentor Wing

The flow field about an augmentor wing is very complicated. For the practical purposes of engineering, the simplified or idealized models of the augmentor wing, such as those presented in the previous introduction, are often used in the analysis of the augmentor wing. These models, however, do not represent the complete augmentor wing aerodynamics.

In the real flow, the viscosity of air causes the development of boundary layers on the aerofoil and flap surfaces, and the entrainment along the jet. The boundary layers change the effective surfaces of the aerofoil and affect the drag and lift on the aerofoil. The entrainment increases the jet thickness and changes the jet momentum downstream. Another problem which complicates the augmentor wing aerodynamics is the mixing of the primary and induced flow inside the augmentor. The mixing process is very difficult to understand fully because of the turbulent nature of the flows and many parameters which affect the mixing, such as the augmentor configuration, the initial jet thickness, and the ratio between the initial jet thickness and augmentor thickness (11).

For the purposes of this analysis the flow is assumed incompressible, irrotational and inviscid, so that potential flow theory can be applied. In addition, the augmentor wing configuration is systematically simplified so that it is possible to solve the problem and to test its results at each stage, from the simplified case to the more complex one.

The simplified two dimensional augmentor wing model consists of a thin aerofoil with a downward deflected flap at the rear portion of the aerofoil and a parallel shroud just above the flap as shown in Fig. 6(a). The augmented jet is ejected between the shroud and the flap at the trailing edge in the direction of the flap chord line. Before studying the model in Fig. 6(a), a more simplified model where the flap and shroud chords are assumed to have zero-length will be examined. In the latter model, as shown in Fig. 6(b), the mixing of the jet and secondary induced flow are assumed to be completed in zero length. Furthermore, the functions of the shroud and flap in controlling the jet exit angle and their effects in turning the free stream flow at the trailing edge and shroud leading edge are assumed to be retained. Thus, the finite thickness jet will be considered to issue from the trailing edge at an angle to the aerofoil chord.

The model is simplified further by assuming that the aerofoil has no camber. The model is shown in Fig. 6(c) and consists of a flat plate at an angle of attack with a thick jet at the trailing edge.

II.3 Straight Uniform Jet

In Chapter 3 of Ref. 14, the technique of replacing two parallel vortices and a uniform flow by a source distribution is discussed. The technique is modified here to represent a jet by source and vortex distributions.

Here the two semi-infinite, parallel vortex distributions on two straight lines $y = \frac{\delta}{2}$ and $y = \frac{-\delta}{2}$, as shown in Fig. 7(a), are added to a source distribution on the y axis and between the two vortex distributions. It can be shown that if the source distribution has equal strength to the two vortex sheets, the resulting flow is a straight uniform jet flow of thickness δ in the region $x > 0$ and between the two vortex sheets (see Appendix A).

It is assumed, in this work, that the thick curved jet in a uniform flow can also be represented by a source distribution and vortex sheets of unknown strength distributions as shown in Fig. 8.

II.4 Mathematical Model of Augmentor Wing

It is desired now to use the concept of distributed vortices to construct a hypothetical model for the augmentor wing of Fig. 6(c).

The flat plate is replaced by a distributed vortex with unknown strength along its lines, and the jet is replaced by two vortex sheets at its boundaries and a source distribution at the trailing edge (Fig. 9). Their strengths are to be determined.

Thus, the resultant flow field is made up of the uniform flow, and the velocities induced by the distributed vortices and distributed sources. Because the velocity potential of the uniform flow, vortices and sources individually satisfy the Laplace equation, which is a linear equation, the potential of the resultant flow also satisfies the Laplace equation. The main boundary conditions are that the flow is tangential to the aerofoil surface and jet boundaries, and is undisturbed from the uniform stream (except in the jet) far from the aerofoil.

CHAPTER III

FORMULATION OF THE PROBLEM

III.1 Boundary Conditions

III.1.1 Kinematic boundary conditions

In using vortex sheets to represent the aerofoil and the jet, one of the physical conditions needed in determining the strength of the vortex distribution is that there will be no flow across the aerofoil and jet boundaries.

Generally, without knowing the type of vortex distribution, this condition means the vortex sheets should assume strength distributions that induce a velocity field such that the aerofoil and jet boundaries are streamlines. Mathematically, the velocities induced by the vortex sheets at any point on the boundary, when combined with the velocities induced by the source distribution and the uniform flow velocity should make a velocity tangential with the boundary at that point, or

$$\frac{U_\infty \sin \alpha + v_i}{U_\infty \cos \alpha + u_i} = \tan (\psi_i), \tag{1}$$

where α is the angle of attack (Fig. 9) and $\tan (\psi_i)$ is the slope of the streamline at point "i". Also v_i and u_i are vertical and horizontal components of the induced velocity, and U_∞ is the main stream velocity for upstream.

III.1.2 Conditions at infinity

At downstream infinity the effects of the disturbances caused by the aerofoil and jet are negligible and the free stream velocity, U, is assumed to approach U_∞.

Concerning the jet trajectory, the physical condition requires the finite thickness jet to be aligned with the free stream at downstream infinity. Thus the jet velocity at infinity must be $(U_\infty + q_\infty)$ where $q_\infty\delta$ is the primary jet flow rate. The jet momentum coefficient measured at infinity is

$$C_{J_\infty} = \frac{J_\infty}{\frac{1}{2}\rho U_\infty^2 c} = \frac{\rho(U_\infty + q_\infty)^2\delta}{\frac{1}{2}\rho U_\infty^2 c}, \qquad (2)$$

where J_∞ is the augmented jet momentum flux at infinity, δ and ρ are the jet thickness and density respectively, and c is the chord length, taken to be unity. The primary and augmented jet densities are assumed to be equal and constant. In this work C_{J_∞} is called the augmented jet momentum coefficient at infinity.

III.1.3 Dynamic Boundary Condition

The dynamic boundary condition of the jet is the requirement for the forces acting on the jet to be in balance.

A curved, thick, two dimensional jet in a co-flowing external field is sketched in Fig. 10. Its trajectory is determined by the radius of curvature R of its center line.

The analysis, similar to that of Spence, Ref. 3, assumes an inviscid, incompressible flow in the main stream and in the jet, and the flow is everywhere irrotational except at the jet origin and at the boundaries of the jet, where the pressure is continuous but the velocity and density are both discontinuous.

The velocity and the pressure at the jet center line vary along the jet; there are only two independent physical quantities that are constant: the mass flow and the total pressure. A polar element of the jet is shown in Fig. 10. The analysis of the jet is presented in Appendix B where a dynamic boundary condition is obtained, and expressed by the relation between the distributed vortex strengths on the jet boundaries and the jet velocities and position. The expression is

$$\frac{1}{R} = \left(\frac{\gamma_u + \gamma_\ell}{U_\infty}\right) \Big/ \left(\frac{\delta V_a^2}{U_\infty^2} - \frac{\delta V_a}{U_\infty}\right) \tag{3}$$

where R is the jet radius of curvature, and γ_u and γ_ℓ are the vortex strengths at the upper and lower jet boundaries respectively. V_a is the average jet velocity, defined as

$$V_a = \frac{V_u + V_\ell}{2} \quad , \tag{4}$$

where V_u and V_ℓ are the jet velocities at the upper and lower jet boundaries respectively. The average jet velocity can be used to define the jet augmented momentum $J = \rho V_a^2 \delta$, which is constant along the jet.

The augmented jet momentum coefficient is defined as

$$C_J = \frac{J}{\frac{1}{2} \rho_\infty U_\infty^2 c} \quad , \tag{5}$$

and assumed constant along the jet. Thus,

$$C_J = C_{J_\infty} \quad . \tag{6}$$

The dynamic boundary condition, Equation (3) is rewritten in terms of C_J as

$$\frac{1}{R} = \left(\frac{\gamma_u}{U_\infty} + \frac{\gamma_\ell}{U_\infty}\right) \Bigg/ \left\{\frac{C_J c}{2} \left[1 - \left(\frac{2\delta}{C_J c}\right)^{1/2}\right]\right\} \quad . \tag{7}$$

In the limiting case where the jet thickness approaches zero this boundary condition, Equation (7), reduces to that used by Spence (3) for the jet flap problem.

It is more practical to express the dynamic boundary condition, Equation (7), in terms of the primary jet momentum. For the present mathematical model the primary jet is assumed to issue uniformly across the jet thickness (δ) at the trailing edge. The primary jet momentum flux, J', is defined as the momentum flux when the main stream velocity is zero so that

$$J' = \rho\, q^2\, \delta \quad .^{*} \tag{8}$$

Because the jet mass flow is conserved

$$q = q_\infty \tag{9}$$

Thus the primary jet momentum coefficient is

$$C_{J'} = \frac{J'}{\frac{1}{2}\rho_\infty U_\infty^2 c} \quad . \tag{10}$$

The augmented jet momentum is now expressed in terms of the primary jet momentum. Using Equations (6) and (9), Equation (2) is

---

*It should be noted that the primary jet momentum flux, J', is different than the power jet momentum flux. In practice, the primary jet is often underexpanded so that it continues to accelerate after the nozzle exit. The power jet momentum flux is defined as the product of the jet mass flow and the velocity which the jet would achieve if the gas expanded isentropically to ambient pressure. However, J', as defined in Equation (8), corresponds to the primary jet momentum at the exit of the zero-length augmentor assuming incompressible flow. The relation between J' and the power jet momentum must be determined empirically.

rewritten as

$$C_J = \frac{\rho(U_\infty + q)^2 \ \delta}{\frac{1}{2}\rho_\infty U_\infty^2 c} , \tag{11}$$

or

$$C_J = \frac{\rho U_\infty^2 \ \delta}{\frac{1}{2}\rho_\infty U_\infty^2 c} + \frac{2\rho U_\infty q \ \delta}{\frac{1}{2}\rho_\infty U_\infty^2 c} + \frac{\rho q^2 \ \delta}{\frac{1}{2}\rho_\infty U_\infty^2 c} . \tag{12}$$

Thus

$$C_J = \frac{2\delta}{c} + \frac{4q\delta}{U_\infty c} + C_{J'} . \tag{13}$$

Substituting Equation (13) into Equation (7) gives

$$\frac{1}{R} = \left(\frac{\gamma_u}{U_\infty} + \frac{\gamma_\ell}{U_\infty}\right) \Bigg/ \left\{ \left(\delta + 2\frac{q\delta}{U_\infty} + \frac{C_{J'}c}{2}\right) \left[1 - \left(\frac{2\delta}{2\delta + 4\frac{q\delta}{U_\infty} + C_{J'}c}\right)^{1/2}\right] \right\} . \tag{14}$$

This form of the dynamic boundary condition has been produced by using an approach similar to that used by Spence. On the face of it, it appears attractive in that the radius of curvature is defined in terms of the local vortex strengths, γ_u and γ_ℓ, which are the main dependent variables in the mathematical problem. However, two approximations

$$V_a \simeq \frac{V_u + V_\ell}{2} \tag{15}$$

and

$$U_\infty \simeq \frac{U_u + U_\ell}{2} \tag{16}$$

have been made which are valid within the linearizing restrictions of Spence's jet flap theory. These approximations are not necessary for the numerical computation except that they reduce the computer memory requirements. In Appendix B it is shown that the dynamic boundary condition is

$$\frac{1}{R} = \frac{(V_u - V_\ell)^2}{U_u^2 - U_\ell^2} \frac{2}{\delta} , \tag{17}$$

when expressed in terms of the local velocities rather than averages.

III.2 Geometrical Construction of the Problem

From the mathematical model of the augmentor wing, the vortex sheets are divided into a chosen number of finite length segments, except that the last two downstream elements on the jet upper and lower boundaries are semi-infinite. The vortex strengths on the segments are originally unknown. The segments are approximated by the straight lines as shown in Fig. 11(a). This approximation is reasonable when the segment lengths are small or the radii of curvature of the segments are large. The latter condition is true in the case of plate aerofoils of small camber and shallow jet trajectories. Since a large number of segments taken will result in more unknown vortex strengths to be determined, it would result in longer computing time. Thus, for better approximation of vortex strength distribution with less computing time the segment lengths may vary according to the behavior of the vortex distributions. Shorter segments are used in the regions of rapidly changing strengths (i.e., adjacent to the leading and trailing edges where there are singularities of the vortex distributions), and longer segments are used when the vortex strengths do not change significantly.

There are two coordinate systems applied: the (x, y) and (ξ, η) systems [Fig. 11(b)]. The (x, y) system is fixed and has its origin, 0, at the leading edge and the x-axis is on the chord line. The (ξ, η) system is temporarily attached to any vortex segment, with its origin, 0', at the upstream end of the segment and the ξ-axis aligned with the segment.

From the concept of different length segments described earlier, the coordinates of the segment end points on the chord are taken from the expression

$$\frac{x_i}{c} = (1 - \cos \Theta_i)/2, \tag{18}$$

where Θ_i is an arbitrary angle varying from 0 to Π with equal increments. Thus, the leading and trailing edge positions correspond to the values of Θ_i of 0 and Π respectively, and shorter segments are crowded near the leading and trailing edges as shown in Fig. 11(a).

On the lower jet boundaries, the first few segment lengths from the trailing edge are taken similarly to those in the first half of the chord [Fig. 11(a)]. Further downstream, the segment lengths are increased by a constant increment until the end point of the last segment is at five chord length away from the trailing edge, where a semi-infinite segment aligned with the free stream is attached.

The coordinates of the segment end points on the upper jet boundary are calculated from those on the lower jet boundary and the jet thickness, as shown in Appendix C. The results give a similar segment length arrangement as on the lower jet boundary, so that there are pairs of parallel segments on the jet two boundaries as shown in Fig. 11(a).

Finally, the mid-points of all the finite length segments are taken as the control points [Fig. 11(a)] where the kinematic boundary condition is satisfied.

For easy reference, the distributed vortex elements are numbered starting at one at the element adjacent to the leading edge increasing to the last finite element downstream on the jet lower boundary, and continuing on the jet upper boundary elements from the element nearest to the trailing edge to the last finite element downstream. The control points are also numbered in the same manner so that they have the same order as the elements that they are situated on [Fig. 11(a)].

III.3 Types of Vortex Strength Distributions

Based on the results of vortex strength distributions in the jet flap problem Refs. 3, 15, linear distributions of vortex strengths are assumed on all the vortex segments except those adjacent to the leading and trailing edges and the two semi-infinite elements. At the leading and trailing edges where the flow makes the sudden turns to satisfy the kinematic boundary condition, the vortex strengths must be infinite. These points are called the singularities. However, the integration of the vortex strengths over the chord and the jet trajectory, which is proportional to the lift, must be finite. Spence showed in Ref. 3 that the proper singular functions are logarithmic. For the two semi-infinite elements, constant strength vortex distributions are assumed such that the condition at downstream infinity is satisfied.

III.3.1 Linear vortex strength distributions

An example of the linearly distributed vortex strength over a segment A_1A_2 is shown in Fig. 12. The vortex strength, in this case, decreases (or increases) linearly from the strength of γ_{A_1} at A_1 to γ_{A_2} at A_2. This will be called a trapezoidal distribution of vortex strength.

For the convenience of the calculations as seen later, the trapezoidal distribution is divided into two triangular distributions: one in which the vortex strength increases linearly from zero at A_1 to γ_{A_2} at A_2 and another in which the vortex strength decreases linearly from γ_{A_1} at A_1 to zero at A_2.

Furthermore, consider, for example, three consecutive vortex segments as shown in Fig. 12. There are trapezoidal vortex distributions over segments A_1A_2, A_2A_3 and A_3A_4, with the common vortex strengths at A_2 and A_3. The vortex strengths at A_1, A_2, A_3, and A_4 are γ_{A_1}, γ_{A_2}, γ_{A_3} and γ_{A_4} respectively. These trapezoidal distributions are divided into the overlapped triangular distributions with the peak vortex strengths of γ_{A_1}, γ_{A_2}, γ_{A_3} and γ_{A_4} as shown in Fig. 12.

III.3.2 Logarithmic vortex strength distributions

The logarithmic distributions of vortex strengths over the chord segments adjacent to the leading and trailing edges are

$$\gamma_1 = K_1 \frac{\ln(1 - x)}{x^{3/2}}, \quad (0 < x < x_2) \tag{19}$$

and

$$\gamma_{NC} = K_{NC} \frac{\ln(1 - x)}{x^{3/2}}, \quad (x_{NC} < x < 1) \tag{20}$$

respectively, where K_1 and K_{NC} are the constants to be determined, and x_2 and x_{NC} are the coordinates of the downstream end point and upstream end point of the chord segments adjacent to the leading and trailing edges respectively. The logarithmic distributions of vortex strengths over the lower and upper jet segments nearest to the trailing edge are

$$\gamma_{NC1} = K_{NC1} \frac{\ln(x - 1)}{x^{3/2}}, \quad (1 < x < x_{NC2}) \tag{21}$$

and

$$\gamma_{N1} = K_{N1} \frac{\ln(x - x_{N2})}{x^{3/2}}, \quad (x_{N2} < x < x_{N3}) \tag{22}$$

respectively, where K_{NC1} and K_{N1} are the constants to be determined and x_{N2} is the x-coordinate of the starting point of the jet upper boundary.

The typical logarithmic and linear vortex strength distributions over the chord and the jet boundaries are shown in Fig. 13. It is noted from Fig. 13 that if there are only the logarithmic distributions over the vortex segments adjacent to the singularities, the number of vortex peak strengths which are originally unknown is less than the number of control points. In order to have an equal number of control points with the number of unknown vortex strengths, the triangular vortex distributions are superimposed on the logarithmic distribution as shown in Fig. 13. The added triangular distributions have their peak-strengths at the leading and trailing edges and at the origin of the jet upper boundary (see Fig. 13).

III.3.3 Constant vortex strength distributions

It is recalled from the mathematical model that if there is no uniform flow, the thick jet issuing from the aerofoil trailing edge can be represented by a source distribution of strength q at the jet origin and two straight semi-infinite vortex sheets of strength -q and q on the upper and lower jet boundaries respectively. When the inclined uniform flow is added, the pressure difference across the jet curves its trajectory until the jet is asymptotically aligned with the free stream at infinity, where the pressure difference becomes nil.

That part of the jet which sustains negligible pressure difference is represented by semi-infinite elements aligned with the main stream with constant vortex strength of -q and q on the upper and lower surfaces, respectively.

CHAPTER IV

THE ITERATIVE METHOD OF SOLUTION

IV.1 General Principle of the Iterative Method

If the aerofoil and the jet boundaries are known, they can be treated as the solid boundaries in the uniform flow. It is then possible to write the integro-differential equation which specifies the vortex strength distributions that will satisfy the kinematic boundary condition, Equation 1, at every control point .

In this problem, the positions of the jet boundaries are not known initially: they must be determined by an iterative process. A jet trajectory is assumed and the vortex strengths calculated. The vortex strengths are then used to calculate the jet curvature by Equation 14. Integration of the curvature gives the jet shape which can be used as a new starting point for the next iteration. The process is continued until there is no significant change in the jet trajectories .

IV.2 The Set of Linear Equations for Vortex Strengths

IV.2.1 Formulae for induced velocities

a) Velocities induced by a constant strength distributed source:

Consider a constant strength source distribution on the η-axis from $\eta = 0$ to $\eta = \delta$, as shown in Fig. 14. The velocity components induced at a point P in the flow field by this source distribution are given by (see Appendix A).

$$u'_{P-s} = \frac{q}{2\Pi} (\theta_1 - \theta_2), \tag{23}$$

and

$$v'_{P-s} = \frac{q}{2\Pi} \ell n \frac{r_2}{r_1} , \tag{24}$$

where u'_{P-s} and v'_{P-s} are the ξ and η components, respectively, r_1 and r_2 are the distances from P to the upper and lower ends of the distributed source segment, and θ_1 and θ_2 are the angles measured from η-axis to r_1 and r_2 respectively. The angles θ_1 and θ_2 vary positively clockwise from 0 to 2Π.

In this problem, the distributed source segment is assumed to be perpendicular to the jet boundary at the trailing edge (Fig. 9). The jet deflection angle at the trailing edge is τ, measured positively clockwise from the x-axis. Thus, the source segment inclines from the y-axis by an angle τ (Fig. 9). The x and y components of the velocities induced by this inclined distributed source segment are obtained by resolving u'_{P-s} and v'_{P-s} into x and y components by using the coordinate transformation

$$\begin{bmatrix} \cos|\tau| & \sin|\tau| \\ -\sin|\tau| & \cos|\tau| \end{bmatrix} \begin{bmatrix} u'_{P-s} \\ v'_{P-s} \end{bmatrix} = \begin{bmatrix} u_{P-s} \\ v_{P-s} \end{bmatrix} \tag{25}$$

where u_{P-S} and v_{P-S} are the x and y components, respectively, of the velocity induced by the source distribution at point P.

Thus,

$$u_{P-S} = u'_{P-S} \cos|\tau| + v'_{P-S} \sin|\tau|, \tag{26}$$

and

$$v_{P-S} = -u'_{P-S} \sin|\tau| + v'_{P-S} \cos|\tau|. \tag{27}$$

b) Velocities induced by the distributed vortices:

Consider a distributed vortex on the segment O'A of the ξ axis as shown in Fig. 15. One end of the segment is chosen at the origin, O', just for convenience. The velocity components induced by the distributed vortex at point $P(\xi_p, \eta_p)$ in the flow field are (Ref. 13)

$$u'_{P-\gamma} = \frac{1}{2\Pi} \int_0^{\xi_A} \gamma \frac{\eta_P}{(\xi_P - \xi)^2 + \eta_P^2} d\xi, \tag{28}$$

and

$$v'_{P-\gamma} = \frac{-1}{2\Pi} \int_0^{\xi_A} \gamma \frac{\xi_P - \xi}{(\xi_P - \xi)^2 + \eta_P^2} d\xi, \tag{29}$$

where $u'_{P-\gamma}$ and $v'_{P-\gamma}$ are the ξ and η components of the induced velocity at P, and γ is the vortex strength which is a function of ξ.

i) Velocities induced by a constant strength vortex distribution:

When γ is equal to a constant, equations (28) and (29) become

$$u'_{P-\gamma_k} = \frac{\gamma_k}{2\Pi} \int_0^{\xi_A} \frac{\eta_P}{(\xi_P - \xi)^2 + \eta_P^2} \, d\xi \ , \tag{30}$$

and

$$v'_{P-\gamma_k} = \frac{-\gamma_k}{2\Pi} \int_0^{\xi_A} \frac{\xi_P - \xi}{(\xi_P - \xi)^2 + \eta_P^2} \, d\xi \ , \tag{31}$$

where $u'_{P-\gamma_k}$ and $v'_{P-\gamma_k}$ are the ξ and η components of the velocity induced by a constant strength vortex distribution having the strength of γ_k. The integrations of Equations (30) and (31) are given in Ref. 13 and summarized in Ref. 15, and the results are

$$u'_{P-\gamma_k} = \frac{\gamma_k}{2\Pi} \ (\phi_2 - \phi_1) \ , \tag{32}$$

and

$$v'_{P-\gamma_k} = \frac{\gamma_k}{2\Pi} \ \ell n \ \frac{r_2}{r_1} \ , \tag{33}$$

where ϕ_1 and ϕ_2 are the angles measured positively anti-clockwise from the ξ axis to $O'P$ and AP respectively, and r_1 and r_2 are the magnitudes of $O'P$ and AP respectively (Fig. 15).

ii) Velocities induced by a distributed vortex of linearly increasing strength:

In the triangular vortex distribution, the linearly increasing vortex strength has the form of

$$\gamma_{\ell i} = \frac{\gamma_{ps}}{\xi_A} \xi \ , \tag{34}$$

where $\gamma_{\ell i}$ is the linearly increasing vortex strength and γ_{ps} is the vortex peak strength at A (Fig. 15).

Rewriting Equations (28) and (29) by replacing γ by $\gamma_{\ell i}$ and using Equation (34) gives

$$u'_{P-\gamma_{\ell i}} = \frac{1}{2\Pi} \frac{\gamma_{ps}}{\xi_A} \int_0^{\xi_A} \frac{\eta_P \quad \xi}{(\xi_P - \xi)^2 + \eta_P^2} d\xi \ , \tag{35}$$

and

$$v'_{P-\gamma_{\ell i}} = \frac{-1}{2\Pi} \frac{\gamma_{ps}}{\xi_A} \int_0^{\xi_A} \frac{\xi \ (\xi_P - \xi)}{(\xi_P - \xi)^2 + \eta_P^2} d\xi \ , \tag{36}$$

where $u'_{P-\gamma_{\ell i}}$ and $v'_{P-\gamma_{\ell i}}$ are the ξ and η components, respectively, of the velocity induced at P by the linearly increasing vortex strength distribution. The integrations of Equations (35) and (36) are performed in Appendix D, and the results are

$$u'_{P-\gamma_{\ell i}} = \frac{\eta_P}{2\Pi} \frac{\gamma_{ps}}{\xi_A} \left\{ \ell n \left[\frac{(\xi_P - \xi_A)^2 + \eta_P^2}{\xi_P^2 + \eta_P^2} \right]^{1/2} \right.$$

$$\left. - \frac{\xi_P}{|\eta_P|} \left[\tan^{-1} \frac{|\eta_P|}{\xi_P} - \tan^{-1} \frac{|\eta_P|}{\xi_P - \xi_A} \right] \right\} , \tag{37}$$

and

$$v'_{P-\gamma_{\ell i}} = \frac{1}{2\Pi} \frac{\gamma_{ps}}{\xi_A} \left\{ \xi_P \, \ell n \left[\frac{(\xi_P - \xi_A)^2 + \eta_P^2}{\xi_P^2 + \eta_P^2} \right]^{1/2} \right.$$

$$\left. + \, \eta_P \left[\tan^{-1} \frac{|\eta_P|}{\xi_P} - \tan^{-1} \frac{|\eta_P|}{\xi_P - \xi_A} \right] + |\xi_A| \right\} \; . \qquad (38)$$

The resultant components of $u'_{P-\gamma_{\ell i}}$ and $v'_{P-\gamma_{\ell i}}$ in the x, y coordinate system are

$$u_{P-\gamma_{\ell i}} = u'_{P-\gamma_{\ell i}} \cos \psi + v'_{P-\gamma_{\ell i}} \sin \psi \qquad (39)$$

$$v_{P-\gamma_{\ell i}} = -u'_{P-\gamma_{\ell i}} \sin \psi + v'_{P-\gamma_{\ell i}} \cos \psi \qquad (40)$$

Using Equations (37) and (38), it is convenient to rewrite Equations (39) and (40) as

$$u_{P-\gamma_{\ell i}} = \gamma_{ps} \, F_j \; , \qquad (41)$$

and

$$v_{P-\gamma_{\ell i}} = \gamma_{ps} \, H_j \qquad (42)$$

where F_j and H_j are functions of ξ_A, ξ_p, η_p and ψ.

iii) Velocities induced by a distributed vortex of linearly decreasing strength:

In the triangular vortex strength distribution, the linearly decreasing vortex strength has the form of

$$\gamma_{\ell d} = - \frac{\gamma_{ps}}{\xi_A} \xi + \gamma_{ps} \tag{43}$$

where $\gamma_{\ell d}$ is the linearly decreasing vortex strength and γ_{ps} is the vortex peak strength at $0'$ (Fig. 15).

Equation (43) shows that the linearly decreasing vortex strength is the difference between the constant vortex strength γ_{ps} and the linearly increasing vortex strength, $\frac{\gamma_{ps}}{\xi_A} \xi$. Thus the velocity induced by the linearly decreasing vortex strength is the difference between the velocities induced by the constant vortex strength and by the linearly increasing vortex strength. The formulae for the latter velocities are presented by Equations (32), (33), (37) and (38). After substituting γ_{ps} for γ_k in Equations (32) and (33), the induced velocities are obtained by subtracting Equation (37) from Equation (32) and Equation (38) from Equation (33). Thus

$$u'_{P-\gamma_{\ell d}} = \frac{\gamma_{ps}}{2\Pi} \left\{ (\phi_2 - \phi_1) - \frac{\eta_P}{\xi_A} \left[\ell n \left(\frac{(\xi_P - \xi_A)^2 + \eta_P^2}{\xi_P^2 + \eta_P^2} \right)^{1/2} \right. \right.$$

$$\left. \left. - \frac{\xi_P}{|\eta_P|} \left[\tan^{-1} \frac{|\eta_P|}{\xi_P} - \tan^{-1} \frac{|\eta_P|}{\xi_P - \xi_A} \right] \right] \right\} , \tag{44}$$

and

$$v'_{P-\gamma_{\ell d}} = \frac{\gamma_{ps}}{2\Pi} \left\{ \ell n \frac{r_2}{r_1} - \frac{1}{\xi_A} \left[\xi_P \ \ell n \left(\frac{(\xi_P - \xi_A)^2 + \eta_P^2}{\xi_P^2 + \eta_P^2} \right)^{1/2} \right. \right.$$

$$\left. \left. + \eta_P \left(\tan^{-1} \frac{|\eta_P|}{\xi_P} - \tan^{-1} \frac{|\eta_P|}{\xi_P - \xi_A} \right) + |\xi_A| \right] \right\} , \tag{45}$$

where $u'_{P-\gamma_{\ell d}}$ and $v'_{P-\gamma_{\ell d}}$ are the ξ and η components, respectively, of the velocity induced at P by the distributed vortex of linearly decreasing strength.

The resultant components of $u'_{P-\gamma_{\ell d}}$ and $v'_{P-\gamma_{\ell d}}$ in the x and y directions are

$$u_{P-\gamma_{\ell d}} = u'_{P-\gamma_{\ell d}} \cos \psi + v'_{P-\gamma_{\ell d}} \sin \psi , \tag{46}$$

and

$$v_{P-\gamma_{\ell d}} = -u'_{P-\gamma_{\ell d}} \sin \psi + v'_{P-\gamma_{\ell d}} \cos \psi . \tag{47}$$

Using Equations (44) and (45), it is convenient to rewrite Equations (46) and (47) as

$$u_{P-\gamma_{\ell d}} = \gamma_{ps} \ L_j \ , \tag{48}$$

and

$$v_{P-\gamma_{\ell d}} = \gamma_{ps} \ M_j \tag{49}$$

where L_j and M_j are functions of ξ_A, ξ_P, η_P and ψ.

iv) Velocities induced by the logarithmic strength distributed vortex on the chord segment adjacent to the leading edge:

In the (x, y) coordinate system where the ξ-axis is coincident with the x-axis, Equations (28) and (29) become

$$u_{P-\gamma} = \frac{1}{2\Pi} \int_{x_{O'}}^{x_A} \gamma \ \frac{y_P}{(x_P - x)^2 + y_P^2} \, dx \ , \tag{50}$$

and

$$v_{P-\gamma} = \frac{-1}{2\Pi} \int_{x_{O'}}^{x_A} \gamma \ \frac{x_P - x}{(x_P - x)^2 + y_P^2} \, dx \ , \tag{51}$$

where $u_{P-\gamma}$ and $v_{P-\gamma}$ are the x and y components, respectively, of the velocity induced at $P(x_P, y_P)$ by the vortex distribution γ, and $x_{O'}$ and x_A are the x coordinates of O' and A respectively.

Using Equation (19) to substitute γ_1 for γ, and noting that the limits of integration for the leading edge element are

$x_{0'} = 0$ and x_2, yields

$$u_{P-\gamma_1} = \frac{K_1}{2\Pi} \int_0^{x_2} \frac{\ell n\ (1 - x)}{x^{3/2}} \frac{y_P}{(x_P - x)^2 + y_P^2}\, dx\ , \qquad (52)$$

and

$$v_{P-\gamma_1} = \frac{-K_1}{2\Pi} \int_0^{x_2} \frac{\ell n\ (1 - x)}{x^{3/2}} \frac{x_P - x}{(x_P - x)^2 + y_P^2}\, dx \qquad (53)$$

where $u_{P-\gamma_1}$ and $v_{P-\gamma_1}$ are the x and y components, respectively, of the velocity induced at P by the logarithmic γ_1 distribution.

The integrals of Equations (52) and (53) become singular when the integrands become infinite within the range of integration. The treatments of the singularities and the integrations of Equations (52) and (53) are presented in Appendix E.

v) Velocities induced by the logarithmic strength distributed vortex on the chord segment adjacent to the trailing edge:

The induced velocities are obtained by substituting γ_{NC} for γ in Equations (50) and (51) and using Equation (20) for the distributed strength of γ_{NC}. Equations (50) and (51) become

$$u_{P-\gamma_{NC}} = \frac{K_{NC}}{2\Pi} \int_{x_{NC}}^{1} \frac{\ell n\ (1 - x)}{x^{3/2}} \frac{y_P}{(x_P - x)^2 + y_P^2}\, dx\ , \qquad (54)$$

and

$$v_{P-\gamma_{NC}} = -\frac{K_{NC}}{2\pi} \int_{x_{NC}}^{1} \frac{\ell n\ (1 - x)}{x^{3/2}} \frac{x_P - x}{(x_P - x)^2 + y_P^2} dx \tag{55}$$

where $u_{P-\gamma_{NC}}$ and $v_{P-\gamma_{NC}}$ are the x and y components, respectively, of the velocity induced at P by γ_{NC} distribution. The integrals of Equations (54) and (55) are also singular. The treatments of the singularities and the integrations of Equations (54) and (55) are presented in Appendix F.

vi) Velocities induced by the logarithmic strength distributed vortex on the jet lower boundary segment nearest to the trailing edge:

The equations for the induced velocities, Equations (50) and (51) are rewritten by changing x and y coordinates into ξ and η coordinates as

$$u'_{P-\gamma} = \frac{1}{2\pi} \int_{0}^{\ell_\gamma} \gamma \frac{\eta_P}{(\xi_P - \xi)^2 + \eta_P^2} d\xi\ , \tag{56}$$

and

$$v'_{P-\gamma} = \frac{-1}{2\pi} \int_{0}^{\ell_\gamma} \gamma \frac{\xi_P - \xi}{(\xi_P - \xi)^2 + \eta_P^2} d\xi\ . \tag{57}$$

The induced velocities are obtained by substituting $\gamma_{NC\ell}$ for γ in Equations (56) and (57), and using Equation (21) for the distributed strength of $\gamma_{NC\ell}$. Equations (56) and (57) become

$$u'_{P-\gamma_{NCl}} = \frac{K_{NCl}}{2\Pi} \int_0^{\ell_{\gamma_{NCl}}} \frac{\ell n\ (x - 1)}{x^{3/2}} \frac{\eta_P}{(\xi_P - \xi)^2 + \eta_P^2}\, d\xi\ , \qquad (58)$$

and

$$v'_{P-\gamma_{NCl}} = \frac{-K_{NCl}}{2\Pi} \int_0^{\ell_{\gamma_{NCl}}} \frac{\ell n\ (x - 1)}{x^{3/2}} \frac{\xi_P - \xi}{(\xi_P - \xi)^2 + \eta_P^2}\, d\xi \qquad (59)$$

where $u'_{P-\gamma_{NCl}}$ and $v'_{P-\gamma_{NCl}}$ are the ξ and η components, respectively, of the velocity induced at P by the γ_{NCl} distribution. The treatment of the singularities and the integrations of Equations (58) and (59) are presented in Appendix G.

vii) Velocities induced by the logarithmic strength distributed vortices on the jet upper boundary segment nearest to the trailing edge:

The induced velocities are obtained by substituting γ_{Nl} for γ in Equations (56) and (57) and using Equation (22) for the distributed strength of γ_{Nl}. Equations (56) and (57) become

$$u'_{P-\gamma_{Nl}} = \frac{K_{Nl}}{2\Pi} \int_0^{\ell_{\gamma_{Nl}}} \frac{\ell n\ (x - x_{N2})}{x^{3/2}} \frac{\eta_P}{(\xi_P - \xi)^2 + \eta_P^2}\, d\xi\ , \qquad (60)$$

and

$$v'_{P-\gamma_{Nl}} = \frac{-K_{Nl}}{2\Pi} \int_0^{\ell_{\gamma_{Nl}}} \frac{\ell n\ (x - x_{N2})}{x^{3/2}} \frac{\xi_P - \xi}{(\xi_P - \xi)^2 + \eta_P^2}\, d\xi\ , \qquad (61)$$

where $u'_{P-\gamma_{Nl}}$ and $v'_{P-\gamma_{Nl}}$ are the ξ and η components, respectively, of the velocity induced at P by γ_{Nl} distribution. The integrations of

Equations (60) and (61) are presented in Appendix G.

IV.2.2 The resulting velocity components induced at a control point by all the finite distributed vortex segments:

The velocity induced at a control point by the j^{th} vortex element which is not adjacent to the singularities is the sum of the velocities induced by the linearly decreasing and linearly increasing vortex distributions whose peak strengths are at the j^{th} and $(j + 1)^{th}$ division points respectively.

Thus, using Equations (41), (42), (48) and (49), the components of the velocity induced at the control point "i" by such j^{th} vortex element are

$$u_{i-j} = \gamma_j \; L_j + \gamma_{j+1} \; F_j \tag{62}$$

and

$$v_{i-j} = \gamma_j \; M_j + \gamma_{j+1} \; H_j \tag{63}$$

where γ_j and γ_{j+1} are the vortex strengths at the j^{th} and $(j + 1)^{th}$ division points, respectively.

However, the velocities induced at a control point by the distributed vortex elements adjacent to the singularities are the sums of the velocities induced at that point by the superimposed distributed vortices of linear and logarithmic strengths. For instance, the induced velocity components due to the vortex element adjacent to the leading edge are

$$u_{i-1} = \left(\gamma_{ps}\right)_1 L_1 + K_1 W, \tag{64}$$

and

$$v_{i-1} = \left(\gamma_{ps}\right)_1 M_1 + K_1 Z \tag{65}$$

where W and Z are the coefficients of K_1 in Equations (52) and (53) respectively. K_1 can be expressed in terms of γ_2 by satisfying the condition that at $x = x_2$ the logarithmic vortex distribution on the first element and the linear vortex distribution on the second element have the common strength, γ_2, or

$$K_1 \left. \frac{\ln (1 - x)}{x^{3/2}} \right|_{x = x_2} = \left(\gamma_{ps}\right)_2 \tag{66}$$

Thus

$$K_1 = \frac{\left(\gamma_{ps}\right)_2}{\dfrac{\ln (1 - x_2)}{x_2^{3/2}}} \;. \tag{67}$$

Substituting (67) into (64) and (65) gives

$$u_{i-1} = \left(\gamma_{ps}\right)_1 L_1 + \left(\gamma_{ps}\right)_2 S_1, \tag{68}$$

and

$$v_{i-1} = \left(\gamma_{ps}\right)_1 M_1 + \left(\gamma_{ps}\right)_2 T_1 \tag{69}$$

where

$$S_1 = \frac{W}{\frac{\ln (1 - x_2)}{x_2^{3/2}}}, \tag{70}$$

and

$$T_1 = \frac{Z}{\frac{\ln (1 - x_2)}{x_2^{3/2}}}. \tag{71}$$

Similarly, the velocities induced by the other vortex elements adjacent to the singularities are obtained.

The induced velocity components due to the NCth vortex element are:

$$u_{i-NC} = \left(\gamma_{ps}\right)_{NC1} F_{NC} + \left(\gamma_{ps}\right)_{NC} S_2, \tag{72}$$

and

$$v_{i-NC} = \left(\gamma_{ps}\right)_{NC1} H_{NC} + \left(\gamma_{ps}\right)_{NC} T_2. \tag{73}$$

Also, the induced velocity components due to the NC1th vortex element are

$$u_{i-NC1} = \left(\gamma_{ps}\right)_{NC1} L_{NC1} + \left(\gamma_{ps}\right)_{NC2} S_3, \tag{74}$$

and

$$v_{i-NC1} = \left(\gamma_{ps}\right)_{NC1} M_{NC1} + \left(\gamma_{ps}\right)_{NC2} T_3, \tag{75}$$

Finally, the induced velocity components due to the N1th vortex element are

$$u_{i-N1} = \left(\gamma_{ps}\right)_{N1} L_{N1} + \left(\gamma_{ps}\right)_{N2} S_4, \tag{76}$$

and

$$v_{i-N1} = \left(\gamma_{ps}\right)_{N1} M_{N1} + \left(\gamma_{ps}\right)_{N2} T_4. \tag{77}$$

The resulting velocity components induced by all the finite distributed vortex elements are the summations of the induced velocity components due to each vortex element. The resulting velocity components are obtained as

$$\sum_{j=1}^{N} u_{i-j} = \sum_{j=1}^{N} D_{i-j} \left(\gamma_{ps}\right)_j , \tag{78}$$

and

$$\sum_{j=1}^{N} v_{i-j} = \sum_{j=1}^{N} E_{i-j} \left(\gamma_{ps}\right)_j , \tag{79}$$

where D_{i-j} and E_{i-j} are functions of the coordinates of the control point "i" and the end points of the j^{th} vortex element.

IV.2.3 The kinematic boundary condition rewritten as a set of linear equations:

Far downstream, the asymptotic value of vorticity along the jet lower boundary is γ_q and equal to the jet source strength, q, whilst along the upper boundary the asymptotic value is $-\gamma_q$. The jet boundary vorticity is considered to be made up of two parts;

$\gamma_\ell = \gamma' + \gamma_q$ along the lower boundary,

$\gamma_u = \gamma'' - \gamma_q$ along the upper boundary, where the γ_q components are constant and related to the jet momentum coefficient by Equation (8). The γ_q components make no contribution to the total lift because of their contra-rotation. The γ' and γ'' components can be considered to be responsible for the jet curvature and lift. Further, let the lifting components of vorticity over the chord and jet boundaries be denoted by γ_j at the j^{th} segment. The induced velocity at any point can then be considered to be made up of a component due to the lifting vorticity over the chord and jet, a component due to the source at the jet origin, and a component due to the non-lifting vorticity of the jet. Then

$$u_i = \sum_{j=1}^{N} u_{i-j} + \sum_{j=NC1}^{N} u_{i-(\gamma_q)j} + u_{i-s} \tag{80}$$

and

$$v_i = \sum_{j=1}^{N} v_{i-j} + \sum_{j=NC1}^{N} v_{i-(\gamma_q)j} + v_{i-s} \; . \tag{81}$$

Here, u_{i-j} is the u-velocity at i induced by the lifting vorticity, γ, at j;

u_{i-s} is the u-velocity at i induced by the source distribution across the jet origin;

$u_{i-(\gamma_q)j}$ is the u-velocity at i induced by the non-lifting vorticity, γ_q, at j.

It is seen that the first terms of the RHS of Equation (80) and (81) depend on the unknown vorticity, γ, whilst the other terms are dependent on the pre-specified jet momentum and jet shape.

The kinematic boundary condition of Equation (1) can be re-written as

$$v_i - u_i \tan \psi_i = U_\infty \cos \alpha \tan \psi_i - U_\infty \sin \alpha . \qquad (82)$$

Substitution of Equation (80) and (81) into Equation (82) leads to

$$\sum_{j=1}^{N} v_{i-j} - \tan \psi_i \sum_{j=1}^{N} u_{i-j} = U_\infty \cos \alpha \tan \psi_i - U_\infty \sin \alpha$$

$$- (v_{i-s} - u_{i-s} \tan \psi_i) - \left(\sum_{j=NC1}^{N} v_{i-(\gamma_q)j} - \sum_{j=NC1}^{N} u_{i-(\gamma_q)j} \tan \psi_i \right) . \qquad (83)$$

Providing the positions of all the distributed vortex and source elements are known, and the source and γ_q strengths are calculated from the jet momentum, Equation (8), the velocities induced by the source distribution and by γ_q distribution, which are presented in the right hand side of Equation (83), are also known. Thus, all the terms in the right hand side of Equation (83) are known from the given initial conditions such as the angle of attack, α, and the original jet momentum.

However, the induced velocities in the left hand side of Equation (83) are unknown because the distributed vortex strengths are originally not known. Instead of solving Equation (83) for the unknown induced velocities v_{i-j} and u_{i-j}, it is much simpler to replace the velocities by the expressions presented in Equations (78) and (79) to form a set of linear equation with the unknown vortex strengths. This method is applied here.

The set of linear equations can be written in the matrix form as

$$[A_{i-j}]\,[\gamma_j] = [B_i], \tag{84}$$

where

$$A_{i-j} = E_{i-j} - \tan\psi_i\, D_{i-j} \quad , \tag{85}$$

and B_i is the right hand side of Equation (83). Equation (84) is solved by Gaussian Elimination method.

IV.3 Differential Equation for the Jet Trajectory

In the jet dynamic boundary condition, Equation (7), the radius of curvature, R, can be related to the first and second derivatives of the jet center line trajectory as

$$\frac{1}{R} = \frac{y''}{(1 + y'^2)^{3/2}} \quad . \tag{86}$$

Substituting Equation (86) into Equation (7) gives

$$\frac{y''}{(1 + y'^2)^{3/2}} = \left(\frac{\gamma_u}{U_\infty} + \frac{\gamma_\ell}{U_\infty}\right) \Bigg/ \left\{ \frac{C_J c}{2} \left[1 - \frac{2\delta}{C_J c}^{\,1/2}\right] \right\} \quad . \tag{87}$$

In each iteration, except the first iteration, using the vortex strengths γ_u and γ_ℓ obtained from the previous iteration, Equation (87) is integrated over each segment length of the jet center line to give the coordinates of the jet center line trajectory.

The differential equation, Equation (87), is solved in Appendix H and the result is

$$y = \frac{-1}{C_1} \left[1 - (C_1 x + C_2)^2 \right]^{1/2} + C_3 \tag{88}$$

where C_1 is the right hand side of Equation (87), and C_2 and C_3 are determined by

$$C_2 = \frac{y'_{oj}}{(1 + y'^{2}_{oj})^{1/2}} - C_1 x_{oj} \ , \tag{89}$$

and

$$C_3 = y_{oj} + \frac{1}{C_1} [1 - (C_1 x_{oj} + C_2)^2]^{1/2} \ . \tag{90}$$

The subscript oj denotes the initial conditions of each jet center line segment; e.g., for the segment nearest to the trailing edge, y'_{oj} is the initial jet deflection slope, tan $(-\tau)$.

IV.4 Discussion of Convergence

The iterative process described in Section IV.1 was tried and it was found that this simple iterative process led to divergent solutions. Successive iterations produced jet trajectories which were alternately too low and too high by greater and greater amounts as illustrated in Fig. 16. It was noted from Fig. 16 that the typical input shape and the result of the subsequent iteration formed an envelope setting upper and lower limits for the correct jet shape.

A method of setting the upper and lower limits of the jet trajectories closer after each iteration was developed in Ref. 15 and is repeated in Appendix I for completeness. The method succeeded in yielding convergence in many cases but failed when an iterated solution crossed over the input jet trajectory. Because the method used the position of the end point of the last finite jet center line segment as an indication of the low or high position of the whole jet trajectory (see Appendix I), it was unable to allow for the fact that trajectories had crossed and therefore wrong upper and lower boundaries could be selected for the envelope.

The reason for the cross over of the jet trajectories was due to the choice of the initial jet shape. It was found that Spence's solutions for the jet-flapped aerofoil could be used to construct the initial jet shape for the thin jet augmentor wing. Solution for the thick jet was satisfactory if the initial shape was for slightly thinner jet.

An alternative method of predicting the correct jet shape after each iteration was tested. Assuming the jet center line trajectory before an iteration is $y_1 = y_1\ (x)$ and the jet center line obtained after an iteration is $y_2 = y_2\ (x)$, the predicted correct jet shape, y, used for the next iteration was calculated from the relation

$$y = y_1 + k\ (y_2 - y_1), \tag{91}$$

where k was a factor (less than one) which was determined arbitrarily.

A large value of k meant the predicted jet shape was close to y_2. One difficulty with this method was the determining of k for each solution. There was no guide line for choosing k except by trial and error. It was found that smaller values of k, down to 0.15, were needed for an augmentor with a thicker jet ($\delta = 0.09$ c).

IV.5 Lift Coefficient and Pitching Moment Coefficient

The lift coefficient is given by

$$C_L = \frac{L}{\frac{1}{2} \rho_\infty U_\infty^2 c} , \tag{92}$$

where C_L is the lift coefficient and L is the total lift, per unit span, on the aerofoil. The total lift is given by

$$L = L_c + L_{J'} , \tag{93}$$

where L_c is the lift related to the circulation on the aerofoil and L_J is the lift due to the vertical reaction of the primary jet momentum. Thus,

$$L_c = \rho_\infty U_\infty \sum_{j=1}^{N_c} \Gamma_j , \tag{94}$$

where Γ_j is the circulation over the jet segment and N_c is the number of vortex segments on the aerofoil, and

$$L_{J'} = J' \sin (\tau + \alpha) . \tag{95}$$

Substituting Equation (93) into Equation (92), and using Equations

(94) and (95) gives

$$C_L = 2 \sum_{j=1}^{N_c} \frac{\Gamma_j}{U_\infty c} + \frac{J'}{\frac{1}{2} \rho_\infty U_\infty^2 c} \sin(\tau + \alpha) , \tag{96}$$

or

$$C_L = 2 \sum_{j=1}^{N_c} \frac{\Gamma_j}{U_\infty c} + C_{J'} \sin(\tau + \alpha) . \tag{97}$$

The circulation, Γ_j, is given by

$$\Gamma_j = \int_{x_j}^{x_j + 1} \gamma_j \, dx \tag{98}$$

where x_j and x_{j+1} are the coordinates of the upstream and downstream end points, respectively, of the j^{th} segment.

The pitching moment coefficient about the leading edge is given by

$$C_M = \int_0^\infty \frac{\rho_\infty U_\infty \gamma x}{\frac{1}{2} \rho_\infty U_\infty^2 c^2} dx$$

$$= \int_0^c \frac{\rho_\infty U_\infty \gamma x}{\frac{1}{2} \rho_\infty U_\infty^2 c^2} dx + \int_c^\infty \frac{\rho_\infty U_\infty \gamma x}{\frac{1}{2} \rho_\infty U_\infty^2 c^2} dx \tag{99}$$

or

$$C_M = 2 \int_0^c \frac{\gamma x}{U_\infty c^2} dx + C_{J'} \sin(\tau + \alpha) \tag{100}$$

because the contribution to the moment from the jet vorticity is equal to the moment due to the jet reaction lift.

Equation (100) is rewritten in an approximate form as

$$C_M = 2 \sum_{j=1}^{N_c} \frac{x_{ctj} \Gamma_j}{U_\infty c^2} + C_{J'} \sin(\tau + \alpha), \tag{101}$$

where x_{ctj} is the distance from the leading edge to the center of the j^{th} vortex segment.

The computer program for the solution of the uniform jet is presented in Appendix K.

CHAPTER V

NON-UNIFORM JET AUGMENTOR WING

V.1 Introduction

It will be recalled that in the augmentor wing arrangement (Fig. 4), the primary jet issuing from a nozzle mixes with the secondary induced flow in the augmentor and the resulting flow emerges at the trailing edge as an augmented jet. The augmented jet momentum and velocity distributions across the jet thickness depend on the degree of mixing which has taken place in the augmentor. A complete mixing was assumed previously to simplify the augmentor wing model for studying the effect of the jet thickness. In practice, the mixing is not complete and the discharge jet velocities are not uniformly distributed.

In this Chapter, a method of solution for the effect of the non-uniform jet on the lift coefficient is presented.

V.2 Mathematical Model of the Non-Uniform Jet

The velocity distribution across the thickness of a non-uniform jet can be approximated by step-distributions such that the non-uniform jet is considered to be made up of the successive uniform jets of different momentums, as shown in Fig. 18(a).

In this work, a simple example of a non-uniform jet is considered to be represented by two successive uniform jets sharing a common boundary but having different momentums [Fig. 18(b)]. First, considering a straight non-uniform jet (Fig. 19) co-flowing in a stream of velocity U_∞, each straight uniform jet is represented by two semi-infinite vortex sheets and a source distribution as presented in Chapter II.3. Let the velocities be $U_\infty + q_u$ and $U_\infty + q_\ell$ in the upper and lower halves of the jet respectively, then the source strengths are q_u and q_ℓ for the upper and lower halves of the jet, and the strengths of the vortex sheets are: $\gamma_u = -q_u$, $\gamma_\ell = q_\ell$, and $\gamma_m = q_u - q_\ell$, where γ_m is the distributed vortex strength on the common boundary of the two assumed uniform jets (Fig. 19).

By arguments similar to those in Chapter II.4, the curved non-uniform jet is considered to be represented by two source distributions, q_u and q_ℓ, at the trailing edge and three semi-infinite vortex sheets of unknown strengths (Fig. 20).

V.3 Non-Uniform Jet Boundary Condition

Applying Bernoulli's equation to the free stream and the jet flows at the jet element shown in Fig. 21 gives

$$p_u + \frac{1}{2} \rho U_u^2 = p_\ell + \frac{1}{2} \rho U_\ell^2 , \tag{102}$$

$$p_1 + \frac{1}{2} \rho V_1^2 = p_2 + \frac{1}{2} \rho V_2^2 , \tag{103}$$

and

$$p_3 + \frac{1}{2} \rho V_3^2 = p_4 + \frac{1}{2} \rho V_4^2 , \tag{104}$$

where p_1 and p_4 are the pressures of the jet at the jet upper and lower boundaries respectively, and p_2 and p_3 are the pressures on the upper and lower side of the common boundary of the two uniform jets. Similar subscripts, 1 to 4, are used for the jet velocity, V.

The assumption of irrotational flow in the jet, except on the jet boundaries, is applied to yield

$$V_1 R_1 = V_2 R_2 \tag{105}$$

and

$$V_3 R_3 = V_4 R_4 \ . \tag{106}$$

The upper and lower uniform jets are assumed to share a common boundary, thus

$$R_2 = R_3 \ . \tag{107}$$

Furthermore, the pressures are assumed to be continuous on the jet boundaries, so that

$$p_u = p_1 \quad , \tag{108}$$

$$p_\ell = p_4 \quad , \tag{109}$$

$$p_2 = p_3 \quad . \tag{110}$$

These basic equations, from Equation (102) to Equation (110), are used in Appendix J to relate the jet centerline radius of curvature to the free stream and jet velocities; the result is

$$\frac{1}{R} = \frac{2}{\delta} \; \frac{(k_V V_1 - V_4)^2}{U_u^2 - U_\ell^2 + (k_V^2 - 1)(V_1^2 - V_2^2)} \; , \qquad (111)$$

where $k_V = V_3/V_2$.

Equation (111) is the dynamic boundary condition of the non-uniform jet.

V.4 Method of Solution for the Non-Uniform Jet

The numerical method of solution for the non-uniform jet was similar to that used for the uniform jet. The vortex sheet on the aerofoil and the three semi-infinite vortex sheets were divided into finite length segments except that the last three segments far downstream are semi-infinite. All the vortex segments were approximated by straight line segments, and the control points were taken at the mid-point of each segment.

The vortex strengths were initially unknown, and assumed to be linearly distributed everywhere except near the singularities where the logarithmic distributions were assumed. The singularities include those described in Chapter III.3 and an additional one at the start of the jet middle vortex sheet. The logarithmic distribution of the vortex strength on the segment adjacent to the latter singularity was expressed by Equation (22) with x_{N2} being replaced by the x-coordinate of the upstream end-point of the segment.

The iterative method described in Chapter IV was applied to find the solutions for the distributed vortex strengths and the jet trajectory.

As the starting iteration for the non-uniform jet solution, the jet trajectory for the uniform jet of the same primary jet momentum coefficient and thickness as those of the non-uniform jet was used as an initial jet shape.

The computer program for the solution of the non-uniform jet is presented in Appendix L.

CHAPTER VI

RESULTS AND DISCUSSIONS

VI.1 Thin Jet

The potential flow solutions for an augmentor wing having a thin jet were obtained and typical results of vortex strength distributions and jet center line trajectories are presented in Fig. 22 and Fig. 23. In this analysis, the jet thickness of .005c was considered to be "thin". Vortex strength distributions on the aerofoil chord and jet boundaries are presented in Fig. 22, where the vortex segment lengths are shown by the division marks on the x-axis. The separate γ-distributions on the upper and lower jet boundaries, shown in Fig. 22(a), represent the difference between the jet and external flow velocities at the respective boundaries. It will be remembered from the mathematical model that the difference $(\gamma_u - \gamma_\ell)$ is a measure of the jet strength whilst the sum $(\gamma_u + \gamma_\ell)$, plotted in Fig. 22(b), represents the contribution to lift. It is seen that γ_u is very nearly equal to $-\gamma_\ell$ for $x/c > 3.0$ which is partial justification for putting $\gamma_u = -\gamma_\ell$ for $x/c > 5$ in the computations.

Spence's (3) linearized, thin jet solutions are shown in Fig. 22(b) and Fig. 23 for comparison. The resultant vortex strength distributions and the jet center line trajectories show very good ~~agreements~~ agreement, although Spence's method results in a slightly shallower jet trajectory. This is because Spence assumed the vortex distribution to be along the x-axis. Herold (6) also found that allowing the vorticity to be on the jet center line gave a bigger jet displacement for low values of C_j'.

Fig. 24 presents the effects of momentum coefficient on the lift coefficient. Comparison with Spence's results shows that the linear theory has underestimated the lift coefficient for the values of C_J' less than 1.5 in the case of $\tau = 55.5°$, and for the values of C_J' less than 3 in the case of $\tau = 30°$. The lower lift is consistent with shallower jet trajectories.

Foley's (16) experimental results of the lift of a two dimensional jet flap wing are shown in Fig. 25 together with the predicted values. Foley's model had a small hinged flap (0.083c) so that his tests represented a jet-augmented flap. This is why the present theory underestimates the lift. A correction, based on Spence's (7) results for a jet-augmented flap, was applied to the present results. The corrected values are now slightly greater than Foley's experimental results; this remaining difference may be attributed to boundary layer effects.

The variations of lift coefficient with angle of attack and jet initial deflection angle are presented in Fig. 26 and Fig. 27 respectively. The results show a very good agreement with Spence's solution (3) for the jet flapped aerofoil.

VI.2 Thick Uniform Jet

The results of the distributed vortex strengths and jet shapes for a two dimensional augmentor wing, corresponding to different jet thicknesses, were obtained.

Fig. 28 shows the vortex strength distributions on the aerofoil and jet boundaries for the case where the jet thickness is 0.09c, the attack and jet deflection angles are 0° and 30° respectively, and the primary jet momentum coefficient is 1.75. The results of vortex strength distributions for the case of jet thickness of 0.005c are also presented in Fig. 28 for comparison. It was found that increasing the jet thickness alters the vorticity distribution over the aerofoil slightly. For the thicker jet, the vortex strengths are greater over the first three-quarters of the chord leading to a decreased nose-down pitching moment. The pitching moments are -1.818 and -1.808, and the lift coefficients are 3.071 and 3.147 corresponding to the jet thicknesses of .005c and .09c respectively.

The effect of the jet thickness on the jet trajectory is presented in Fig. 29. There is a little change in the jet center line shapes for the two extreme cases of δ = .005c and δ = .09c. If the lower jet boundaries were drawn for the two cases, it would be found that the lower jet boundary for δ = .09c had slightly deeper penetration.

Fig. 30 presents the lift coefficients corresponding to different jet thicknesses. It shows an insignificant increase in the lift coefficient over the range of δ from .005c to .09c. An examination of the dynamic boundary condition offers some explanation.

The jet dynamic boundary condition as defined by Equation (7) can be rewritten and combined with Equation (13) to give

$$\frac{1}{R} = \frac{\gamma_u + \gamma_\ell}{U_\infty} \Bigg/ \left\{ \frac{C_J c}{2} \left[1 - \left(\frac{2\delta}{C_J c} \right)^{1/2} \right] \right\} \tag{112}$$

$$= \frac{\gamma_u + \gamma_\ell}{U_\infty} \Bigg/ \left[\frac{C_{J'} c}{2} + \left(\frac{C_{J'} c}{2} \right)^{1/2} \delta^{1/2} \right] . \tag{113}$$

Equation (113) shows that for an increment in the jet thickness, the coefficient of $\frac{\gamma_u + \gamma_\ell}{U_\infty}$ changes less for smaller values of $C_{J'}$. This means the jet dynamic boundary condition is less affected by the change of the jet thickness for small values of $C_{J'}$. Based on this argument and the results found for $C_{J'} = 1.75$, it is reasonable to predict that, in the practical range of $C_{J'}$ $(0.4 < C_{J'} < 1)$, the jet thickness has a very little effect on the lift coefficient.

The fact that the vortex strength distribution on the upper jet boundary becomes infinite at the jet start seems to indicate that a significant lift might be carried by the shroud. As noticed from Fig. 22a, the vortex strength drops so sharply over the first small element of the jet upper boundary that its integration, which is finite because of the nature of the singularity, is very small. Therefore the circulation around such an element, and hence the shroud lift, is small.

A solution for an augmentor wing with the jet thickness $\delta = 0.09c$ was also obtained using the jet dynamic boundary condition in terms of velocities near the jet edges given by Equation (17). The results of vortex distributions which are shown in Fig. 31 are very close to the results obtained using the approximate jet dynamic boundary condition (expressed in terms of average velocities) Equation (14). However, the use of the dynamic boundary condition, Equation (17), required more computing time and memory to compute the velocities and is not considered justified.

VI.3 Thick Non-Uniform Jet

The effects of the velocity distributions across the jet thickness on the lift coefficient were studied by comparing the solutions of the lift coefficient for different velocity distributions provided that the mass flow rate and the momentum coefficient of the primary jet are kept constant.

The mass flow rate and momentum coefficient of the primary jet are defined as

$$\dot{m} = \int_0^\delta \rho q d\eta \ , \tag{114}$$

and

$$C_{J'} = \frac{\int_0^\delta \rho q^2 d\eta}{\frac{1}{2} \rho U_\infty^2 c} \ , \tag{115}$$

respectively, where the η-axis coincides with the source distribution segments and its origin is at the trailing edge.

The general non-uniformity was simplified into a jet consisting of two uniform parts and, in particular of equal thicknesses. The primary flow velocities in the upper and lower parts of the jet are q_u and q_ℓ (as discussed in Chapter V.2). The integrations of Equations (114) and (115) give

$$\dot{m} = \rho q_u \frac{\delta}{2} + q_\ell \frac{\delta}{2} \rho \, , \tag{116}$$

and

$$C_{J'} = \frac{\rho q_u^2 \frac{\delta}{2}}{\frac{1}{2} \rho U_\infty^2 c} + \frac{\rho q_\ell^2 \frac{\delta}{2}}{\frac{1}{2} \rho U_\infty^2 c} \, , \tag{117}$$

respectively.

If the mass flow and momentum coefficient are to be kept the same as for a uniform jet so that

$$\dot{m} = \rho q \delta \, , \tag{118}$$

and

$$C_{J'} = \frac{\rho q^2 \delta}{\frac{1}{2} \rho U_\infty^2 c} \tag{119}$$

then the only possible solution of Equations (116), (117), (118), and (119) is for $q_u = q_\ell = q$. To provide some basis for comparison, $C_{J'}$

was kept constant and the mass flow was allowed to take on the values required to satisfy Equation (116).

Two different non-uniform jets (cases A and B) having the same momentum coefficient and same mass flow can be compared for the special condition represented by

$$[q_u]_A = [q_\ell]_B \; ; \; [q_\ell]_A = [q_u]_B$$

i.e., $\left[\frac{q_u}{q_\ell}\right]_A = 1 \Big/ \left[\frac{q_u}{q_\ell}\right]_B$, where subscripts A and B denote cases A and B respectively.

The vortex distributions solutions for two cases, $\left[\frac{q_u}{q_\ell}\right]_B = 0.6$ and $\left[\frac{q_u}{q_\ell}\right]_A = \frac{1}{0.6}$, are presented in Fig. (32). The vortex distribution on the aerofoil and parts of the vortex distributions on the jet contributing to the lift are shown. It is seen that the distributed vortex strengths on the aerofoil for case B are greater than that for case A, where the velocity in the lower half of the jet is smaller than the velocity in the upper half. The distributed vortex strengths on the jet middle vortex sheet are small compared to the vortex strengths on the jet boundaries.

At the initial singularity on the jet middle vortex sheet, the vortex strengths for cases A and B approach negative and positive infinity respectively. The reason for this behaviour may be due to the difference in the jet trajectories in the two cases (Fig. 33). The jet trajectories give the general flow direction. The local flow in the neighborhood of the jet start is discussed later. The jet center line trajectory in case A is much shallower than in case B.

Solutions for a range of values of $\frac{q_u}{q_\ell}$ have been obtained and the effect on lift coefficient is shown in Fig. 34. The primary jet momentum coefficient was kept constant at 1.75. The jet thickness was 0.09c, and the angle of attack and jet initial deflection angles were 0° and 30° respectively.

By comparing the pairs of points of the same mass flow rates in Fig. 34, it shows that the lift coefficients are higher for the smaller values of $\frac{q_u}{q_\ell}$. This means higher lift is obtained when the primary jet velocity in the lower half of the jet is greater than that in the upper half of the jet.

It should be noted that when $\frac{q_u}{q_\ell}$ is equal to 1, the non-uniform jet becomes a uniform one. The "non-uniform jet" solution for $\frac{q_u}{q_\ell} = 1$ was compared to the solutions obtained by using the uniform jet model having the same initial conditions.

The results of the lift coefficient, C_L, are shown in Fig. 34. It is noted that the result of lift coefficient at $q_u/q_\ell = 1$ differs by 4 percent from the result obtained by using the uniform jet model.

Furthermore, the γ_m strength distribution was expected to be nil so that the results of the vortex strength distributions could be consistent with the results obtained by using the uniform jet model. However, this was not the case. The strengths of γ_m distribution are small, but they are not negligible.

To try to understand these inconsistancies in the lift coefficients and vortex distributions, the flow conditions in the neighbourhood of the jet start for the uniform jet model were sought by calculating the velocities in this region. The flow directions are shown in Fig. 35(a). Also the velocities at 10 points equally spaced across the jet start were found and presented in Fig. 35(b).

Figs. 35(a) and 35(b) show that at the jet start, the slope of the velocity decreases from tan τ at the trailing edge to a shallow slope nearer the jet upper boundary. Therefore, when the non-uniform jet model was used to represent the uniform jet flow, the middle vortex sheet, which was assumed to have the initial deflection angle of τ, was subjected to an oncoming flow with an angle less than τ. This flow condition created the circulation around the jet middle vortex sheet, which affected the overall circulation and so the lift coefficient.

However, taking into account of the small discrepancy in the lift coefficient (only 4%), Fig. 34 can be used to show the trend of the effect of the velocity ratio on the lift coefficient. There are no other results (either experimental or theoretical) with which these present results can be compared.

CHAPTER VII

CONCLUSION

A method of potential flow solution for a simplified two dimensional augmentor wing has been developed. The simplification involved the reduction of the aerofoil to a flat plate, and the reduction of the augmentor length to zero. This was in order to concentrate on the effects of jet thicknesses and velocity profiles. The method used a mathematical model of distributed vortices and sources to represent the augmented jet, and the jet shape was calculated by an iterative process which required special treatment to ensure convergence.

The good agreement between the present solution for the thin jet and the well known linearized solution demonstrates that the method gives good results for calculating the vortex strength distributions, jet trajectories and lift coefficient curves at the limiting case where the jet thickness is very small. Besides, the comparison verifies the accuracy of the linearized solution for the jet flap problem.

Solutions for a range of jet thickness indicate that the lift coefficient and the jet trajectory are not affected very much by the jet thickness provided the primary jet momentum coefficient is kept constant. However, there is a difficulty in applying these results in practice because of the difference between the definitions of the primary jet momentum used in the present model and the power jet momentum used in practice. The relation between these momentums must be determined empirically.

A solution for a non-uniform jet was attempted by dividing the jet into several uniform layers and results were obtained for the special case of two equal thickness layers. It was found that, for a constant primary jet momentum coefficient, a higher lift was developed when the lower part of the jet had a higher velocity than the upper part. The method does not completely represent the flow at the start of the jet but the results indicate the lift trends due to jet non-uniformity. The drawback of the model is outweighed by the simplicity and practicality of the method in predicting the performance of the augmentor wing.

For future work, the effects of the flap and shroud can be studied by incorporating the flap and shroud to the present model in the form of flat surfaces. To take into account the effects of the aerofoil camber and thickness, singularity distributions can be used to replace the solid boundary of the aerofoil. The use of sinks or sink distributions may be considered to represent the entrainment at the augmentor inlet and along the jet boundaries. Regarding the non-uniform jet model, four or five vortex sheets in the jet may be used to represent a non-uniform jet with better approximation for the primary jet velocity distribution.

APPENDIX A

REPRESENTATION OF STRAIGHT UNIFORM JET

Induced Velocities by Two Semi-Infinite Vortex Distributions

Consider two semi-infinite plane parallel uniform vortex distributions of strengths γ_q and $-\gamma_q$ on two lines $y = -\frac{\delta}{2}$ and $y = \frac{\delta}{2}$ as shown in Fig. 7(a). The horizontal components of velocities induced by parts of vortex sheets 1 and 2 which stretch from $x = 0$ to x_{A_1} and x_{A_2} [Fig. 7(b)] are(Ref. 14)

$$u_{P-\gamma_{q_1}} = -\frac{\gamma_q}{2\Pi}(\phi_{11} - \phi_1) \tag{A.1}$$

and

$$u_{P-\gamma_{q_2}} = \frac{\gamma_q}{2\Pi}(\phi_{22} - \phi_2)\ , \tag{A.2}$$

where ϕ_1, ϕ_2, ϕ_{11} and ϕ_{22} increase anti-clockwise from 0 to 2Π.

Adding (A.1) and (A.2) yields

$$u_{P-\gamma_{q_1}} + u_{P-\gamma_{q_2}} = \frac{\gamma_q}{2\Pi}[(\phi_1 - \phi_2) - (\phi_{11} - \phi_{22})]. \tag{A.3}$$

At the limit when x_{A_1} and x_{A_2} go to infinity,

$$\phi_{11} = \phi_{22} = \Pi \tag{A.4}$$

and Equation (A.3) becomes

$$u_{P-\gamma_{q_1}} + u_{P-\gamma_{q_2}} = \frac{\gamma_q}{2\Pi} (\phi_1 - \phi_2) \tag{A.5}$$

The vertical components of the induced velocities are (Ref. 14)

$$v_{P-\gamma_{q_1}} = - \frac{\gamma_q}{2\Pi} \ell n \frac{r_{11}}{r_1} \tag{A.6}$$

and

$$v_{P-\gamma_{q_2}} = \frac{\gamma_q}{2\Pi} \ell n \frac{r_{22}}{r_2} . \tag{A.7}$$

Adding (A.6) and (A.7) gives

$$v_{P-\gamma_{q_1}} + v_{P-\gamma_{q_2}} = \frac{\gamma_q}{2\Pi} (\ell n \frac{r_{22}}{r_2} - \ell n \frac{r_{11}}{r_1}) . \tag{A.8}$$

At the limit when x_{A_1} and x_{A_2} go to infinity, r_{11} is equal to r_{22} and (A.8) becomes

$$v_{P-\gamma_{q_1}} + v_{P-\gamma_{q_2}} = \frac{\gamma_q}{2\Pi} \ell n \frac{r_1}{r_2} . \tag{A.9}$$

Induced Velocities by a Source Distribution

Consider a two dimensional uniform source distribution of strength q on the y axis between $y = -\frac{\delta}{2}$ and $y = \frac{\delta}{2}$ as shown in Fig. 7(b). The two components of the induced velocity at P are

$$u_{P-s} = \frac{q}{2\Pi} \int_{-\frac{\delta}{2}}^{\frac{\delta}{2}} \frac{\sin\theta}{r}\, dy \qquad \text{(A.10)}$$

and

$$v_{P-s} = \frac{q}{2\Pi} \int_{-\frac{\delta}{2}}^{\frac{\delta}{2}} \frac{\cos\theta}{r}\, dy \qquad \text{(A.11)}$$

where subscript s indicates the source.

From Fig. 7(b) it can be written that

$$\tan\theta = \frac{x_P}{y_P - y}\,. \qquad \text{(A.12)}$$

Differentiating both sides of (A.12) with respect to θ and y gives

$$\frac{d\theta}{\cos^2\theta} = \frac{x_P}{(y_P - y)^2}\, dy. \qquad \text{(A.13)}$$

Also, from Fig. 7(b), it can be written that

$$r^2 = x_P^2 + (y_P - y)^2\,. \qquad \text{(A.14)}$$

Differentiating both sides of (A.14) with respect to r and y gives

$$2rdr = -2\,(y_p - y)\,dy \;. \tag{A.15}$$

Using (A.13) and (A.15) to change the variables in the integrals in (A.10) and (A.11) gives, respectively,

$$u_{P-s} = \frac{q}{2\Pi} \int_{\theta_2}^{\theta_1} \frac{\sin\theta}{r} \, \frac{(y_p - y)^2}{x_p} \, \frac{1}{\cos^2\theta} \, d\theta \tag{A.16}$$

or

$$u_{P-s} = \frac{q}{2\Pi} \int_{\theta_2}^{\theta_1} d\theta = \frac{q}{2\Pi}\,(\theta_1 - \theta_2), \tag{A.17}$$

where θ_1 and θ_2 are measured positively clockwise from 0 to 2Π

and

$$v_{P-s} = \frac{q}{2\Pi} \int_{r_2}^{r_1} \frac{\cos\theta}{r} \left(-\frac{r}{y_p - y}\right) dr \tag{A.18}$$

or

$$v_{P-s} = \frac{q}{2\Pi} \int_{r_2}^{r_1} \frac{-dr}{r} = \frac{q}{2\Pi}\,\ell n\,\frac{r_2}{r_1} \;. \tag{A.19}$$

Resultant Induced Velocities by Previous Two Vortex Distributions and the Source Distribution

Assuming the vortex and source strengths per unit length are equal or

$$\gamma_q = q \quad . \tag{A.20}$$

The resultant induced velocities, u_r and v_r, are

$$u_r = (u_{P-\gamma_{q_1}} + u_{P-\gamma_{q_2}}) + u_{P-s} \tag{A.21}$$

and

$$v_r = (v_{P-\gamma_{q_1}} + v_{P-\gamma_{q_2}}) + v_{P-s} \tag{A.22}$$

Substituting (A.5) and (A.17) into (A.21) and applying (A.20) gives

$$u_r = \frac{\gamma_q}{2\Pi}[(\phi_1 - \phi_2) + (\theta_1 - \theta_2)]. \tag{A.23}$$

Similarly, substituting (A.9) and (A.19) into (A.22) and applying (A.20) gives

$$v_r = 0 \tag{A.24}$$

It is desired now to observe the velocity field in some particular regions.

At $x = -\infty$	$u_r = 0$	
At $x = 0+$	$u_r = 0$	for $\|y\| > \frac{\delta}{2}$
	$u_r = \gamma_q$	for $\|y\| < \frac{\delta}{2}$
At $x = +\infty$	$u_r = 0$	for $\|y\| > \frac{\delta}{2}$
	$u_r = \gamma_q$	for $\|y\| < \frac{\delta}{2}$

The resulting flow is a parallel flow in the region between the lines $y = \frac{\delta}{2}$ and $y = -\frac{\delta}{2}$ and for $x > 0$, with constant velocity, $u_r = \gamma_q = q$.

APPENDIX B

ANALYSIS OF A POLAR ELEMENT OF A TWO DIMENSIONAL JET

Consider a polar element of the two dimensional jet whose boundaries are treated as concentric circular arcs subtending an angle $d\psi$ at the centre of curvature (Fig. 10). The pressures p_u and p_ℓ at the upper and lower jet boundaries are continuous across the boundaries.

Bernoulli's equation can be applied to the external and jet flows to give

$$p_u + \frac{1}{2}\rho_\infty U_u^2 = p_\ell + \frac{1}{2}\rho_\infty U_\ell^2 , \tag{B.1}$$

and

$$p_u + \frac{1}{2}\rho V_u^2 = p_\ell + \frac{1}{2}\rho V_\ell^2 , \tag{B.2}$$

where U_u and U_ℓ are main stream velocities just outside the upper and lower boundaries; the jet velocities just inside the upper and lower boundaries are V_u and V_ℓ respectively. Assuming the jet and main stream densities to be the same and constant, Equations (B.1) and (B.2) are combined to yield

$$U_u^2 - U_\ell^2 = V_u^2 - V_\ell^2 \tag{B.3}$$

Since the jet flow is irrotational, the circulation round the jet element is zero and hence

$$V_u \, ds_u = V_\ell ds_\ell \tag{B.4}$$

or

$$V_u \left(R - \frac{\delta}{2}\right) d\psi = V_\ell \left(R + \frac{\delta}{2}\right) d\psi \tag{B.5}$$

where R is the jet radius of curvature.

Rearranging (B.5) gives

$$(V_u - V_\ell) R = \frac{\delta}{2} (V_u + V_\ell) \tag{B.6}$$

or

$$V_u - V_\ell = \frac{\delta}{R} V_a \tag{B.7}$$

where V_a is the jet mean velocity defined as

$$V_a = \frac{1}{2} (V_u + V_\ell) \ . \tag{B.8}$$

This approximation was justified by Spence (3) for jets of small deflection and will be assumed to be reasonable for the larger jet deflection angles to be used in this analysis. Similarly, the external velocities are assumed to have the average

$$\frac{1}{2} (U_u + U_\ell) = U_\infty \ . \tag{B.9}$$

Rewriting (B.3) using (B.7) and (B.8) gives

$$U_u^2 - U_\ell^2 = 2 \frac{\delta}{R} V_a^2 \ . \tag{B.10}$$

Using (B.9), (B.10) becomes

$$U_u - U_\ell = \frac{\delta}{R} \frac{V_a^2}{U_\infty} \quad . \tag{B.11}$$

The velocity discontinuities at the jet boundaries are equivalent to vortex sheets of strengths

$$\gamma_u = U_u - V_u \tag{B.12}$$

and

$$\gamma_\ell = V_\ell - U_\ell \quad , \tag{B.13}$$

so that

$$\gamma_u + \gamma_\ell = (U_u - U_\ell) - (V_u - V_\ell) \ . \tag{B.14}$$

Substituting (B.7) and (B.11) into (B.14) gives

$$\gamma_u + \gamma_\ell = \frac{\delta}{R} \frac{V_a^2}{U_\infty} - \frac{\delta}{R} V_a \quad , \tag{B.15}$$

then nondimensionalizing (B.15) and rearranging gives

$$\frac{1}{R} = \frac{\gamma_u + \gamma_\ell}{U_\infty} \Bigg/ \left(\frac{\delta V_a^2}{U_\infty^2} - \frac{\delta V_a}{U_\infty} \right) \quad . \tag{B.16}$$

This is one form of the jet dynamic boundary condition, which expresses R in terms of γ_u and γ_ℓ. Another form of the dynamic boundary condition expressed in terms of the velocities at the jet boundaries (without averaging them) is derived from Equations (B.3) and (B.6) as

$$\frac{1}{R} = \frac{2}{\delta} \; \frac{V_u - V_\ell}{V_u + V_\ell} \tag{B.17}$$

or

$$\frac{1}{R} = \frac{2}{\delta} \; \frac{(V_u - V_\ell)^2}{V_u^2 - V_\ell^2} \quad , \tag{B.18}$$

thus

$$\frac{1}{R} = \frac{2}{\delta} \; \frac{(V_u - V_\ell)^2}{U_u^2 - U_\ell^2} \quad . \tag{B.19}$$

APPENDIX C

CONSTRUCTION OF THE COORDINATES OF DIVISION POINTS ON THE JET UPPER BOUNDARY

From Fig. 11(c), assuming the coordinates of A_ℓ, a division point on the jet lower boundary, are known, the coordinates of A_u, a corresponding division point on the jet upper boundary, is calculated as follows.

The length $\overline{A_u A_\ell}$ is found from the jet thickness δ and χ, half the angle formed by the two adjacent vortex segments, as

$$\overline{A_u A_\ell} = \frac{\delta}{\sin(\chi)} \quad . \tag{C.1}$$

Thus, the coordinates of A_u are

$$x_{A_u} = x_{A_\ell} + \overline{A_u A_\ell} \cdot \cos(\lambda) \tag{C.2}$$

or

$$= x_{A_\ell} + \left|\frac{\delta}{\sin(\chi)}\right| \cos(\lambda) \tag{C.3}$$

and

$$y_{A_u} = y_{A_\ell} + \left|\frac{\delta}{\sin(\chi)}\right| \sin(\lambda) \tag{C.4}$$

where λ is the angle measured positively anti-clockwise from the x-axis to $\overline{A_\ell A_u}$.

APPENDIX D

VELOCITIES INDUCED BY A LINEARLY INCREASING STRENGTH DISTRIBUTED VORTEX

Considering a distributed vortex segment O'A on the ξ axis as shown in Fig. 15, the vortex strength, γ, increases linearly as

$$\gamma = \gamma_{ps} \frac{\xi}{\xi_A} , \tag{D.1}$$

where γ_{ps} is the vortex peak strength at ξ = A.

The differential induced velocity, dV', at point P (ξ_p, η_p) due to a very small element of distributed vortex having a strength of $\gamma d\xi$ at ξ is

$$dV' = \frac{\gamma d\xi}{2\Pi\ [(\xi_p - \xi)^2 + \eta_p^2]^{1/2}} . \tag{D.2}$$

Resolving dV' into ξ and η components gives

$$du' = dV' \sin \phi \tag{D.3}$$

or

$$du' = \frac{\gamma d\xi}{2\Pi\ [\xi_p - \xi)^2 + \eta_p^2]^{1/2}} \cdot \frac{\eta_p}{[(\xi_p - \xi)^2 + \eta_p^2]^{1/2}}$$

$$= \frac{\gamma \eta_p\ d\ \xi}{2\Pi\ [(\xi_p - \xi)^2 + \eta_p^2]} , \tag{D.4}$$

and

$$dv' = - dV' \cos \phi \tag{D.5}$$

or

$$dv' = \frac{- \gamma d\xi}{2\Pi \, [(\xi_p - \xi)^2 + \eta_p^2]^{1/2}} \cdot \frac{\xi_p - \xi}{[(\xi_p - \xi)^2 + \eta_p^2]^{1/2}}$$

$$= - \frac{(\xi_p - \xi) \, \gamma d\xi}{2\Pi \, [(\xi_p - \xi)^2 + \eta_p^2]} \quad . \tag{D.6}$$

The resultant velocities induced by the distributed vortex segment O'A are obtained by integrating (D.4) and (D.6) over the segment length. From (D.4),

$$u' = \frac{\eta_p}{2\Pi} \int_0^{\xi_A} \frac{\gamma d\xi}{(\xi_p - \xi)^2 + \eta_p^2} \quad . \tag{D.7}$$

Substituting (D.1) into (D.7) gives

$$u' = \frac{\eta_p}{2\Pi} \, \frac{\gamma_{ps}}{\xi_A} \int_0^{\xi_A} \frac{\xi d\xi}{(\xi_p - \xi)^2 + \eta_p^2} \tag{D.8}$$

or

$$u' = \frac{\eta_p}{2\Pi} \, \frac{\gamma_{ps}}{\xi_A} \left\{ \ln \left[\frac{(\xi_p - \xi_A)^2 + \eta_p^2}{\xi_p^2 + \eta_p^2} \right]^{1/2} \right.$$

$$\left. - \frac{\xi_p}{|\eta_p|} \left[\tan^{-1} \frac{|\eta_p|}{\xi_p} - \tan^{-1} \frac{|\eta_p|}{\xi_p - \xi_A} \right] \right\} \tag{D.9}$$

Similarly, by substituting (D.1) into (D.6) and integrating, the η- component of induced velocity is obtained as

$$v' = -\frac{\gamma_{ps}}{2\Pi\xi_A}\int_0^{\xi_A}\frac{(\xi_p - \xi)\quad \xi d\xi}{(\xi_p - \xi)^2 + \eta_p^2} \tag{D.10}$$

or

$$v' = \frac{1}{2\Pi}\frac{\gamma_{ps}}{\xi_A}\left\{\xi_p \ \ell n\left[\frac{(\xi_p - \xi_A)^2 + \eta_p^2}{\xi_p^2 + \eta_p^2}\right]^{1/2}\right.$$

$$\left. + \eta_p\left[\tan^{-1}\frac{|\eta_p|}{\xi_p} - \tan^{-1}\frac{|\eta_p|}{\xi_p - \xi_A}\right] + |\xi_A|\right\} \quad . \tag{D.11}$$

APPENDIX E

TREATMENTS OF THE SINGULAR INTEGRALS IN THE EXPRESSIONS OF $u_{P-\gamma_1}$ AND $v_{P-\gamma_1}$

Equation (52) for $u_{P-\gamma_1}$ is

$$u_{P-\gamma_1} = \frac{K_1}{2\Pi} \int_0^{x_2} \frac{\ln (1 - x)}{x^{3/2}} \frac{y_P}{(x_P - x)^2 + y_P^2} \, dx \, . \qquad (E.1)$$

The integral is singular at $x = 0$.

The method used to solve this integral is to separate the integrand into additive parts which are either analytically integrable through the singularity or have no singularity (and hence can be solved accurately enough by a numerical method). In this case the integrand is rearranged so that

$$\frac{u_{P-\gamma_1}}{\frac{K_1}{2\Pi}} = \int_0^{x_2} \left[\frac{\ln (1 - x)}{x^{3/2}} \frac{y_P}{(x_P - x)^2 + y_P^2} - \frac{\ln (1 - x)}{x^{3/2}} \frac{y_P}{x_P^2 + y_P^2}\right]^* dx$$

$$+ \frac{y_P}{x_P^2 + y_P^2} \int_0^{x_2} \frac{\ln (1 - x)}{x^{3/2}} \, dx \qquad (E.2)$$

$$= \int_0^{x_2} [\quad]^* \, dx - \frac{y_P}{x_P^2 + y_P^2} \, 2 \left[\ln \frac{1 + x^{1/2}}{1 - x^{1/2}} + \frac{\ln (1 - x)}{x^{1/2}}\right]_0^{x_2} \qquad (E.3)$$

or

$$\frac{u_{P-\gamma_1}}{\frac{K_1}{2\Pi}} = \int_0^{x_2} [\ ]^* dx - \frac{2\, y_P}{x_P^2 + y_P^2} \left[\ln \frac{1 + x_2^{1/2}}{1 - x_2^{1/2}} + \frac{\ln (1 - x_2)}{x_2^{1/2}} \right] . \qquad (E.4)$$

The integrand in (E.4) is free from singularity at $x = 0$ and can be calculated fairly accurately by a numerical method.*

Equation (53) for $v_{P-\gamma_1}$ is

$$v_{P-\gamma_1} = \frac{-K_1}{2\Pi} \int_0^{x_2} \frac{\ln (1 - x)}{x^{3/2}} \frac{x_P - x}{(x_P - x)^2 + y_P^2} dx . \qquad (E.5)$$

For the values of x_P outside the range of integration, $x_P < 0$ and $x_P > x_2$, the integral is singular at $x = 0$.

Using the method of treatment of the singularity described earlier, the integrand in (E.5) is rewritten as

$$\frac{v_{P-\gamma_1}}{\frac{K_1}{2\Pi}} = - \int_0^{x_2} \left[\frac{\ln (1 - x)}{x^{3/2}} \frac{x_P - x}{(x_P - x)^2 + y_P^2} - \frac{\ln (1 - x)}{x^{3/2}} \frac{x_P}{x_P^2 + y_P^2} \right]^* dx$$

$$- \frac{x_P}{x_P^2 + y_P^2} \int_0^{x_2} \frac{\ln (1 - x)}{x^{3/2}} dx \qquad (E.6)$$

---

* Integration by Gaussian Quadrature was used.

$$= - \int_0^{x_2} [\ ]^* \, dx + \frac{x_p}{x_p^2 + y_p^2} \, 2 \left[\ell n \frac{1 + x^{1/2}}{1 - x^{1/2}} + \frac{\ell n \, (1 - x)}{x^{1/2}} \right]_0^{x_2} \quad (E.7)$$

or

$$\frac{v_{p-\gamma_1}}{\frac{K_1}{2\Pi}} = - \int_0^{x_2} [\ ]^* \, dx + \frac{2 \, x_p}{x_p^2 + y_p^2} \left[\ell n \frac{1 + x_2^{1/2}}{1 - x_2^{1/2}} + \frac{\ell n \, (1 - x_2)}{x_2^{1/2}} \right] \quad (E.8)$$

For values of x_p within the range of integration, $0 < x_p < x_2$, and when y_p is equal to zero, the integral (E.5) is singular at $x = 0$ and $x = x_p$. Equation (E.5) is rewritten as

$$\frac{v_{p-\gamma_1}}{\frac{K_1}{2\Pi}} = - \int_0^{x_2} \left[\frac{\ell n \, (1 - x)}{x^{3/2}} \frac{1}{x_p - x} - \frac{\ell n \, (1 - x)}{x^{3/2}} \frac{1}{x_p} - \frac{\ell n \, (1 - x_p)}{x_p^{3/2}} \right.$$

$$\left. \frac{1}{x_p - x} \right]^* dx - \frac{1}{x_p} \int_0^{x_2} \frac{\ell n \, (1 - x)}{x^{3/2}} \, dx - \frac{\ell n \, (1 - x_p)}{x_p^{3/2}} \int_0^{x_2} \frac{dx}{x_p - x} \quad .$$

or (E.9)

$$\frac{v_{p-\gamma_1}}{\frac{K_1}{2\Pi}} = - \int_0^{x_2} [\ ]^* \, dx + \frac{2}{x_p} \left[\ell n \frac{1 + x_2^{1/2}}{1 - x_2^{1/2}} + \frac{\ell n \, (1 - x_2)}{x_2^{1/2}} \right]$$

$$- \frac{\ell n \, (1 - x_p)}{x_p^{3/2}} \, \ell n \, \frac{x_p}{x_2 - x_p} \quad . \quad (E.10)$$

APPENDIX F

TREATMENTS OF THE SINGULAR INTEGRALS IN THE EXPRESSIONS OF $u_{P-\gamma_{NC}}$ AND $v_{P-\gamma_{NC}}$

Equation (54) for $u_{P-\gamma_{NC}}$ is

$$u_{P-\gamma_{NC}} = \frac{K_{NC}}{2\Pi} \int_{x_{NC}}^{1} \frac{\ln (1 - x)}{x^{3/2}} \; \frac{y_P}{(x_P - x)^2 + y_P^2} \; dx \quad . \tag{F.1}$$

The integral is singular at x = 1.

Using a method of treatment of the singular integrals similar to that described in Appendix E, Equation (F.1) is rewritten as

$$\frac{u_{P-\gamma_{NC}}}{\frac{K_{NC}}{2\Pi}} = \int_{x_{NC}}^{1} \left[\frac{\ln (1 - x)}{x^{3/2}} \; \frac{y_P}{(x_P - x)^2 + y_P^2} - \ln (1 - x) \right.$$

$$\left. \frac{y_P}{(x_P - 1)^2 + y_P^2}\right]^* dx + \frac{y_P}{(x_P - 1)^2 + y_P^2} \int_{x_{NC}}^{1} \ln (1 - x) \; dx \tag{F.2}$$

or

$$\frac{u_{P-\gamma_{NC}}}{\frac{K_{NC}}{2\Pi}} = \int_{x_{NC}}^{1} [\;]^* \; dx + \frac{y_P}{(x_P - 1)^2 + y_P^2} \left[(1 - x_{NC}) \ln (1 - x_{NC}) + x_{NC} - 1\right] \tag{F.3}$$

Equation (55) for $v_{P-\gamma_{NC}}$ is

$$v_{P-\gamma_{NC}} = \frac{-K_{NC}}{2\Pi} \int_{x_{NC}}^{1} \frac{\ell n\ (1 - x)}{x^{3/2}} \frac{(x_P - x)}{(x_P - x)^2 + y_P^2}\ dx\ . \tag{F.4}$$

For the values of x_P outside the range of integration $x_P < x_{NC}$ and $x_P > 1$, the integral is singular at $x = 1$.

Equation (F.4) is rewritten as

$$\frac{v_{P-\gamma_{NC}}}{\frac{K_{NC}}{2\Pi}} = - \int_{x_{NC}}^{1} \left[\frac{\ell n\ (1 - x)}{x^{3/2}} \frac{x_P - x}{(x_P - x)^2 + y_P^2} - \ell n\ (1-x) \frac{x_P - 1}{(x_P - 1)^2 + y_P^2}\right]^* dx - \frac{x_P - 1}{(x_P - 1)^2 + y_P^2} \int_{x_{NC}}^{1} \ell n\ (1 - x)\ dx \tag{F.5}$$

or

$$\frac{v_{P-\gamma_{NC}}}{\frac{K_{NC}}{2\Pi}} = - \int_{x_{NC}}^{1} [\ ]^*\ dx - \frac{x_P - 1}{(x_P - 1)^2 + y_P^2} \left[(1 - x_{NC}\ \ell n\ (1 - x_{NC}) + x_{NC}) - 1\right]\ . \tag{F.6}$$

For values of x_P within the range of integration, $x_{NC} < x_P < 1$, and $y_P = 0$, the integral in Equation (F.4) is singular at $x = 1$ and $x = x_P$.

Equation (F.4) is rewritten as

$$\frac{v_{P-\gamma_{NC}}}{\frac{K_{NC}}{2\Pi}} = - \int_{x_{NC}}^{1} \left[\frac{\ell n\ (1 - x)}{x^{3/2}} \frac{1}{x_P - x} - \frac{\ell n\ (1 - x)}{x_P - 1} - \frac{\ell n\ (1 - x_P)}{x_P^{\ 3/2}} \right.$$

$$\left. \frac{1}{x_P - x} \right]^* dx - \frac{1}{x_P - 1} \int_{x_{NC}}^{1} \ell n\ (1 - x\ )\ dx - \frac{\ell n\ (1 - x_P)}{x_P^{\ 3/2}}$$

$$\int_{x_{NC}}^{1} \frac{dx}{x_P - x} \quad , \tag{F.7}$$

or

$$\frac{v_{P-\gamma_{NC}}}{\frac{K_{NC}}{2\Pi}} = - \int_{x_{NC}}^{1} [\ ]^* \, dx - \frac{1}{x_P - 1} \left[(1 - x_{NC})\ \ell n\ (1 - x_{NC}) + x_{NC} - 1 \right]$$

$$- \frac{\ell n\ (1 - x_P)}{x_P^{3/2}}\ \ell n \quad \frac{x_P - x_{NC}}{1 - x_P} \quad . \tag{F.8}$$

APPENDIX G

TREATMENTS OF THE SINGULAR INTEGRALS IN THE EXPRESSIONS OF $u'_{P-\gamma_{NCI}}$, $v'_{P-\gamma_{NCI}}$, $u'_{p-\gamma_{NI}}$ and $v'_{P-\gamma_{NI}}$

The expressions for $u'_{P-\gamma_{NCI}}$ and $u'_{P-\gamma_{NI}}$ have the general form of

$$u' = \frac{K}{2\Pi} \int_0^{\ell} \frac{\ell n \ (x - k)}{x^{3/2}} \ \frac{\eta_P}{(\xi_P - \xi)^2 + \eta_P^2} \ d\xi \ , \tag{G.1}$$

where k is a constant.

From the geometrical model [Fig. 11(b)]

$$x - k = \xi \cos \tau \tag{G.2}$$

Substituting (G.2) into (G.1) gives

$$\frac{u'}{\frac{K}{2\Pi}} = \int_0^{\ell} \frac{\ell n \ (\xi \cos \tau)}{(\xi \cos \tau + k)^{3/2}} \ \frac{\eta_P}{(\xi_P - \xi)^2 + \eta_P^2} \ d\xi \tag{G.3}$$

Using a method of treatment of the singularity similar to that described in Appendix E, Equation (G.3) is rewritten as

$$\frac{u'}{\frac{K}{2\Pi}} = \int_0^{\ell} \left[\frac{\ell n \ (\xi \cos \tau)}{(\xi \cos \tau + k)^{3/2}} \ \frac{\eta_P}{(\xi_P - \eta_P)^2 + \eta_P^2} - \ell n \ (\xi \cos \tau) \right.$$

$$\left. \frac{\eta_P}{k^{3/2} \ (\xi_P^2 + \eta_P^2)} \right]^* d\xi + \frac{\eta_P}{k^{3/2} \ (\xi_P^2 + \eta_P^2)} \int_0^{\ell} \ell n \ (\xi \cos \tau) \ d\xi \tag{G.4}$$

or

$$\frac{u'}{\frac{K}{2\Pi}} = \int_0^{\ell} [\ ]^* \, d\xi + \frac{\eta_p}{k^{3/2}\ (\xi_p^2 + \eta_p^2)}\ \ell \left[\ell n\ (\ell \cos \tau) - 1\right]. \qquad (G.5)$$

The expressions for $v'_{P-\gamma_{NC}}$ and $v'_{P-\gamma_{N}}$ have the general form of

$$v' = - \frac{-K}{2\Pi} \int_0^{\ell} \frac{\ell n\ (x - k)}{x^{3/2}} \frac{\xi_p - \xi}{(\xi_p - \xi)^2 + \eta_p^2} \, d\xi \qquad (G.6)$$

Substituting (G.2) into (G.6) gives

$$\frac{v'}{\frac{K}{2\Pi}} = - \int_0^{\ell} \frac{\ell n\ (\xi \cos \tau)}{(\xi \cos \tau + k)^{3/2}} \frac{\xi_p - \xi}{(\xi_p - \xi)^2 + \eta_p^2} \, d\xi \quad . \qquad (G.7)$$

For values of ξ_p outside the range of integration, the integral in Equation (G.7) is singular at $\xi = 0$. Equation (G.7) is rewritten as

$$\frac{v'}{\frac{K}{2\Pi}} = - \int_0^{\ell} \left[\frac{\ell n\ (\xi \cos \tau)}{(\xi \cos \tau + k)^{3/2}} \frac{\xi_p - \xi}{(\xi_p - \xi)^2 + \eta_p^2} - \ell n\ (\xi \cos \tau) \right.$$

$$\left. \frac{\xi_p}{k^{3/2}\ (\xi_p^2 + \eta_p^2)}\right]^* d\xi - \frac{\xi_p}{k^{3/2}\ (\xi_p^2 + \eta_p^2)} \int_0^{\ell} \ell n\ (\xi \cos \tau) \, d\xi \qquad (G.8)$$

or

$$\frac{v'}{\frac{K}{2\Pi}} = - \int_0^{\ell} [\ ]^* d\xi - \frac{\xi_p}{(\xi_p^2 + \eta_p^2)\ k^{3/2}}\ \ell \left[\ell n\ (\xi \cos \tau) - 1\right] \quad . \qquad (G.9)$$

For values of ξ_p within the range of integration, and $\eta_p = 0$, the integral in Equation (G.7) is singular at $\xi = 0$ and $\xi = \xi_p$. Equation (G.7) is rewritten as

$$\frac{v'}{\frac{K}{2\Pi}} = - \int_0^{\ell} \left[\frac{\ell n\ (\xi \cos \tau)}{(\xi \cos \tau + k)^{3/2}} \frac{1}{\xi_p - \xi} - \frac{1}{\xi_p\, k^{3/2}} \ell n\ (\xi \cos \tau) \right.$$

$$\left. - \frac{\ell n\ (\xi_p \cos \tau)}{(\xi_p \cos \tau + k)^{3/2}} \frac{1}{\xi_p - \xi} \right]^* d\xi \ - \frac{1}{\xi_p\, k^{3/2}} \int_0^{\ell} \ell n\ (\xi \cos \tau)\ d\xi$$

$$- \frac{\ell n\ (\xi_p \cos \tau)}{(\xi_p \cos \tau + k)^{3/2}} \int_0^{\ell} \frac{d\xi}{\xi_p - \xi} \qquad \text{(G.10)}$$

or

$$\frac{v'}{\frac{K}{2\Pi}} = - \int_0^{\ell} [\ ]^*\ d\xi - \frac{1}{\xi_p\, k^{3/2}}\, \ell \left[\ell n\ (\xi \cos \tau) - 1 \right]$$

$$- \frac{\ell n\ (\xi_p \cos \tau)}{(\xi_p \cos \tau + k)^{3/2}}\ \ell n\ \frac{\xi_p}{\ell - \xi_p} \qquad \text{(G.11)}$$

APPENDIX H

SOLUTION TO A DIFFERENTIAL EQUATION

Rewriting Equation (87) gives

$$\frac{y''}{(1 + y'^2)^{3/2}} = C_1 \tag{H.1}$$

where C_1 is the right hand side of Equation (87) which is assumed constant along each vortex segment.

Let

$$g = y', \tag{H.2}$$

then (H.1) becomes

$$\frac{g'}{(1 + g^2)^{3/2}} = C_1 \quad . \tag{H.3}$$

Both sides of (H.3) can be integrated to give

$$\int \frac{dg}{(1 + g^2)^{3/2}} = C_1 \int dx \quad , \tag{H.4}$$

$$\frac{g}{(1 + g^2)^{1/2}} = C_1 \; x + C_2 \; , \tag{H.5}$$

where C_2 is determined by letting (H.5) satisfy the initial slope of the jet center line segment

$$C_2 = \frac{y'_{oj}}{(1 + y'^2_{oj})^{1/2}} - C_1 \; x_{oj} \tag{H.6}$$

Solving (H.5) gives

$$g = \frac{C_1 \; x + C_2}{[1 - (C_1 \; x + C_2)^2]^{1/2}} \quad . \tag{H.7}$$

Rewriting (H.7) letting $X = C_1 \; x + C_2$ and substituting $\frac{dy}{dx}$ for g gives

$$\frac{dy}{dx} = \frac{X}{(1 - X^2)^{1/2}} \quad , \tag{H.8}$$

or

$$dy = \frac{X}{(1 - X^2)^{1/2}} \, dx \quad . \tag{H.9}$$

But

$$dx = \frac{dX}{C_1} \quad , \tag{H.10}$$

therefore substituting (H.10) into (H.9) and integrating (H.9) gives

$$y = - \frac{(1 - X^2)^{1/2}}{C_1} + C_3 \quad . \tag{H.11}$$

Rewriting (H.11) in term of x gives

$$y = - \frac{1}{C_1} [1 - (C_1 \; x + C_2)^2]^{1/2} + C_3 \quad , \tag{H.12}$$

where C_3 is determined by letting (H.12) satisfy the initial location of the jet center line segment, and is given by

$$C_3 = y_{oj} + \frac{1}{C_1} [1 - (C_1 \; x_{oj} + C_2)^2]^{1/2} \quad . \tag{H.13}$$

APPENDIX I

CONVERGENCE OF ITERATIONS

The basic iterative solution consists of two steps:

Step 1

An assumed jet shape is used to evaluate the vortex strength distribution.

Step 2

The vortex strength distribution is used to evaluate the jet shape to be used in the next "Step 1".

Application of this technique produces divergent solutions as illustrated in Fig. 16. An additional step (Step 3) is introduced to produce a modified jet shape for input to Step 1.

Any pair of successive jet shapes forms an envelope within which the true shape lies. Because the first assumed jet shape may cross the true shape, it was found to be unwise to take it as a boundary to the envelope. The first envelope is therefore taken as the two jet shapes resulting from the first two applications of Step 2.

Suppose the envelope is bounded by the curves y_1, y_2 (with y_1 above y_2) as on Fig. 17. The next input shape is given by

$$y_3 = \frac{1}{2}(y_1 + y_2)$$

and produces the curve y_4 which may lie in any of four regions. The end points are denoted by $(y_4)_{1,\ 2,\ 3,\ 4}$ as shown on Fig. 17 and are used in the computer programme for determining the input for the next iteration. Also, the end points of the curves y_1, y_2 and y_3 are denoted by (y_1), (y_2) and (y_3) respectively. Consider the four possibilities.

$\underline{(y_4)_1;\ (y_4)_1 < (y_2)}$

To produce a curve with $(y_4)_1 < (y_2)$, the (y_3) value would have had to be above (y_1) because of the divergent nature of the solutions. Therefore $(y_4)_1$ cannot exist.

$\underline{(y_4)_2;\ (y_3) < (y_4)_2 < (y_2)}$

Since the iterative solutions diverge, y_3 and y_4 must represent a more restrictive envelope than y_1, y_2 and this new envelope is retained for comparison in the next iteration for which the input is taken as $\frac{1}{2}(y_3 + y_4)$.

$\underline{(y_4)_3;\ (y_1) < (y_4)_3 < (y_3)}$

A similar case to $(y_4)_2$. The new envelope is y_4 and y_3 and the input for the next iteration is $\frac{1}{2}(y_3 + y_4)$.

$\underline{(y_4)_4;\ (y_4)_4 > (y_1)}$

In this case, $(y_4)_4$ is outside the original envelope and is rejected. The new envelope is specified by y_1 and y_3 and the next input is $\frac{1}{2}(y_1 + y_3)$.

A similar set of arguments is used if the curve y_2 lies above curve y_1.

APPENDIX J

NON-UNIFORM JET DYNAMIC BOUNDARY CONDITION

In this Appendix, the non-uniform jet dynamic boundary condition is derived from the nine equations given in Chapter V.3, from Equations (102) to (110). For convenience, these equations are rewritten here.

$$p_u + \frac{1}{2} \rho U_u^2 = p_\ell + \frac{1}{2} \rho U_\ell^2 \tag{J.1}$$

$$p_1 + \frac{1}{2} \rho V_1^2 = p_2 + \frac{1}{2} \rho V_2^2 \tag{J.2}$$

$$p_3 + \frac{1}{2} \rho V_3^2 = p_4 + \frac{1}{2} \rho V_4^2 \tag{J.3}$$

$$V_1 R_1 = V_2 R_2 \tag{J.4}$$

$$V_3 R_3 = V_4 R_4 \tag{J.5}$$

$$R_2 = R_3 \tag{J.6}$$

$$p_u = p_1 \tag{J.7}$$

$$p_\ell = p_4 \tag{J.8}$$

$$p_2 = p_3 \tag{J.9}$$

Substituting (J.6) into (J.5), and combining (J.4) and (J.5) give

$$\frac{V_1}{V_4} R_1 = \frac{V_2}{V_3} R_4 \quad . \tag{J.10}$$

Substituting $R_1 = R - \frac{\delta}{2}$ and $R_4 = R + \frac{\delta}{2}$ into (J.10),

$$\frac{V_1}{V_4} (R - \frac{\delta}{2}) = \frac{V_2}{V_3} (R + \frac{\delta}{2}) \quad . \tag{J.11}$$

Rearranging (J.11) gives

$$\frac{1}{R} = \frac{V_1 V_3 - V_2 V_4}{V_1 V_3 + V_2 V_4} \cdot \frac{2}{\delta} \quad . \tag{J.12}$$

Let

$$k_V = \frac{V_3}{V_2} \quad , \tag{J.13}$$

(J.12) is rewritten as

$$\frac{1}{R} = \frac{k_V V_1 - V_4}{k_V V_1 + V_4} \cdot \frac{2}{\delta} \quad , \tag{J.14}$$

or

$$\frac{1}{R} = \frac{(k_V V_1 - V_4)^2}{k_V^2 V_1^2 - V_4^2} \cdot \frac{2}{\delta} \quad . \tag{J.15}$$

Rewriting (J.1) gives

$$p_\ell - p_u = \frac{1}{2} \rho (U_u^2 - U_\ell^2) \tag{J.16}$$

Combining (J.2) and (J.3) and using (J.9) yields

$$p_4 - p_1 = \frac{1}{2} \rho (V_1^2 - V_4^2) + \frac{1}{2} \rho (V_3^2 - V_2^2) \tag{J.17}$$

Combining (J.16) and (J.17) using (J.7) and (J.8) gives

$$U_u^2 - U_\ell^2 = V_1^2 - V_4^2 + V_3^2 - V_2^2 , \tag{J.18}$$

Adding and substracting $k_V^2\, V_1^2$ to the right hand side of (J.18),

$$U_u^2 - U_\ell^2 = k_V^2\, V_1^2 - V_4^2 - (k_v^2 - 1)\, V_1^2 + V_3^2 - V_2^2 \tag{J.19}$$

Using (J.13) , substituting V_3 by $k_V V_2$, (J.19) becomes

$$U_u^2 - U_\ell^2 = k_V^2\, V_1^2 - V_4^2 - (k_V^2 - 1)\, V_1^2 + k_V^2\, V_2^2 - V_2^2 \ . \tag{J.20}$$

Rearranging (J.20) gives

$$k_V^2\, V_1^2 - V_4^2 = (U_u^2 - U_\ell^2) + (k_V^2 - 1)\, (V_1^2 - V_2^2) \ . \tag{J.21}$$

Substituting (J.21) into (J.15) gives

$$\frac{1}{R} = \frac{(k_V V_1 - V_4)^2}{(U_u^2 - U_\ell^2) + (k_V^2 - 1)\, (V_1^2 - V_2^2)} \cdot \frac{2}{\delta} \ . \tag{J.22}$$

APPENDIX K

FLOW CHART AND COMPUTER PROGRAM FOR THE SOLUTION OF THE UNIFORM JET

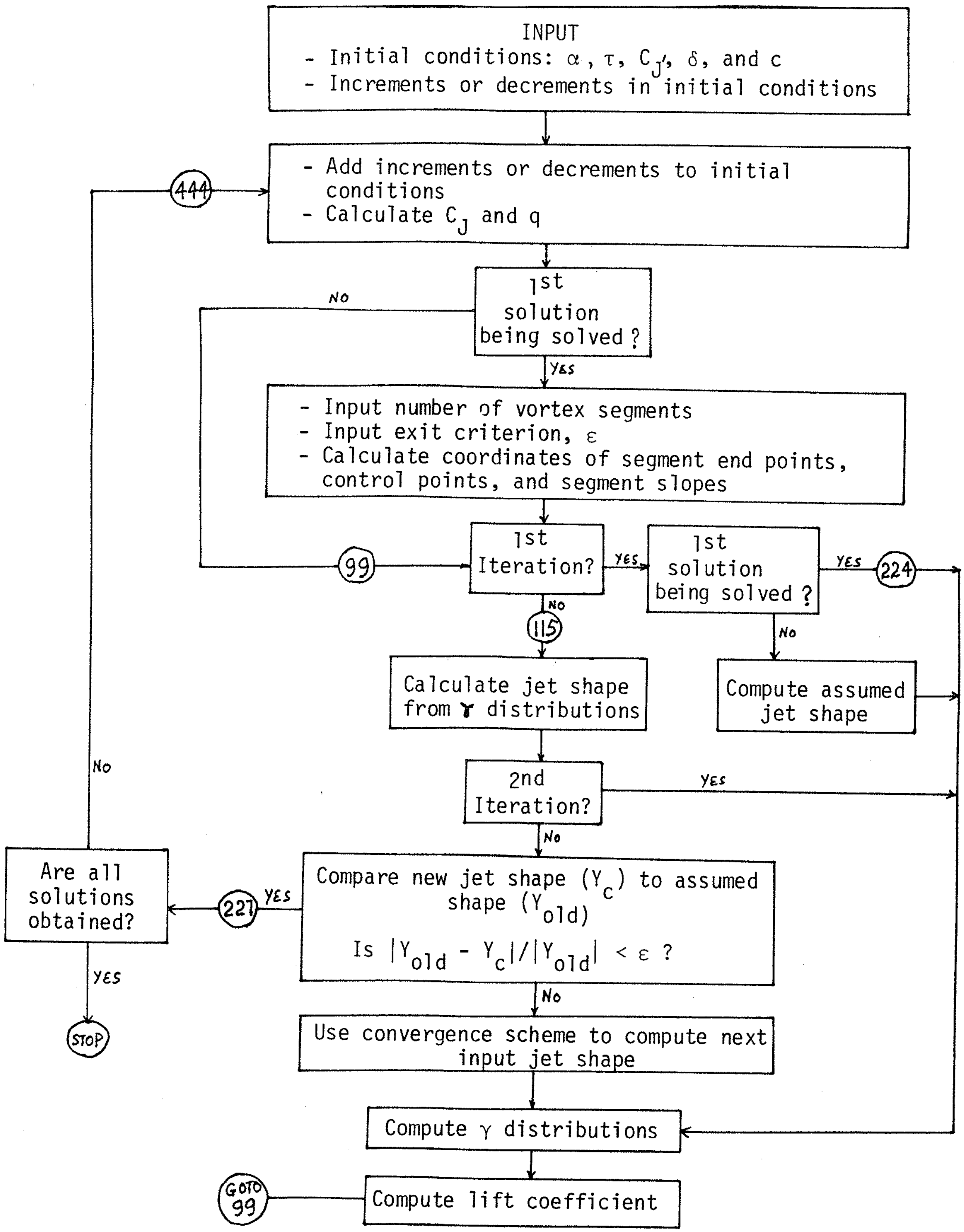

INPUT
- Initial conditions: α, τ, C_J', δ, and c
- Increments or decrements in initial conditions
444
- Add increments or decrements to initial conditions
- Calculate C_J and q
1st solution being solved?
NO
YES
- Input number of vortex segments
- Input exit criterion, ε
- Calculate coordinates of segment end points, control points, and segment slopes
99
1st Iteration?
YES
1st solution being solved?
YES
224
NO
115
NO
Calculate jet shape from γ distributions
Compute assumed jet shape
2nd Iteration?
YES
NO
NO
Are all solutions obtained?
227
YES
Compare new jet shape (Y_c) to assumed shape (Y_old)
Is |Y_old - Y_c|/|Y_old| < ε ?
YES
STOP
NO
Use convergence scheme to compute next input jet shape
Compute γ distributions
GOTO 99
Compute lift coefficient

```
$JOB   WATFIV    TANG,TIME=120,LIBLIST,LINES=50
        DIMENSION X(60),Y(60),XP(60),YP(60),SLOPE(60),
       CB(60),A(60,60),IW1(60),IW2(60),YOLD(60),YMAX(60),YMIN(60)
       C,G(60),XC(60),YC(60),XK(60),AS(60,60),SU1(60),SV1(60)
       C,SYOL(30,30),UIND(20)
C---
C---   PRINCIPAL SYMBOLS
C---
C       A(I,J)       COEFFICIENT MATRIX IN THE SET OF LINEAR
C                    EQUATIONS
C       ALPHA        ANGLE OF ATTACK (RADIAN)
C       ALFAD        ANGLE OF ATTACK (DEGREE)
C       B(I)         COLUMN MATRIX IN THE SET OF LINEAR EQUATIONS
C                    THIS MATRIX IS ERASED AFTER THE SOLUTION
C                    OF THE SET OF LINEAR EQUATIONS IS FOUND,AND
C                    THE MATRIX IS USED TO STORE THE SOLUTION
C       CHORD        CHORD LENGTH
C       CJ           AUGMENTED JET MOMENTUM COEFFICIENT
C       CPJ          PRIMARY JET MOMENTUM COEFFICIENT
C       DALPHA       INCREMENT IN ANGLE OF ATTACK
C       DCPJ         INCREMENT IN PRIMARY JET MOMENTUM COEFFICIENT
C       DDEL         INCREMENT IN JET THICKNESS
C       DEL          JET THICKNESS
C       DTAU         INCREMENT IN INITIAL JET DEFLECTION ANGLE
C       EPS          EXIT CRITERION
C       MAXIT        MAXIMUM NUMBER OF ITERATIONS PER SOLUTION
C       N            NUMBER OF FINITE VORTEX SEGMENTS ON THE CHORD
C                    AND LOWER JET BOUNDARY
C       NC           NUMBER OF VORTEX SEGMENTS ON THE CHORD
C       NT           TOTAL NUMBER OF FINITE VORTEX SEGMENTS
C       PHI          ANGLE MADE BY THE VORTEX SEGMENT AND THE X-AXIS
C       Q            PRIMARY JET VELOCITY
C       R1           DISTANCE FROM UPSTREAM END POINT OF VORTEX
C                    SEGMENT TO CONTROL POINT
C       R2           DISTANCE FROM DOWNSTREAM END POINT OF VORTEX
C                    SEGMENT TO CONTROL POINT
C       SL           FINITE VORTEX SEGMENT LENGTH
C       SLOPE(I)     SLOPES OF THE VORTEX SEGMENTS
C       TAU          INITIAL JET DEFLECTION ANGLE (RADIAN)
C       TAUD         INITIAL JET DEFLECTION ANGLE(DEGREE)
C       TETA1        ANGLE MEASURED FROM VORTEX SEGMENT TO
C                    THE LINE OF R1
C       TETA2        ANGLE MEASURED FROM VORTEX SEGMENT TO
C                    THE LINE OF R2
C       U            X-COMPONENT OF VELOCITY INDUCED BY ALL THE
C                    DISTRIBUTED VORTICES CONTRIBUTING TO LIFT
C       US           X-COMPONENT OF VELOCITY INDUCED BY SOURCE
C                    DISTRIBUTION
C       USINF        X-COMPONENT OF VELOCITY INDUCED BY
C                    SEMI-INFINITE VORTEX ELEMENTS
```

```
C       V               Y-COMPONENT OF VELOCITY INDUCED BY ALL THE
C                       DISTRIBUTED VORTICES CONTRIBUTING TO LIFT
C       VS              Y-COMPONENT OF VELOCITY INDUCED BY SOURCE
C                       DISTRIBUTION
C       VSINF           Y-COMPONENT OF VELOCITY INDUCED BY
C                       SEMI-INFINITE VORTEX ELEMENTS
C       X(I)            X-COORDINATES OF FINITE VORTEX SEGMENT
C                       END POINTS
C       XCONP           ZETA-COORDINATES OF CONTROL POINTS
C       XC(I)           X-COORDINATES OF FINITE SEGMENT END POINTS
C                       ON JET CENTER LINE
C       XLC             LIFT COEFFICIENT
C       XLCJ            JET LIFT COEFFICIENT (JET LIFT IS OBTAINED
C                       FROM THE INTEGRATION OF VORTEX DISTRIBUTIONS
C                       FROM THE TRAILING EDGE TO INFINITY)
C       XP(I)           X-COORDINATES OF CONTROL POINTS
C       Y(I)            Y-COORDINATES OF FINITE VORTEX SEGMENT
C                       END POINTS
C       YCONP            ETA-COORDINATES OF CONTROL POINTS
C       YC(I)           Y-COORDINATES OF FINITE SEGMENT END POINTS
C                       ON JET CENTER LINE
C       YP(I)           Y-COORDINATES OF CONTROL POINTS
C       YOLD(I)         Y-COORDINATES OF FINITE SEGMENT END POINTS ON
C                       JET CENTER LINE OF THE PRECEDING ITERATION
C---
C---    INITIAL CONDITIONS
C---
        ALPHA=0.
        TAU=-3.14159266/6.
        CPJ=1.75
        DEL=0.005
        CHORD=1.
C       INCREMENTS IN VARIABLES
C---    IN THIS EXAMPLE, JET THICKNESS IS A VARIABLE.
C---    THAT IS WHILE OTHER INITIAL CONDITIONS ARE KEPT
C---    CONSTANT, SOLUTIONS FOR DIFFERENT JET THICKNESSES
C                    ARE CALCULATED
        DALFA=0.
        DTAU=0.
        DCPJ=0.
        DDEL=0.001
        INP=0
  444   CONTINUE
        INP=INP+1
        CPJ=CPJ+DCPJ
        ALPHA=ALPHA+DALFA
        TAU=TAU+DTAU
        DEL=DEL+DDEL
C---    AUGMENTED JET MOMENTUM COEFFICIENT AND
C                    PRIMARY JET VELOCITY
```

```
      CJ=(SQRT(2.*DEL/CHORD)+SQRT(CPJ))**2
      Q=SQRT(CJ*CHORD/(2.*DEL))-1.
      DELH=DEL/2
      ALFAD=ALPHA*180./3.14159266
      TAUD=TAU*180./3.14159266
      IF(INP.GT.1) GOTO 445
C---
C___  INPUT DATA
C---
      EPS=0.C5
      MAXIT=6
      ERMAX=0.1
C---   NT=TOTAL ELEMENT IN THE THICK JET
      NT=38
      N=24
      NC=10
      NT1=NT+1
      NT2=NT+2
      NL2=N-2
      NC1=NC+1
      NC2=NC+2
      NCL1=NC-1
      NCL2=NC-2
      NTC=NT-NC
      NJ=N-NC
      NJ1=NJ+1
      NJL1=NJ-1
      N1=N+1
      N2=N+2
      N3=N+3
C---  X AND Y COORDINATES OF SEGMENT END POINTS ON THE AEROFOIL
      DO 23 I=1,NC1
      Y(I)=0.
      ARG=3.1415926*(I-1.)/NC
      X(I)=0.5*CHORD*(1.-COS(ARG))
   23 CONTINUE
      X(NC1)=1.
C---  READ X AND Y COORDINATES OF VORTEX SEGMENT END POINTS
C---  ON THE LOWER JET BOUNDARY
      READ(5,21) (X(I),I=NC2,N1)
      READ(5,21) (Y(I),I=NC2,N1)
   21 FORMAT(6F10.6)
      X(N2)=-DEL*SIN(TAU)+X(NC1)
      Y(N2)=DEL*COS(TAU)+Y(NC1)
C---  X AND Y COORDINATES OF VORTEX SEGMENT END POINTS ON UPPER
C---  JET BOUNDARY AND JET CENTER LINE
      DO 60 I=1,NJ
      TSG1=ATAN2((Y(I+NC)-Y(I+NC1)),(X(I+NC)-X(I+NC1)))
      IF(I.EQ.NJ) GOTO 61
      TSG2=ATAN2((Y(I+NC2)-Y(I+NC1)),(X(I+NC2)-X(I+NC1)))
```

```
 61   CONTINUE
      IF(I.EQ.NJ) TSG2=ALPHA
      THALF=(TSG1-TSG2)/2.
      PSG=(TSG1+TSG2)/2.
      X(I+N2)=X(I+NC1)+DEL*COS(PSG)/SIN(THALF)
      Y(I+N2)=Y(I+NC1)+DEL*SIN(PSG)/SIN(THALF)
      XC(I+1)=(X(I+NC1)+X(I+N2))/2.
      YC(I+1)=(Y(I+NC1)+Y(I+N2))/2.
 60   CONTINUE
      YC(1)=(Y(N2)+Y(NC1))/2
      XC(1)=(X(N2)+X(NC1))/2
      DO 24 I=1,NC
      XP(I)=(X(I+1)+X(I))/2.
      YP(I)=(Y(I+1)+Y(I))/2.
      SLOPE(I)=(Y(I+1)-Y(I))/(X(I+1)-X(I))
 24   CONTINUE
C---
C---  STARTING ITERATION PROCESS
C---
 445  CONTINUE
      MAXD=1
      ITR=0
 99   ITR=ITR+1
      IF(ITR.EQ.1.AND.INP.EQ.1) GOTO 224
      IF(ITR.NE.1) GOTO 115
      SXN2=X(N2)
      SYN2=Y(N2)
      X(N2)=-DEL*SIN(TAU)+X(NC1)
      Y(N2)=DEL*COS(TAU)+Y(NC1)
      XC(1)=(X(N2)+X(NC1))/2.
      YC(1)=(Y(N2)+Y(NC1))/2.
      IF(DTAU.NE.0.) GOTO 451
      DO 450 I=2,NJ1
      XC(I)=-DDEL*SIN(TAU)/2.+XC(I)
      YC(I)=DDEL*COS(TAU)/2.+YOLD(I)
      YOLD(I)=YC(I)
 450  CONTINUE
      GOTO 107
 451  CONTINUE
      DXTAU=(X(N2)-SXN2)/2.
      DYTAU=(Y(N2)-SYN2)/2.
      DO 452 I=2,NJ1
      XC(I)=XC(I)+DXTAU
      YC(I)=((YOLD(I)+DYTAU)-YC(1))*TAN(TAU)/TAN(TAU-DTAU)
     C+YC(1)
      YOLD(I)=YC(I)
 452  CONTINUE
      GOTO 107
 115  CONTINUE
C---
```

```
C---  JET SHAPE CALCULATION
C---
      B(NT1)=0.
      G(1)=TAN(TAU)
      DO 220 I=1,NJ
      IF(I.GT.1) GOTO 221
      AU=SAU/(X(N3)-X(N2))
      AL=SAL/(X(NC2)-X(NC1))
      GOTO 222
221   CONTINUE
      IF(I.EQ.NJ) B(NC1+I)=0.
      AL=(B(NC+I)+B(NC1+I))/2
      AU=(B(N+I)+B(N1+I))/2
222   CONTINUE
      XK(I)=(AU+AL)/(CJ*CHORD*(1.-(2.*DEL/(CJ*CHORD))**0.5)/2.)
      C1=G(I)/(1.+G(I)**2)**0.5-XK(I)*XC(I)
      G(I+1)=(XK(I)*XC(I+1)+C1)/(1.-(XK(I)*XC(I+1)
     C+C1)**2)**.5
      C2=YC(I)+(1.-(XK(I)*XC(I)+C1)**2)**.5/XK(I)
      YC(I+1)=-(1.-(XK(I)*XC(I+1)+C1)**2)**.5/XK(I)+C2
      IF(INP.GT.1) GOTO 220
      IF(ITR.GT.2) GOTO 220
      YOLD(I+1)=YC(I+1)
220   CONTINUE
      PRINT,'JET SHAPE CALCULATED DIRECTLY FROM GAMA DISTRIBUTION'
      PRINT 52,(YC(I),I=1,NJ1)
      IF(ITR.EQ.2.AND.INP.EQ.1) GOTO 107
C---
C---  EXIT CRITERIA
C---
      DO 225 I=2,NJ1
      DISP=ABS(YOLD(I)-YC(I))/ABS(YOLD(I))
      IF(I.EQ.2) GOTO 226
      IF(DD.LT.DISP) DD=DISP
      GOTO 225
226   CONTINUE
      DD=DISP
225   CONTINUE
      PRINT,'JET DEVIATION'
      PRINT 55,DD
55    FORMAT(F10.3////)
      IF(DD.LT.EPS) GOTO 227
      IF(DD.LT.ERMAX) MAXD=2
      IF(ITR.LE.MAXIT) GOTO 449
      IF(MAXD.EQ.2) GOTO 227
      GOTO 448
C
C---  CONVERGENCE SCHEME
C
449   CONTINUE
```

```
      IF(YC(NJ1).GT.YOLD(NJ1)) GOTO 70
      IF(ITR.NE.3.AND.INP.EQ.1) GOTO 71
      IF(ITR.NE.2.AND.INP.GT.1) GOTO 71
   74 DO 72 I=2,NJ1
      YMAX(I)=YOLD(I)
   72 YMIN(I)=YC(I)
      GOTO 73
   71 CONTINUE
      IF(LL.GE.2) GOTO 74
      IF(YC(NJ1).GT.YMIN(NJ1)) GOTO 74
      KK=KK+1
      DO 75 I=2,NJ1
      YC(I)=(YOLD(I)+YMIN(I))/2.
   75 YOLD(I)=YC(I)
      GOTO 107
   70 CONTINUE
      IF(ITR.NE.3.AND.INP.EQ.1) GOTO 76
      IF(ITR.NE.2.AND.INP.GT.1) GOTO 76
   79 DO 77 I=2,NJ1
      YMAX(I)=YC(I)
   77 YMIN(I)=YOLD(I)
   73 CONTINUE
      KK=1
      LL=1
      DO 78 I=2,NJ1
      YC(I)=(YMAX(I)+YMIN(I))/2.
   78 YOLD(I)=YC(I)
      GOTO 107
   76 CONTINUE
      IF(KK.GE.2) GOTO 79
      IF(YC(NJ1).LT.YMAX(NJ1)) GOTO 79
      LL=LL+1
      DO 80 I=2,NJ1
      YC(I)=(YOLD(I)+YMAX(I))/2.
   80 YOLD(I)=YC(I)
C
C---  X AND Y COORDINATES OF FINITE VORTEX SEGMENT END POINTS
C---  ON THE JET LOWER AND UPPER BOUNDARIES
C
  107 CONTINUE
      DO 202 I=1,NJ
      TSG1=ATAN2((YC(I)-YC(I+1)),(XC(I)-XC(I+1)))
      IF(I.EQ.NJ) GOTO 203
      TSG2=ATAN2((YC(I+2)-YC(I+1)),(XC(I+2)-XC(I+1)))
  203 CONTINUE
      IF(I.EQ.NJ) TSG2=ALPHA
      THALF=(TSG1-TSG2)/2.
      PSG=(TSG1+TSG2)/2.
      X(I+N2)=XC(I+1)+DELH*COS(PSG)/SIN(THALF)
      Y(I+N2)=YC(I+1)+DELH*SIN(PSG)/SIN(THALF)
```

```
      X(I+NC1)=2.*XC(I+1)-X(I+N2)
      Y(I+NC1)=2.*YC(I+1)-Y(I+N2)
  202 CONTINUE
  224 CONTINUE
      DO 228 I=NC1,NT
      IF(I.GT.N) GOTO 229
      XP(I)=(X(I+1)+X(I))/2.
      YP(I)=(Y(I+1)+Y(I))/2.
      SLOPE(I)=(Y(I+1)-Y(I))/(X(I+1)-X(I))
      GOTO 228
  229 CONTINUE
      XP(I)=(X(I+2)+X(I+1))/2.
      YP(I)=(Y(I+2)+Y(I+1))/2.
      SLOPE(I)=(Y(I+2)-Y(I+1))/(X(I+2)-X(I+1))
  228 CONTINUE
C---
C---  COEFFICIENT MATRIX
C---
      DO 1 I=1,NT
      UGAMA=0.
      VGAMA=0.
      SYP=YP(I)
      SXP=XP(I)
      IK=1
      DO 2 J=1,NT
      IF(ITR.EQ.1) GOTO 3
      IF(I.GT.NC) GOTO 3
      IF(J.GT.NC) GOTO 3
      A(I,J)=AS(I,J)
      GOTO 2
    3 CONTINUE
      IF(J.EQ.N1) IK=1
      IF(IK.EQ.2) GOTO 4
      K=0
      IF(J.GT.N) K=1
      K1=K+1
      PHI=ATAN2((Y(J+K1)-Y(J+K)),(X(J+K1)-X(J+K)))
      SL=SQRT((Y(J+K1)-Y(J+K))**2+(X(J+K1)-X(J+K))**2)
      YCONP=-(SXP-X(J+K))*SIN(PHI)+(SYP-Y(J+K))*COS(PHI)
      XCONP=(SXP-X(J+K))*COS(PHI)+(SYP-Y(J+K))*SIN(PHI)
      R1=SQRT(XCONP**2+YCONP**2)
      R2=SQRT((XCONP-SL)**2+YCONP**2)
      DCP=1.
      IF(YCONP.LT.0.) DCP=-1.
      TETA1=ATAN2(ABS(YCONP),XCONP)
      IF(TETA1.LT.0.) TETA1=TETA1+2.*3.14159266
      TETA2=ATAN2(ABS(YCONP),(XCONP-SL))
      IF(TETA2.LT.0.) TETA2=TETA2+2.*3.14159266
      IK=2
      GOTO 5
```

```
    4 CONTINUE
      IF(J.EQ.2) GOTO 8
      IF(J.EQ.NC2) GOTO 9
      IF(J.EQ.N2) GOTO 9
      UU=(YCONP*ALOG(R2/R1)-XCONP*DCP*(TETA1-TETA2))/SL
      VV=1.+(ABS(YCONP)*(TETA1-TETA2)+XCONP*ALOG(R2/R1))/SL
      GOTO 11
    8 CONTINUE
      IF(XP(I).LT.X(2)) GOTO 12
      IEQ=1
      CALL XINT(IEQ,XP,YP,X,Y,I,J,SL,APHI,VV)
      VV=-VV
      IEQ=2
      CALL XINT(IEQ,XP,YP,X,Y,I,J,SL,APHI,UU)
      GOTO 11
   12 CONTINUE
      IEQ=3
      CALL XINT(IEQ,XP,YP,X,Y,I,J,SL,APHI,VV)
      VV=-VV
      UU=0.
      GOTO 11
    9 CONTINUE
      XP(I)=XCONP
      YP(I)=YCONP
      APHI=ABS(PHI)
      IF(J.EQ.NC2) GOTO 10
      L=J+1
      IF(I.EQ.N1) GOTO 14
      GOTO 15
   10 CONTINUE
      L=J
      IF(I.EQ.NC1) GOTO 14
   15 CONTINUE
      IEQ=7
      CALL XINT(IEQ,XP,YP,X,Y,I,L,SL,APHI,VV)
      VV=-VV
      IEQ=8
      CALL XINT(IEQ,XP,YP,X,Y,I,L,SL,APHI,UU)
      XP(I)=SXP
      YP(I)=SYP
      GOTO 11
   14 CONTINUE
      IEQ=9
      CALL XINT(IEQ,XP,YP,X,Y,I,L,SL,APHI,VV)
      VV=-VV
      UU=0.
      XP(I)=SXP
      YP(I)=SYP
   11 CONTINUE
      U1=UU*COS(PHI)-VV*SIN(PHI)
```

```
      V1=UU*SIN(PHI)+VV*COS(PHI)
      IF(ITR.GT.1) GOTO 18
      IF(J.EQ.NC1.AND.I.LE.NC) SU1(I)=U1
      IF(J.EQ.NC1.AND.I.LE.NC) SV1(I)=V1
   18 CONTINUE
      IK=1
      GOTO 3
    5 CONTINUE
      IF(J.NE.NC) GOTO 19
      IF(I.EQ.NC) GOTO 16
      IEQ=4
      CALL XINT(IEQ,XP,YP,X,Y,I,J,SL,APHI,VV)
      VV=-VV
      IEQ=5
      CALL XINT(IEQ,XP,YP,X,Y,I,J,SL,APHI,UU)
      GOTO 17
   16 CONTINUE
      IEQ=6
      CALL XINT(IEQ,XP,YP,X,Y,I,J,SL,APHI,VV)
      VV=-VV
      UU=0.
      GOTO 17
   19 CONTINUE
      PSI1=ATAN2(YCONP,XCONP)
      IF(PSI1.LT.0.) PSI1=PSI1+2.*3.14159266
      PSI2=ATAN2(YCONP,(XCONP-SL))
      IF(PSI2.LT.0.) PSI2=PSI2+2.*3.14159266
      UU=PSI2-PSI1+(XCONP*DCP*(TETA1-TETA2)-
     CYCONP*ALOG(R2/R1))/SL
      VV=(1.-XCONP/SL)*ALOG(R2/R1)-1.-ABS(YCONP)
     C*(TETA1-TETA2)/SL
   17 CONTINUE
      U2=UU*COS(PHI)-VV*SIN(PHI)
      V2=UU*SIN(PHI)+VV*COS(PHI)
      IF(J.EQ.NC1.AND.I.LE.NC) U1=SU1(I)
      IF(J.EQ.NC1.AND.I.LE.NC) V1=SV1(I)
      IF(J.EQ.N1) V1=0.
      IF(J.EQ.N1) U1=0.
      IF(J.EQ.1) U1=0.
      IF(J.EQ.1) V1=0.
      U=U1+U2
      V=V1+V2
      A(I,J)=V-U*SLOPE(I)
      IF(J.LE.NC) GOTO 20
      UG=PSI2-PSI1
      VG=ALOG(R2/R1)
      IF(J.GT.N) VG=-VG
      IF(J.GT.N) UG=-UG
      UGAMA=UG*COS(PHI)-VG*SIN(PHI)+UGAMA
      VGAMA=UG*SIN(PHI)+VG*COS(PHI)+VGAMA
```

```
   20 CONTINUE
      IF(I.GT.NC) GOTO 2
      IF(J.GT.NC) GOTO 2
      AS(I,J)=A(I,J)
    2 CONTINUE
      R1=((XP(I)-X(N2))**2+(YP(I)-Y(N2))**2)**.5
      R2=((XP(I)-X(NC1))**2+(YP(I)-Y(NC1))**2)**.5
      XP(I)=(SXP-X(NC1))*COS(TAU)+(SYP-Y(NC1))*SIN(TAU)
      YP(I)=-(SXP-X(NC1))*SIN(TAU)+(SYP-Y(NC1))*COS(TAU)
      T1=1.57079-ATAN2((YP(I)-DEL),XP(I))
      IF(T1.LT.0.) T1=2.*3.14159+T1
      T2=1.57079-ATAN2(YP(I),XP(I))
      IF(T2.LT.0.) T2=3.14159*2+T2
      XP(I)=SXP
      YP(I)=SYP
      US=(T1-T2)*COS(TAU)+ALOG(R2/R1)*SIN(-TAU)
      VS=-(T1-T2)*SIN(-TAU)+ALOG(R2/R1)*COS(TAU)
      US=US*Q
      VS=VS*Q
      B(I)=-VS+SLOPE(I)*US-(SIN(ALPHA)-COS(ALPHA)*SLOPE(I))
     C*2*3.14159
      RR1=((XP(I)-X(NT2))**2+(YP(I)-Y(NT2))**2)**.5
      RR2=((XP(I)-X(N1))**2+(YP(I)-Y(N1))**2)**.5
      PP1=ATAN2((YP(I)-Y(NT2)),(XP(I)-X(NT2)))
      IF(PP1.LT.0.) PP1=2.*3.1415926+PP1
      PP2=ATAN2((YP(I)-Y(N1)),(XP(I)-X(N1)))
      IF(PP2.LT.0.) PP2=2.*3.1415926+PP2
      VSINF=(PP1-PP2)*SIN(ALPHA)+ALOG(RR1/RR2)*COS(ALPHA)
      USINF=(PP1-PP2)*COS(ALPHA)-ALOG(RR1/RR2)*SIN(ALPHA)
      B(I)=B(I)-(VSINF-USINF*SLOPE(I))*Q
      B(I)=B(I)-(VGAMA-UGAMA*SLOPE(I))*Q
    1 CONTINUE
C---  SOLUTION OF THE SET OF LINEAR EQUATIONS
      CALL LNEQNS(A,60,60,NT,B,IW1,IW2,IER)
C---  LIFT COEFFICIENT
C--
      XLC=0.
      DO 230 I=1,NT
      IF(I.EQ.1) GOTO 231
      IF(I.EQ.NC) GOTO 232
      IF(I.EQ.NC1) GOTO 233
      IF(I.EQ.N) GOTO 236
      IF(I.EQ.NT) GOTO 236
      IF(I.GT.N) GOTO 234
      XLC=XLC+(B(I+1)+B(I))*(X(I+1)-X(I))/2.
      GOTO 230
  231 CONTINUE
      XLC=XLC+B(I)*(X(I+1)-X(I))/2.-2.*B(I+1)*X(I+1)**1.5
     C*(ALOG((1+X(I+1)**.5)/(1-X(I+1)**.5))+
     CALOG(1-X(I+1))/X(I+1)**.5)/ALOG(1-X(I+1))
```

```
           SL1=XLC
           GOTO 230
     232   CONTINUE
           SXLC=XLC
           XLC=XLC+B(NC1)*(X(NC1)-X(NC))/2.-2.*B(NC)*X(NC)**1.5
          C*(2.*ALOG(2.)-ALOG((1+X(NC)**.5)/
          C(1-X(NC)**.5))-ALOG(1-X(NC))/X(NC)**.5)/ALOG(1-X(NC))
           XLCC=XLC*2.
           SLNC=XLC-SXIC
           GOTO 230
     233   CONTINUE
           SXLC=XLC
           XLC=XLC+B(NC1)*(X(NC2)-X(NC1))/2.+B(NC2)*X(NC2)**1.5*(2
          C*(1-
          C1/X(NC2)**.5)*ALOG(X(NC2)**.5-1)-2*(1+1/X(NC2)**.5)*
          CALOG(X(NC2)**.5+1)+4.*ALOG(2.))/ALOG(X(NC2)-1.)
           SAL=XLC-SXLC
           GOTO 230
     234   CONTINUE
           IF(I.EQ.N1) GOTO 235
           XLC=XLC+(B(I+1)+B(I))*(X(I+2)-X(I+1))/2.
           GOTO 230
     235   CONTINUE
           SXLC=XLC
           XLC=XLC+B(N1)*(X(N3)-X(N2))/2.+(2.*(1./X(N2)**.5-
          C1./X(N3)**.5)*ALOG(X(N3)**.5-X(N2)**.5)-
          C2.*(1./X(N2)**.5+1./X(N3)**.5)*ALOG(X(N3)**.5+
          CX(N2)**.5)+4.*ALOG(2.*X(N2)**.5)/X(N2)**.5)
          C*B(N2)*X(N3)**1.5/ALOG(X(N3)-X(N2))
           SAU=XLC-SXLC
           GOTO 230
     236   CONTINUE
           J=I
           IF(I.EQ.NT) J=I+1
           XLC=B(I)*(X(J+1)-X(J))/2.+XLC
     230   CONTINUE
           XLC=XLC*2.
           XLCJ=XLC-XLCC
     C---
     C---  OUTPUTS
     C---
           PRINT,'NUMBER OF ITERATIONS'
           PRINT 54, ITR
     54    FORMAT(5X,I4)
           PRINT,'ANGLE OF ATTACK IN DEGREE'
           PRINT 53,ALFAD
     53    FORMAT(F10.3)
           PRINT,'INITIAL JET DEFLECTICN ANGLE IN DEGREE'
           PRINT 53, TAUD
           PRINT,'POWER JET MOMENTUM CCEFFICIENT'
```

```
          PRINT 53,CPJ
          PRINT,'TOTAL JET MOMENTUM COEFFICIENT'
          PRINT 53,CJ
          PRINT,'X CENTER'
          PRINT 52,(XC(I),I=1,NJ1)
          PRINT,'Y CENTER'
          PRINT 52,(YC(I),I=1,NJ1)
          PRINT,'X COORDINATES OF CONTROL POINTS'
          PRINT 52, (XP(I),I=1,NT)
          PRINT,'Y COORDINATES OF CONTROL POINTS'
          PRINT 52, (YP(I),I=1,NT)
          PRINT,'X COORDINATES OF DIVISION POINTS'
          PRINT 52,(X(I),I=1,NT2)
          PRINT,'Y COORDINATES OF DIVISION POINTS'
          PRINT 52, (Y(I),I=1,NT2)
          PRINT,'VORTEX DISTRIBUTION'
          PRINT 52,(B(I),I=1,NT)
    52    FORMAT(10F10.6)
          PRINT,'LIFT COEFFICIENT'
          PRINT 53,XLC
          PRINT,'JET LIFT COEFFICIENT'
          PRINT 53,XLCJ
          GOTO 99
    227   CONTINUE
          IF(INP.LT.61) GOTO 444
    448   CONTINUE
          STOP
          END
          INTEGRATION USING GAUSSIAN QUADRATURE
          SUBROUTINE XINT(IEQ,XP,YP,X,Y,I,J,SL,APHI,VEL)
          DIMENSION X(60),Y(60),XP(60),YP(60)
          N=24
          NC=10
          N2=N+2
          NC2=NC+2
          G=1.
          IF(J.NE.NC2)G=X(N2)
          IF(IEQ.GT.6) GOTO 421
          IF(IEQ.LT.7.AND.IEQ.GT.3) GOTO 420
          XU=X(J)
          XL=X(J-1)
          GOTO 401
    420   CONTINUE
          XU=X(J+1)
          XL=X(J)
          GOTO 401
    421   CONTINUE
          XU=SL
          XL=0.
    401   CONTINUE
```

```
      A=.5*(XU+XL)
      BB=XU-XL
      C=.4869533*BB
      T=.03333567*(F(IEQ,XP,YP,I,J,X,APHI,A+C)
     C+F(IEQ,XP,YP,I,J,X,APHI,A-C))
      C=.4325317*BB
      T=T+.07472567*(F(IEQ,XP,YP,I,J,X,APHI,A+C)
     C+F(IEQ,XP,YP,I,J,X,APHI,A-C))
      C=.3397048*BB
      T=T+.1095432*(F(IEQ,XP,YP,I,J,X,APHI,A+C)
     C+F(IEQ,XP,YP,I,J,X,APHI,A-C))
      C=.2166977*BB
      T=T+.1346334*(F(IEQ,XP,YP,I,J,X,APHI,A+C)
     C+F(IEQ,XP,YP,I,J,X,APHI,A-C))
      C=.07443717*BB
      T=BB*(T+.1477621*(F(IEQ,XP,YP,I,J,X,APHI,A+C)
     C+F(IEQ,XP,YP,I,J,X,APHI,A-C)))
      GOTO (403,404,405,406,407,408,410,411,412),IEQ
  403 VEL=(T-2.*XP(I)*(ALOG((1.+X(J+0)**.5)/(1.-X(J+0)**.5))+
     CALOG(1.-X(J+0))/X(J+0)**.5)/(XP(I)**2+YP(I)**2))*
     CX(J+0)**1.5/ALOG(1.-X(J+0))
      GOTO 409
  404 VEL=(T-2.*YP(I)*(ALOG((1.+X(J+0)**.5)/(1.-X(J+0)**.5))+
     CALOG(1.-X(J+0))/X(J+0)**.5)/(XP(I)**2+YP(I)**2))*
     CX(J+0)**1.5/ALOG(1.-X(J+0))
      GOTO 409
  405 VEL=T-2.*(ALOG((1+X(J+0)**.5)/(1-X(J+0)**.5))+
     CALOG(1-X(J+0))/X(J+0)**.5)/XP(I)+ALOG(1-XP(I))*
     CALOG(XP(I)/(X(J+0)-XP(I)))/XP(I)**1.5
      VEL=VEL*X(J+0)**1.5/ALOG(1.-X(J+0))
      GOTO 409
  406 VEL=(T+(XP(I)-1.)*
     C((1.-X(J+0))*ALOG(1.-X(J+0))+X(J+0)-1.)/((XP(I)-1.)**2
     C+YP(I)**2))*X(J+0)**1.5/ALOG(1.-X(J+0))
      GOTO 409
  407 VEL=(T+YP(I)*
     C((1.-X(J+0))*ALOG(1.-X(J+0))+X(J+0)-1.)/((XP(I)-1.)**2
     C+YP(I)**2))*X(J+0)**1.5/ALOG(1.-X(J+0))
      GOTO 409
  408 VEL=T+(1.-X(J+0))*(ALOG(1.-X(J+0))-1.)/(XP(I)-1)+
     CALOG(1.-XP(I))*ALOG((XP(I)-X(J+0))/(1-XP(I)))
     C/XP(I)**1.5
      VEL=VEL*X(J+0)**1.5/ALOG(1.-X(J+0))
      GOTO 409
  410 VEL=(T+XP(I)*SL*(ALOG(SL*COS(APHI))-1)/((XP(I)**2+YP(I)
     C**2)*G**1.5))*X(J)**1.5/ALOG(X(J)-G)
      GOTO 409
  411 VEL=(T+YP(I)*SL*(ALOG(SL*COS(APHI))-1)/((XP(I)**2+YP(I)
     C**2)*G**1.5))*X(J)**1.5/ALOG(X(J)-G)
      GOTO 409
```

```
412   VEL=T+SL*(AIOG(SL*COS(APHI))-1.)/(XP(I)*G**1.5)+
     CALOG(XP(I)*COS(APHI))*ALOG(XP(I)/(SL-XP(I)))/
     C(XP(I)*COS(APHI)+G)**1.5
      VEL=VEL*X(J+0)**1.5/ALOG(X(J+0)-G)
409   CONTINUE
      RETURN
      END

      FUNCTION F(IEQ,XP,YP,I,J,X,APHI,S)
      DIMENSION X(60),XP(60),YP(6C)
      N=24
      NC=10
      N2=N+2
      NC2=NC+2
      G=1.
      IF(J.NE.NC2)G=X(N2)
      GOTO (1,2,3,4,5,6,7,8,9),IEQ
1     F=ALOG(1.-S)*(XP(I)-S)/(S**1.5*((XP(I)-S)**2+YP(I)**2))
     C-ALOG(1.-S)*XP(I)/(S**1.5*(XP(I)**2+YP(I)**2))
      GOTO 10
2     F=ALOG(1.-S)*YP(I)/(S**1.5*((XP(I)-S)**2+YP(I)**2))-
     CALOG(1.-S)*YP(I)/(S**1.5*(XP(I)**2+YP(I)**2))
      GOTO 10
3     F=ALOG(1.-S)/(S**1.5*(XP(I)-S))-ALOG(1.-S)/
     C(XP(I)*S**1.5)-ALOG(1.-XP(I))/(XP(I)**1.5*(XP(I)-S))
      GOTO 10
4     F=ALOG(1.-S)*(XP(I)-S)/(S**1.5*((XP(I)-S)**2+YP(I)**2))
     C-ALOG(1.-S)*(XP(I)-1.)/((XP(I)-1.)**2+YP(I)**2)
      GOTO 10
5     F=ALOG(1.-S)*YP(I)/(S**1.5*((XP(I)-S)**2+YP(I)**2))-
     CALOG(1.-S)*YP(I)/((XP(I)-1.)**2+YP(I)**2)
      GOTO 10
6     F=ALOG(1.-S)/(S**1.5*(XP(I)-S))-ALCG(1.-S)/(XP(I)-1.)-
     CALOG(1.-XP(I))/(XP(I)**1.5*(XP(I)-S))
      GOTO 10
7     F=ALOG(S*COS(APHI))*(XP(I)-S)/
     C((S*COS(APHI)+G)**1.5*((XP(I)-S)**2+YP(I)**2))
     C-ALOG(S*COS(APHI))*XP(I)/((XP(I)**2+YP(I)**2)*G**1.5)
      GOTO 10
8     F=ALOG(S*COS(APHI))*YP(I)/
     C((S*COS(APHI)+G)**1.5*((XP(I)-S)**2+YP(I)**2))
     C-ALOG(S*COS(APHI))*YP(I)/((XP(I)**2+YP(I)**2)*G**1.5)
      GOTO 10
9     F=ALOG(S*COS(APHI))/((S*COS(APHI)+G)**1.5*(XP(I)-S))
     C-ALOG(S*COS(APHI))/(XP(I)*G**1.5)-ALOG(XP(I)*COS(APHI))/
     C((XP(I)*COS(APHI)+G)**1.5*(XP(I)-S))
10    CONTINUE
      RETURN
      END
```

```
 SUBROUTINELNEQNS(A,IA,JA,MA,W,IR,IC,IER);DIMENSIONA(IA,JA),W(MA),I
*R(MA),IC(MA);IER=0;R=MA;S=0.;DET=1.0;DO2K=1,MA;IR(K)=0;2:IC(K)=0
  CALLSUBMXS(A,IA,JA,MA,MA,IR,IC,I,J);PIV=A(I,J);DET=PIV*DET;IF(PIV
*.EQ.0.0)GOTO16;IR(I)=J;IC(J)=I;PIV=1.0/PIV;DO6K=1,MA;6:A(I,K)=A(I,
*K)*PIV;W(I)=W(I)*PIV;DO10L=1,MA;IF(IC(L).NE.0)GOTO10;PIV1=A(I,L);D
*O9K=1,MA;9:IF(K.NE.I)A(K,L)=A(K,L)-PIV1*A(K,J);10:CONTINUE;PIV2=W(
*I);DO12K=1,MA;12:IF(K.NE.I)W(K)=W(K)-PIV2*A(K,J);S=S+1.;IF(S.LT.R)
*GOTO3;DO15J=1,MA;K=IC(J);L=IR(J);IF(K.EQ.J)GOTO15;TEMP=W(J);W(J)=W
*(K);W(K)=TEMP;IC(L)=K;IR(K)=L;DET=-DET;15:CONTINUE;16:A(1,1)=DET;I
*F(DET.EQ.0.0)IER=1;RETURN;END
```

APPENDIX L

COMPUTER PROGRAM FOR THE SOLUTION OF THE NON-UNIFORM JET

```
$JOB    WATFIV    TANG,TIME=120,LIBLIST,LINES=50
         DIMENSION X(60),Y(60),XP(60),YP(60),SLOPE(60),
        CB(60),A(60,60),IW1(60),IW2(60),YOLD(60),YMAX(60),YMIN(60)
        C,G(60),XC(60),YC(60),XK(60),AS(60,60),SU1(60),SV1(60),
        CVI(60,60),UI(60,60),UO2(60),VO2(60),UJT1(60),UJT2(60),
        CUJT3(60),UJT4(60),VJT1(60),VJT2(60),VJT3(60),VJT4(60)
         REAL KEP
C---
C---     INITIAL CONDITIONS
C---
         ALPHA=0.
         TAU=-3.14159266/6.
         DEL=0.09
         CPJ=1.75
C---     RADEL        THICKNESS RATIO
         RADEL=0.5
C---     DEL1         THICKNESS OF LOWER LAYER OF THE JET
         DEL1=RADEL*DEL
C---     RAQ          VELOCITY RATIO (Q-UP / Q-LOW)
         RAQ=0.9
         CHORD=1.
C        INCREMENTS IN VARIABLES
         DALFA=0.
         DCPJ=0.
         DTAU=0.
         DDEL=0.
         INP=0
444      CONTINUE
         INP=INP+1
         CPJ=CPJ+DCPJ
         ALPHA=ALPHA+DALFA
         TAU=TAU+DTAU
         DEL=DEL+DDEL
C---     AUGMENTED JET MOMENTUM COEFFICIENT AND PRIMARY JET VELOCITY
         CJ=(SQRT(2.*DEL/CHORD)+SQRT(CPJ))**2
         Q=SQRT(CJ*CHORD/(2.*DEL))-1.
         Q2=Q/(RADEL+RAQ**2*(1-RADEL))**.5
         Q1=RAQ*Q2
         DELH=DEL/2
         ALFAD=ALPHA*180./3.14159266
         TAUD=TAU*180./3.14159266
         IF(INP.GT.1) GOTO 445
C---
C___     INPUT DATA
         EPS=0.03
         MAXIT=6
C---     DF          DAMPING FACTOR
         DF=0.15
         ERMAX=0.1
C---
```

```
C     NTT    TOTAL NUMBER OF FINITE VORTEX SEGMENTS
      NTT=46
      NTT3=NTT+3
      NTM1=NTT-1
      N=22
      NC=10
      NJ=N-NC
      NT=N+NJ
      NT3=NT+3
      NT4=NT+4
      NT1=NT+1
      NT2=NT+2
      NL2=N-2
      NC1=NC+1
      NC2=NC+2
      NCL1=NC-1
      NCL2=NC-2
      NTC=NT-NC
      NJ1=NJ+1
      NJL1=NJ-1
      N1=N+1
      N2=N+2
      N3=N+3
C---  X AND Y COORDINATES OF SEGMENT END POINTS ON THE AEROFOIL
      DO 23 I=1,NC1
      Y(I)=0.
      ARG=3.1415926*(I-1.)/NC
      X(I)=0.5*(1.-COS(ARG))
   23 CONTINUE
      X(NC1)=1.
C---  READ X AND Y COORDINATES OF VORTEX SEGMENT END POINTS
C---  ON THE LOWER JET BOUNDARY
      READ(5,21) (X(I),I=NC2,N1)
      READ(5,21) (Y(I),I=NC2,N1)
   21 FORMAT(6F10.6)
      X(N2)=-DEL1*SIN(TAU)+X(NC1)
      Y(N2)=DEL1*COS(TAU)+Y(NC1)
C---  X AND Y COORDINATES OF VORTEX SEGMENT END POINTS ON THE UPPER
C---  JET BOUNDARY AND JET CENTER LINE
      DO 60 I=1,NJ
      TSG1=ATAN2((Y(I+NC)-Y(I+NC1)),(X(I+NC)-X(I+NC1)))
      IF(I.EQ.NJ) GOTO 61
      TSG2=ATAN2((Y(I+NC2)-Y(I+NC1)),(X(I+NC2)-X(I+NC1)))
   61 CONTINUE
      IF(I.EQ.NJ) TSG2=ALPHA
      THALF=(TSG1-TSG2)/2.
      PSG=(TSG1+TSG2)/2.
      X(I+N2)=X(I+NC1)+DEL1*COS(PSG)/SIN(THALF)
      Y(I+N2)=Y(I+NC1)+DEL1*SIN(PSG)/SIN(THALF)
   60 CONTINUE
```

```
      DO 260 I=1,NJ1
      X(I+NT2)=X(I+NC)+(X(I+N1)-X(I+NC))/RADEL
      Y(I+NT2)=Y(I+NC)+(Y(I+N1)-Y(I+NC))/RADEL
      YC(I)=(Y(I+NT2)+Y(I+NC))/2.
      YOLD(I)=YC(I)
      XC(I)=(X(I+NT2)+X(I+NC))/2.
  260 CONTINUE
      DO 24 I=1,NC
      XP(I)=(X(I+1)+X(I))/2.
      YP(I)=(Y(I+1)+Y(I))/2.
      SLOPE(I)=(Y(I+1)-Y(I))/(X(I+1)-X(I))
   24 CONTINUE
C---
C---  STARTING ITERATION PROCESS
C---
  445 CONTINUE
      MAXD=1
      ITR=0
   99 ITR=ITR+1
      IF(ITR.EQ.1.AND.INP.EQ.1) GOTO 224
      IF(ITR.NE.1) GOTO 115
      SXN2=X(N2)
      SYN2=Y(N2)
      X(N2)=-DEL*SIN(TAU)+X(NC1)
      Y(N2)=DEL*COS(TAU)+Y(NC1)
      XC(1)=(X(N2)+X(NC1))/2.
      YC(1)=(Y(N2)+Y(NC1))/2.
      IF(DTAU.NE.0.) GOTO 451
      DO 450 I=2,NJ1
      XC(I)=-DDEL*SIN(TAU)/2.+XC(I)
      YC(I)=DDEL*COS(TAU)/2.+YOLD(I)
      YOLD(I)=YC(I)
  450 CONTINUE
      GOTO 107
  451 CONTINUE
      DXTAU=(X(N2)-SXN2)/2.
      DYTAU=(Y(N2)-SYN2)/2.
      DO 452 I=2,NJ1
      XC(I)=XC(I)+DXTAU
      YC(I)=YOLD(I)+DYTAU
      YOLD(I)=YC(I)
  452 CONTINUE
      GOTO 107
  115 CONTINUE
C---
C---  JET SHAPE CALCULATION
C---
      DO 323 I=NC1,NTT
      SVI=0.
      SUI=0.
```

```
      DO 324 J=1,NTT
      SVI=SVI+VI(I,J)*B(J)/(2.*3.14159266)
      SUI=SUI+UI(I,J)*B(J)/(2.*3.14159266)
  324 CONTINUE
      K=0
      IF(I.GT.N) K=1
      IF(I.GT.NT) K=2
      PHI=ATAN2((Y(I+K+1)-Y(I+K)),(X(I+K+1)-X(I+K)))
      IF(I.GT.NC1) GOTO 325
      GI=SAL/((X(NC2)-X(NC1))*2.)
      GOTO 326
  325 CONTINUE
      IF(I.EQ.NT1) GOTO 255
      IF(I.EQ.N1) GOTO 327
      IF(I.EQ.N) GOTO 328
      IF(I.EQ.NT) GOTO 328
      IF(I.EQ.NTT) GOTO 328
      GI=(B(I+1)+B(I))/4.
      GOTO 326
  328 CONTINUE
      GI=B(I) /4.
      GOTO 326
  327 CONTINUE
      GI=SAU/((X(N3)-X(N2))*2.)
      GOTO 326
  255 CONTINUE
      GI=SAU3/((X(NT4)-X(NT3))*2.)
  326 CONTINUE
      UQ1=(Q2-Q1)*COS(PHI)/2.
      VQ1=(Q2-Q1)*SIN(PHI)/2.
      UQ2=Q1*COS(PHI)/2.
      VQ2=Q1*SIN(PHI)/2.
      UQ3=-Q2*COS(PHI)/2.
      VQ3=-Q2*SIN(PHI)/2.
      IF(I.GT.N) GOTO 239
      UO2(I)=UO2(I)+SUI-GI*COS(PHI)-UQ2+COS(ALPHA)
      VO2(I)=VO2(I)+SVI-GI*SIN(PHI)-VQ2+SIN(ALPHA)
      UJT4(I)=UO2(I)+2.*(GI*COS(PHI)+UQ2)
      VJT4(I)=VO2(I)+2.*(GI*SIN(PHI)+VQ2)
      GOTO 323
  239 CONTINUE
      IF(I.GT.NT) GOTO 256
      UJT3(I)=UO2(I)+SUI-GI*COS(PHI)-UQ1+COS(ALPHA)
      VJT3(I)=VO2(I)+SVI-GI*SIN(PHI)-VQ1+SIN(ALPHA)
      UJT2(I)=UJT3(I)+2.*(GI*COS(PHI)+UQ1)
      VJT2(I)=VJT3(I)+2.*(GI*SIN(PHI)+VQ1)
      GOTO 323
  256 CONTINUE
      UJT1(I)=UO2(I)+SUI-GI*COS(PHI)-UQ3+COS(ALPHA)
      VJT1(I)=VO2(I)+SVI-GI*SIN(PHI)-VQ3+SIN(ALPHA)
```

```
       UO2(I)=UJT1(I)+2.*(GI*COS(PHI)+UQ3)
       VO2(I)=VJT1(I)+2.*(GI*SIN(PHI)+VQ3)
 323   CONTINUE
       B(NT1)=0.
       G(1)=TAN(TAU)
       DO 220 I=1,NJ
       ULS=UO2(I+NC)**2+VO2(I+NC)**2
       UUS=UO2(I+NT)**2+VO2(I+NT)**2
       UL=ULS**.5
       UU=UUS**.5
       VONE=(UJT1(I+NT)**2+VJT1(I+NT)**2)**.5
       VTWO=(UJT2(I+N)**2+VJT2(I+N)**2)**.5
       VTHR=(UJT3(I+N)**2+VJT3(I+N)**2)**.5
       VFOR=(UJT4(I+NC)**2+VJT4(I+NC)**2)**.5
       KEP=VTHR/VTWO
       PRINT 380,UL,UU,VONE,VTWO,VTHR,VFOR
 380   FORMAT(F10.3,5X,F10.3,5X,F10.3,5X,F10.3,5X,F10.3,5X,
      CF10.3)
       XK(I)=2.*(UUS-ULS+(KEP**2-1.)*(VONE**2
      C-VTWO**2))/(DEL*(KEP*VONE+VFOR)**2)
       C1=G(I)/(1.+G(I)**2)**0.5-XK(I)*XC(I)
       G(I+1)=(XK(I)*XC(I+1)+C1)/(1.-(XK(I)*XC(I+1)
      C+C1)**2)**.5
 381   CONTINUE
       C2=YC(I)+(1.-(XK(I)*XC(I)+C1)**2)**.5/XK(I)
       YC(I+1)=-(1.-(XK(I)*XC(I+1)+C1)**2)**.5/XK(I)+C2
 220   CONTINUE
       PRINT,'JET SHAPE CALCULATED DIRECTLY FROM GAMA DISTRIBUTION'
       PRINT 52,(YC(I),I=1,NJ1)
C---
C---   EXIT CRITERIA
C---
       DO 225 I=2,NJ1
       DISP=ABS(YOLD(I)-YC(I))
       IF(I.EQ.2) GOTO 226
       IF(DD.LT.DISP) DD=DISP
       GOTO 225
 226   CONTINUE
       DD=DISP
 225   CONTINUE
       PRINT,'JET DEVIATION'
       PRINT 55,DD
 55    FORMAT(F10.3////)
       IF(DD.LT.EPS) GOTO 227
       IF(DD.LT.ERMAX) MAXD=2
       IF(ITR.LE.MAXIT) GOTO 449
       IF(MAXD.EQ.2) GOTO 227
       GOTO 448
C
C---   CONVERGENCE SCHEME
```

```
C
  449  CONTINUE
       DO 72 I=2,NJ1
       YC(I)=YOLD(I)+DF*(YC(I)-YOLD(I))
   72  YOLD(I)=YC(I)
C
C
C---   X AND Y COORDINATES OF THE FINITE VORTEX SEGMENT END POINTS
C---   ON THE JET BOUNDARIES
  107  CONTINUE
       DO 202 I=1,NJ
       TSG1=ATAN2((YC(I)-YC(I+1)),(XC(I)-XC(I+1)))
       IF(I.EQ.NJ) GOTO 203
       TSG2=ATAN2((YC(I+2)-YC(I+1)),(XC(I+2)-XC(I+1)))
  203  CONTINUE
       IF(I.EQ.NJ) TSG2=ALPHA
       THALF=(TSG1-TSG2)/2.
       PSG=(TSG1+TSG2)/2.
       X(I+NT3)=XC(I+1)+DELH*COS(PSG)/SIN(THALF)
       Y(I+NT3)=YC(I+1)+DELH*SIN(PSG)/SIN(THALF)
       X(I+NC1)=2.*XC(I+1)-X(I+NT3)
       Y(I+NC1)=2.*YC(I+1)-Y(I+NT3)
       X(I+N2)=(X(I+NT3)-X(I+NC1))*RADEL+X(I+NC1)
       Y(I+N2)=(Y(I+NT3)-Y(I+NC1))*RADEL+Y(I+NC1)
  202  CONTINUE
  224  CONTINUE
       KP=1
       DO 228 I=NC1,NTT
       IF(I.GT.N) KP=2
       IF(I.GT.NT) KP=3
       XP(I)=(X(I+KP)+X(I+KP-1))/2.
       YP(I)=(Y(I+KP)+Y(I+KP-1))/2.
       SLOPE(I)=(Y(I+KP)-Y(I+KP-1))/(X(I+KP)-X(I+KP-1))
  228  CONTINUE
C---
C---   COEFFICIENT MATRIX
C---
       DO 1 I=1,NTT
       UL1=0.
       VL1=0.
       UJU1=0.
       VJU1=0.
       UGAMA=0.
       VGAMA=0.
       SYP=YP(I)
       SXP=XP(I)
       IK=1
       DO 2 J=1,NTT
       IF(ITR.EQ.1) GOTO 3
       IF(I.GT.NC) GOTO 3
```

```
      IF(J.GT.NC) GOTO 3
      A(I,J)=AS(I,J)
      GOTO 2
    3 CONTINUE
      IF(J.EQ.N1) IK=1
      IF(J.EQ.NT1) IK=1
      IF(IK.EQ.2) GOTO 4
      K=0
      IF(J.GT.N.AND.J.LE.NT) K=1
      IF(J.GT.NT) K=2
      K1=K+1
      PHI=ATAN2((Y(J+K1)-Y(J+K)),(X(J+K1)-X(J+K)))
      SL=SQRT((Y(J+K1)-Y(J+K))**2+(X(J+K1)-X(J+K))**2)
      YCONP=-(SXP-X(J+K))*SIN(PHI)+(SYP-Y(J+K))*COS(PHI)
      XCONP=(SXP-X(J+K))*COS(PHI)+(SYP-Y(J+K))*SIN(PHI)
      R1=SQRT(XCONP**2+YCONP**2)
      R2=SQRT((XCONP-SL)**2+YCONP**2)
      DCP=1.
      IF(YCONP.LT.0.) DCP=-1.
      TETA1=ATAN2(ABS(YCONP),XCONP)
      IF(TETA1.LT.0.) TETA1=TETA1+2.*3.14159266
      TETA2=ATAN2(ABS(YCONP),(XCONP-SL))
      IF(TETA2.LT.0.) TETA2=TETA2+2.*3.14159266
      IK=2
      GOTO 5
    4 CONTINUE
      IF(J.EQ.2) GOTO 8
      IF(J.EQ.NC2) GOTO 9
      IF(J.EQ.N2) GOTO 9
      IF(J.EQ.NT2) GOTO 9
      UU=(YCONP*ALOG(R2/R1)-XCONP*DCP*(TETA1-TETA2))/SL
      VV=1.+(ABS(YCONP)*(TETA1-TETA2)+XCONP*ALOG(R2/R1))/SL
      IF(I+1.EQ.J) UU=0.
      GOTO 11
    8 CONTINUE
      IF(XP(I).LT.X(2)) GOTO 12
      IEQ=1
      CALL XINT(IEQ,XP,YP,X,Y,I,J,SL,APHI,VV)
      VV=-VV
      IEQ=2
      CALL XINT(IEQ,XP,YP,X,Y,I,J,SL,APHI,UU)
      GOTO 11
   12 CONTINUE
      IEQ=3
      CALL XINT(IEQ,XP,YP,X,Y,I,J,SL,APHI,VV)
      VV=-VV
      UU=0.
      GOTO 11
    9 CONTINUE
      XP(I)=XCONP
```

```
      YP(I)=YCCNP
      APHI=ABS(PHI)
      IF(J.EQ.NC2) GOTO 10
      IF(J.EQ.N2) GOTC 250
      L=J+2
      IF(I.EQ.NT1) GOTO 14
      GOTO 15
250   CONTINUE
      L=J+1
      IF(I.EQ.N1) GOTO 14
      GOTO 15
10    CONTINUE
      L=J
      IF(I.EQ.NC1) GOTO 14
15    CONTINUE
      IEQ=7
      CALL XINT(IEQ,XP,YP,X,Y,I,L,SL,APHI,VV)
      VV=-VV
      IEQ=8
      CALL XINT(IEQ,XP,YP,X,Y,I,L,SL,APHI,UU)
      XP(I)=SXP
      YP(I)=SYP
      GOTO 11
14    CONTINUE
      IEQ=9
      CALL XINT(IEQ,XP,YP,X,Y,I,L,SL,APHI,VV)
      VV=-VV
      UU=0.
      XP(I)=SXP
      YP(I)=SYP
11    CONTINUE
      U1=UU*COS(PHI)-VV*SIN(PHI)
      V1=UU*SIN(PHI)+VV*COS(PHI)
      IF(ITR.GT.1) GOTO 18
      IF(J.EQ.NC1.AND.I.LE.NC) SU1(I)=U1
      IF(J.EQ.NC1.AND.I.LE.NC) SV1(I)=V1
18    CONTINUE
      IK=1
      GOTO 3
5     CONTINUE
      IF(J.NE.NC) GOTO 19
      IF(I.EQ.NC) GOTC 16
      IEQ=4
      CALL XINT(IEQ,XP,YP,X,Y,I,J,SL,APHI,VV)
      VV=-VV
      IEQ=5
      CALL XINT(IEQ,XP,YP,X,Y,I,J,SL,APHI,UU)
      GOTO 17
16    CONTINUE
      IEQ=6
```

```
      CALL XINT(IEQ,XP,YP,X,Y,I,J,SL,APHI,VV)
      VV=-VV
      UU=0.
      GOTO 17
19    CONTINUE
      PSI1=ATAN2(YCONP,XCONP)
      IF(PSI1.LT.0.) PSI1=PSI1+2.*3.14159266
      PSI2=ATAN2(YCONP,(XCONP-SL))
      IF(PSI2.LT.0.) PSI2=PSI2+2.*3.14159266
      UU=PSI2-PSI1+(XCONP*DCP*(TETA1-TETA2)-
     CYCONP*ALOG(R2/R1))/SL
      VV=(1.-XCONP/SL)*ALOG(R2/R1)-1.-ABS(YCONP)
     C*(TETA1-TETA2)/SL
      IF(I.EQ.J) UU=0.
17    CONTINUE
      U2=UU*COS(PHI)-VV*SIN(PHI)
      V2=UU*SIN(PHI)+VV*COS(PHI)
      IF(J.EQ.NC1.AND.I.LE.NC) U1=SU1(I)
      IF(J.EQ.NC1.AND.I.LE.NC) V1=SV1(I)
      IF(J.EQ.NT1) V1=0
      IF(J.EQ.NT1) U1=0
      IF(J.EQ.N1) V1=0.
      IF(J.EQ.N1) U1=0.
      IF(J.EQ.1) U1=0.
      IF(J.EQ.1) V1=0.
      U=U1+U2
      V=V1+V2
      A(I,J)=V-U*SLOPE(I)
      IF(I.LE.NC) GOTO 340
      VI(I,J)=V
      UI(I,J)=U
340   CONTINUE
      IF(J.LE.NC) GOTO 20
      UG=PSI2-PSI1
      IF(I.EQ.J) UG=0.
      VG=ALOG(R2/R1)
      IF(J.GT.N.AND.J.LE.NT) VG=(Q2-Q1)*VG
      IF(J.GT.N.AND.J.LE.NT) UG=(Q2-Q1)*UG
      IF(J.LE.N) VG=Q1*VG
      IF(J.LE.N) UG=Q1*UG
      IF(J.GT.NT) VG=-Q2*VG
      IF(J.GT.NT) UG=-Q2*UG
      UGAMA=UG*COS(PHI)-VG*SIN(PHI)+UGAMA
      VGAMA=UG*SIN(PHI)+VG*COS(PHI)+VGAMA
20    CONTINUE
      IF(I.GT.NC) GOTO 2
      IF(J.GT.NC) GOTO 2
      AS(I,J)=A(I,J)
2     CONTINUE
      R1=((XP(I)-X(N2))**2+(YP(I)-Y(N2))**2)**.5
```

```
      R2=((XP(I)-X(NC1))**2+(YP(I)-Y(NC1))**2)**.5
      R3=((XP(I)-X(NT3))**2+(YP(I)-Y(NT3))**2)**.5
      XP(I)=(SXP-X(NC1))*COS(TAU)+(SYP-Y(NC1))*SIN(TAU)
      YP(I)=-(SXP-X(NC1))*SIN(TAU)+(SYP-Y(NC1))*COS(TAU)
      T3=1.57079-ATAN2((YP(I)-DEL),XP(I))
      IF(T3.LT.0) T3=T3+2.*3.14159266
      T2=1.57079-ATAN2(YP(I),XP(I))
      IF(T2.LT.0.) T2=3.14159*2+T2
      T1=1.57079-ATAN2((YP(I)-DEL1),XP(I))
      IF(T1.LT.0) T1=2.*3.14159266+T1
      US1=((T1-T2)*COS(TAU)+ALOG(R2/R1)*SIN(-TAU))*Q1
      VS1=(-(T1-T2)*SIN(-TAU)+ALOG(R2/R1)*COS(TAU))*Q1
      US2=((T3-T1)*COS(TAU)+ALOG(R1/R3)*SIN(-TAU))*Q2
      VS2=(-(T3-T1)*SIN(-TAU)+ALOG(R1/R3)*COS(TAU))*Q2
      US=US1+US2
      VS=VS1+VS2
      XP(I)=SXP
      YP(I)=SYP
      B(I)=-VS+SLOPE(I)*US-(SIN(ALPHA)-COS(ALPHA)*SLOPE(I))
     C*2*3.14159
      RR1=((XP(I)-X(NT2))**2+(YP(I)-Y(NT2))**2)**.5
      RR2=((XP(I)-X(N1))**2+(YP(I)-Y(N1))**2)**.5
      RR3=((XP(I)-X(NTT3))**2+(YP(I)-Y(NTT3))**2)**.5
      PP1=ATAN2((YP(I)-Y(NT2)),(XP(I)-X(NT2)))
      IF(PP1.LT.0.) PP1=2.*3.1415926+PP1
      PP2=ATAN2((YP(I)-Y(N1)),(XP(I)-X(N1)))
      IF(PP2.LT.0.) PP2=2.*3.1415926+PP2
      PP3=ATAN2((YP(I)-Y(NTT3)),(XP(I)-X(NTT3)))
      IF(PP3.LT.0) PP3=PP3+2.*3.14159266
      VINF2=((PP3-PP1)*SIN(ALPHA)+ALOG(RR3/RR1)*COS(ALPHA))*Q2
      UINF2=((PP3-PP1)*COS(ALPHA)-ALOG(RR3/RR1)*SIN(ALPHA))*Q2
      VINF1=((PP1-PP2)*SIN(ALPHA)+ALOG(RR1/RR2)*COS(ALPHA))*Q1
      UINF1=((PP1-PP2)*COS(ALPHA)-ALOG(RR1/RR2)*SIN(ALPHA))*Q1
      B(I)=B(I)-VINF1-VINF2+(UINF1+UINF2)*SLOPE(I)
      B(I)=B(I)-VGAMA+UGAMA*SLOPE(I)
      IF(I.LE.NC) GOTO 1
      UO2(I)=(UGAMA+UINF1+UINF2+US)/(2.*3.14159266)
      VO2(I)=(VGAMA+VINF1+VINF2+VS)/(2.*3.14159266)
1     CONTINUE
C---  SOLUTION OF THE SET OF LINEAR EQUATIONS
      CALL LNEQNS(A,60,60,NTT,B,IW1,IW2,IER)
C---  LIFT COEFFICIENT
C--
      XLC=0.
      DO 230 I=1,NTT
      IF(I.EQ.1) GOTO 231
      IF(I.EQ.NC) GOTO 232
      IF(I.EQ.NC1) GOTO 233
      IF(I.EQ.N) GOTO 236
      IF(I.EQ.NT) GOTO 236
```

```
          IF(I.EQ.NTT) GOTO 236
          IF(I.GT.N) GOTO 234
          XLC=XLC+(B(I+1)+B(I))*(X(I+1)-X(I))/2.
          GOTO 230
  231     CONTINUE
          XLC=XLC+B(I)*(X(I+1)-X(I))/2.-2.*B(I+1)*X(I+1)**1.5
         C*(ALOG((1+X(I+1)**.5)/(1-X(I+1)**.5))+
         CALOG(1-X(I+1))/X(I+1)**.5)/ALOG(1-X(I+1))
          SL1=XLC
          GOTO 230
  232     CONTINUE
          SXLC=XLC
          XLC=XLC+B(NC1)*(X(NC1)-X(NC))/2.-2.*B(NC)*X(NC)**1.5
         C*(2.*ALCG(2.)-ALOG((1+X(NC)**.5)/
         C(1-X(NC)**.5))-ALOG(1-X(NC))/X(NC)**.5)/ALOG(1-X(NC))
          XLCC=XLC*2.
          SLNC=XLC-SXIC
          GOTO 230
  233     CONTINUE
          SXLC=XLC
          XLC=XLC+B(NC1)*(X(NC2)-X(NC1))/2.+B(NC2)*X(NC2)**1.5*(2
         C*(1-
         C1/X(NC2)**.5)*AIOG(X(NC2)**.5-1)-2*(1+1/X(NC2)**.5)*
         CALOG(X(NC2)**.5+1)+4.*ALOG(2.))/ALOG(X(NC2)-1.)
          SAL=XLC-SXLC
          GOTO 230
  234     CONTINUE
          IF(I.GT.NT) GCTC 251
          IF(I.EQ.N1) GOTO 235
          XLC=XLC+(B(I+1)+B(I))*(X(I+2)-X(I+1))/2.
          GOTO 230
  235     CONTINUE
          SXLC=XLC
          XLC=XLC+B(N1)*(X(N3)-X(N2))/2.+(2.*(1./X(N2)**.5-
         C1./X(N3)**.5)*ALOG(X(N3)**.5-X(N2)**.5)-
         C2.*(1./X(N2)**.5+1./X(N3)**.5)*ALOG(X(N3)**.5+
         CX(N2)**.5)+4.*ALOG(2.*X(N2)**.5)/X(N2)**.5)
         C*B(N2)*X(N3)**1.5/ALOG(X(N3)-X(N2))
          SAU=XLC-SXLC
          GOTO 230
  251     CONTINUE
          IF(I.EQ.NT1) GOTO 252
          XLC=XLC+(B(I+1)+B(I))*(X(I+3)-X(I+2))/2.
          GOTO 230
  252     CONTINUE
          SXLC=XLC
          XLC=XLC+B(NT1)*(X(NT4)-X(NT3))/2.+(2.*(1/X(NT3)**.5-
         C1/X(NT4)**.5)*ALOG(X(NT4)**.5-X(NT3)**.5)-2*(1/X(NT3)**
         C.5+1/X(NT4)**.5)*ALOG(X(NT4)**.5+X(NT3)**.5)+4*ALOG(2*
         CX(NT3)**.5)/X(NT3)**.5)*B(NT2)*X(NT4)**1.5/
```

```
          CALOG(X(NT4)-X(NT3))
           SAU3=XLC-SXLC
           GOTO 230
      236  CONTINUE
           J=I
           IF(I.EQ.NT) J=I+1
           IF(I.EQ.NTT)J=I+2
           XLC=B(I)*(X(J+1)-X(J))/2.+XLC
      230  CONTINUE
           XLC=XLC*2.
           XLCJ=XLC-XLCC
C---
C---       OUTPUTS
C---
           PRINT,'NUMBER OF ITERATIONS'
           PRINT 54, ITR
      54   FORMAT(5X,I4)
           PRINT,'ANGLE OF ATTACK IN DEGREE'
           PRINT 53,ALFAD
      53   FORMAT(F10.3)
           PRINT,'INITIAL JET DEFLECTION ANGLE IN DEGREE'
           PRINT 53, TAUD
           PRINT,'JET THICKNESS'
           PRINT 53, DEL
           PRINT,'POWER JET MOMENTUM COEFFICIENT'
           PRINT 53,CPJ
           PRINT,'TOTAL JET MOMENTUM COEFFICIENT'
           PRINT 53,CJ
           PRINT,'X CENTER'
           PRINT 52,(XC(I),I=1,NJ1)
           PRINT,'Y CENTER'
           PRINT 52,(YC(I),I=1,NJ1)
           PRINT,'X COORDINATES OF CONTROL POINTS'
           PRINT 52, (XP(I),I=1,NTT)
           PRINT,'Y COORDINATES OF CONTROL POINTS'
           PRINT 52, (YP(I),I=1,NTT)
           PRINT,'X COORDINATES OF DIVISION POINTS'
           PRINT 52,(X(I),I=1,NTT3)
           PRINT,'Y COORDINATES OF DIVISION POINTS'
           PRINT 52, (Y(I),I=1,NTT3)
           PRINT,'VORTEX DISTRIBUTION'
           PRINT 52,(B(I),I=1,NTT)
      52   FORMAT(10F10.6)
           PRINT,'LIFT COEFFICIENT'
           PRINT 53,XLC
           PRINT,'JET LIFT COEFFICIENT'
           PRINT 53,XLCJ
           PRINT,'POWERJET VELOCITY'
           PRINT 53,Q
           PRINT,'Q1'
```

```
      PRINT 53,Q1
      PRINT,'Q2'
      PRINT 53, Q2
      PRINT,'VELOCITY DISTRIBURICNS'
      GOTO 99
227   CONTINUE
448   CONTINUE
      STOP
      END

      SUBROUTINE XINT(IEQ,XP,YP,X,Y,I,J,SL,APHI,VEL)
      DIMFNSICN X(60),Y(60),XP(60),YP(60)
      N=22
      N2=N+2
      NC=10
      NC2=NC+2
      NT=N+(N-NC)
      NT2=NT+2
      NT3=NT+3
      G=1.
      IF((J-1).EQ.N2) G=X(N2)
      IF((J-2).EQ.NT2) G=X(NT3)
      IF(IEQ.GT.6) GOTC 421
      IF(IEQ.LT.7.AND.IEQ.GT.3) GCTO 420
      XU=X(J)
      XL=X(J-1)
      GOTO 401
420   CONTINUE
      XU=X(J+1)
      XL=X(J)
      GOTO 401
421   CONTINUE
      XU=SL
      XL=0.
401   CONTINUE
      A=.5*(XU+XL)
      BB=XU-XL
      C=.4869533*BB
      T=.03333567*(F(IEQ,XP,YP,I,J,X,APHI,A+C)
     C+F(IEQ,XP,YP,I,J,X,APHI,A-C))
      C=.4325317*EB
      T=T+.07472567*(F(IEQ,XP,YP,I,J,X,APHI,A+C)
     C+F(IEQ,XP,YP,I,J,X,APHI,A-C))
      C=.3397048*BB
      T=T+.1C95432*(F(IEQ,XP,YP,I,J,X,APHI,A+C)
     C+F(IEQ,XP,YP,I,J,X,APHI,A-C))
      C=.2166977*BB
      T=T+.1346334*(F(IEQ,XP,YP,I,J,X,APHI,A+C)
     C+F(IEQ,XP,YP,I,J,X,APHI,A-C))
      C=.07443717*BB
```

```
      T=BB*(T+.1477621*(F(IEQ,XP,YP,I,J,X,APHI,A+C)
     C+F(IEQ,XP,YP,I,J,X,APHI,A-C)))
      GOTO (403,404,405,406,407,408,410,411,412),IEQ
  403 VEL=(T-2.*XP(I)*(ALOG((1.+X(J+0)**.5)/(1.-X(J+0)**.5))+
     CALOG(1.-X(J+0))/X(J+0)**.5)/(XP(I)**2+YP(I)**2))*
     CX(J+0)**1.5/ALOG(1.-X(J+0))
      GOTO 409
  404 VEL=(T-2.*YP(I)*(ALOG((1.+X(J+0)**.5)/(1.-X(J+0)**.5))+
     CALOG(1.-X(J+0))/X(J+0)**.5)/(XP(I)**2+YP(I)**2))*
     CX(J+0)**1.5/ALOG(1.-X(J+0))
      GOTO 409
  405 VEL=T-2.*(ALOG((1+X(J+0)**.5)/(1-X(J+0)**.5))+
     CALOG(1-X(J+0))/X(J+0)**.5)/XP(I)+ALOG(1-XP(I))*
     CALOG(XP(I)/(X(J+0)-XP(I)))/XP(I)**1.5
      VEL=VEL*X(J+0)**1.5/ALOG(1.-X(J+0))
      GOTO 409
  406 VEL=(T+(XP(I)-1.)*
     C((1.-X(J+0))*ALOG(1.-X(J+0))+X(J+0)-1.)/((XP(I)-1.)**2
     C+YP(I)**2))*X(J+0)**1.5/ALOG(1.-X(J+0))
      GOTO 409
  407 VEL=(T+YP(I)*
     C((1.-X(J+0))*ALOG(1.-X(J+0))+X(J+0)-1.)/((XP(I)-1.)**2
     C+YP(I)**2))*X(J+0)**1.5/ALOG(1.-X(J+0))
      GOTO 409
  408 VEL=T+(1.-X(J+0))*(ALOG(1.-X(J+0))-1.)/(XP(I)-1)+
     CALOG(1.-XP(I))*ALOG((XP(I)-X(J+0))/(1-XP(I)))
     C/XP(I)**1.5
      VEL=VEL*X(J+0)**1.5/ALOG(1.-X(J+0))
      GOTO 409
  410 VEL=(T+XP(I)*SI*(ALOG(SL*COS(APHI))-1)/((XP(I)**2+YP(I)
     C**2)*G**1.5))*X(J)**1.5/ALOG(X(J)-G)
      GOTO 409
  411 VEL=(T+YP(I)*SI*(ALOG(SL*COS(APHI))-1)/((XP(I)**2+YP(I)
     C**2)*G**1.5))*X(J)**1.5/ALOG(X(J)-G)
      GOTO 409
  412 VEL=T+SL*(ALOG(SL*COS(APHI))-1.)/(XP(I)*G**1.5)+
     CALOG(XP(I)*COS(APHI))*ALOG(XP(I)/(SL-XP(I)))/
     C(XP(I)*COS(APHI)+G)**1.5
      VEL=VEL*X(J+0)**1.5/ALOG(X(J+0)-G)
  409 CONTINUE
      RETURN
      END

      FUNCTION F(IEQ,XP,YP,I,J,X,APHI,S)
      DIMENSION X(60),XP(60),YP(60)
      N=22
      N2=N+2
      NC=10
      NT=N+(N-NC)
      NT2=NT+2
```

```
      NT3=NT+3
      NC2=NC+2
      G=1.
      IF((J-2).EQ.NT2) G=X(NT3)
      IF((J-1).EQ.N2) G=X(N2)
      GOTO (1,2,3,4,5,6,7,8,9),IEQ
    1 F=ALOG(1.-S)*(XP(I)-S)/(S**1.5*((XP(I)-S)**2+YP(I)**2))
     C-ALOG(1.-S)*XP(I)/(S**1.5*(XP(I)**2+YP(I)**2))
      GOTO 10
    2 F=ALOG(1.-S)*YP(I)/(S**1.5*((XP(I)-S)**2+YP(I)**2))-
     CALOG(1.-S)*YP(I)/(S**1.5*(XP(I)**2+YP(I)**2))
      GOTO 10
    3 F=ALOG(1.-S)/(S**1.5*(XP(I)-S))-ALOG(1.-S)/
     C(XP(I)*S**1.5)-ALOG(1.-XP(I))/(XP(I)**1.5*(XP(I)-S))
      GOTO 10
    4 F=ALOG(1.-S)*(XP(I)-S)/(S**1.5*((XP(I)-S)**2+YP(I)**2))
     C-ALOG(1.-S)*(XP(I)-1.)/((XP(I)-1.)**2+YP(I)**2)
      GOTO 10
    5 F=ALOG(1.-S)*YP(I)/(S**1.5*((XP(I)-S)**2+YP(I)**2))-
     CALOG(1.-S)*YP(I)/((XP(I)-1.)**2+YP(I)**2)
      GOTO 10
    6 F=ALOG(1.-S)/(S**1.5*(XP(I)-S))-ALCG(1.-S)/(XP(I)-1.)-
     CALOG(1.-XP(I))/(XP(I)**1.5*(XP(I)-S))
      GOTO 10
    7 F=ALOG(S*COS(APHI))*(XP(I)-S)/
     C((S*COS(APHI)+G)**1.5*((XP(I)-S)**2+YP(I)**2))
     C-ALOG(S*COS(APHI))*XP(I)/((XP(I)**2+YP(I)**2)*G**1.5)
      GOTO 10
    8 F=ALOG(S*COS(APHI))*YP(I)/
     C((S*CCS(APHI)+G)**1.5*((XP(I)-S)**2+YP(I)**2))
     C-ALOG(S*COS(APHI))*YP(I)/((XP(I)**2+YP(I)**2)*G**1.5)
      GOTO 10
    9 F=ALOG(S*COS(APHI))/((S*COS(APHI)+G)**1.5*(XP(I)-S))
     C-ALOG(S*COS(APHI))/(XP(I)*G**1.5)-ALOG(XP(I)*COS(APHI))/
     C((XP(I)*COS(APHI)+G)**1.5*(XP(I)-S))
   10 CONTINUE
      RETURN
      END
```

REFERENCES

1. Hagedorn, H. and Ruden, P., "Windkanahintersuchungen an cinem Junkers-Doppelflugel nit Ausblaseschlitz am Heck des Hauptflugels", Institut Fur Aeromechanik und Flugtechnik der Technischen Hochschule Hannover, LGL Beridit A64, 1938, pp. 38-56; R.A.E. Translation 442, Dec., 1953.

2. Davidson, M., "The Jet Flap", Journal of the Royal Aeronautical Society, Vol. 60, Jan., 1956, p. 25.

3. Spence, D.A., "The Lift Coefficient of a Thin Jet-Flapped Wing", Proc. Roy. Soc. (London), ser. A, pp. 46-68, Dec. 4, 1956.

4. Leamon, R.G. and Plotkin, A., "An Improved Solution of the Two Dimensional Jet-Flapped Airfoil Problem", Journal of Aircraft, Vol. 9, No. 9, pp. 631-635, September, 1972.

5. Sato, J., "Discrete Vortex Method of Two-Dimensional Jet Flaps", AIAA Journal, pp. 968-973, July, 1973.

6. Herold, A.C., "A Two Dimensional, Iterative Solution for the Jet Flap", NASA CR-2190, Feb., 1973.

7. Spence, D.A., "The Lift on a Thin Aerofoil with a Jet-Augmented Flap", Aeronautical Quarterly, Vol. 9, pt. 3, 1958.

8. Whittley, D.C., "The Augmentor Wing: A New Means of Engine Air-frame Integration for STOL Aircraft", Fourth ICAS Conference, Paris, 1964, AIAA Paper No. 64-574.

9. Whittley, D.C., "Ejector-Powered Lift Systems for VISTOL Aircraft", Canadian Aeronautics and Space Journal, Vol. 20, No. 5, May, 1974.

10. Chan, Y.Y., "The Lift on a Two Dimensional Augmentor Wing", NRC Aeronautical Report, LR-523, April, 1969.

11. Woolard, H.W., "Thin Aerofoil Theory of an Ejector-Flapped Wing Section", Journal of Aircraft, Vol. 12, No. 1, Jan., 1975.

12. Wilson, J.D., Loth, J.L., and Chandra, A., "Thrust Augmented Wing Sections in Potential Flow", West Virginia University, Aerospace Engineering TR-25, August, 1974.

13. Mises, R.V., "Theory of Flight", Dover Publications, Inc., 1959.

14. Kuchemann and Weber, "Aerodynamics of Propulsion", McGraw-Hill, 1953.

15. Tang, V.Q., "A Distributed Vortex Theory for the Augmentor Wing", M.Sc. Thesis, Dept. of Mechanical Engineering, The University of Manitoba, Sept., 1974.

16. Foley, W.M., "An Experimental Study of Jet Flap Thrust Recovery", Ph.D. Thesis, Dept. of Aeronautics and Astronautics, Stanford University, SUDAER No. 135, 1962.

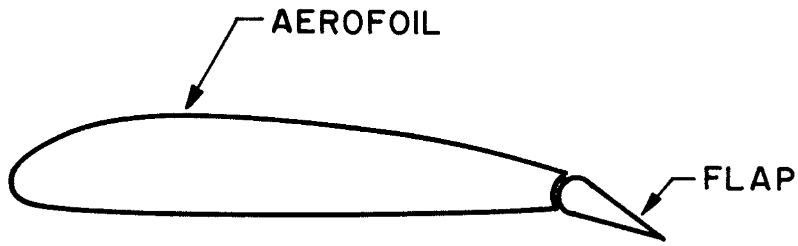

Fig. 1. Aerofoil with Mechanical Flap.

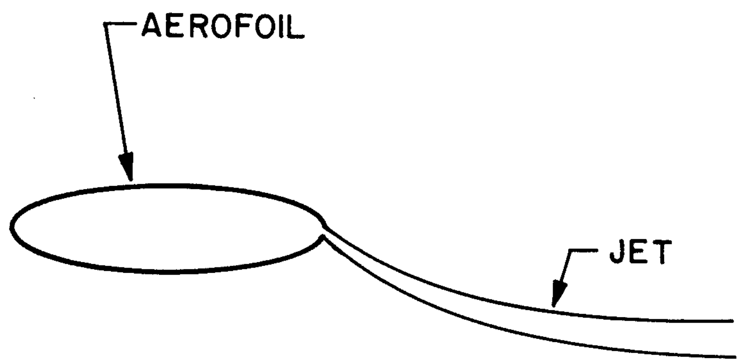

Fig. 2. Elliptic Aerofoil with Jet Flap.

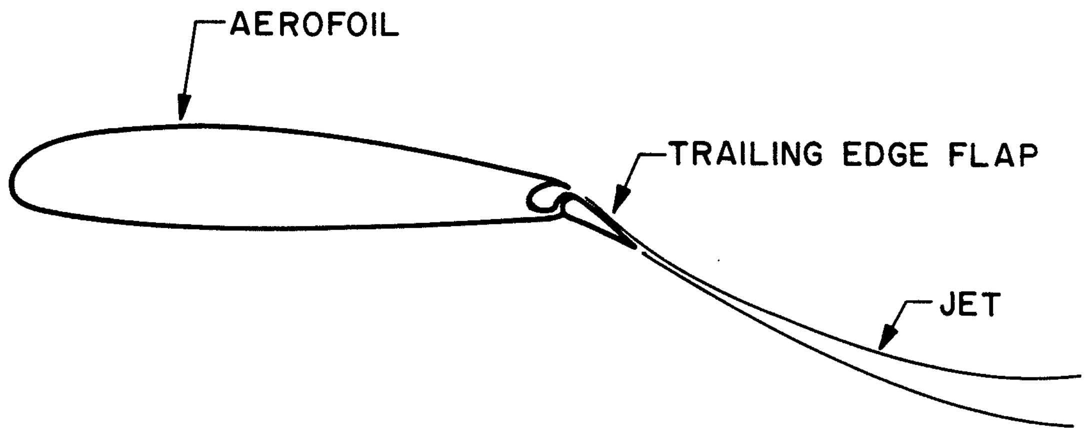

Fig. 3. Aerofoil with Jet Augmented Flap.

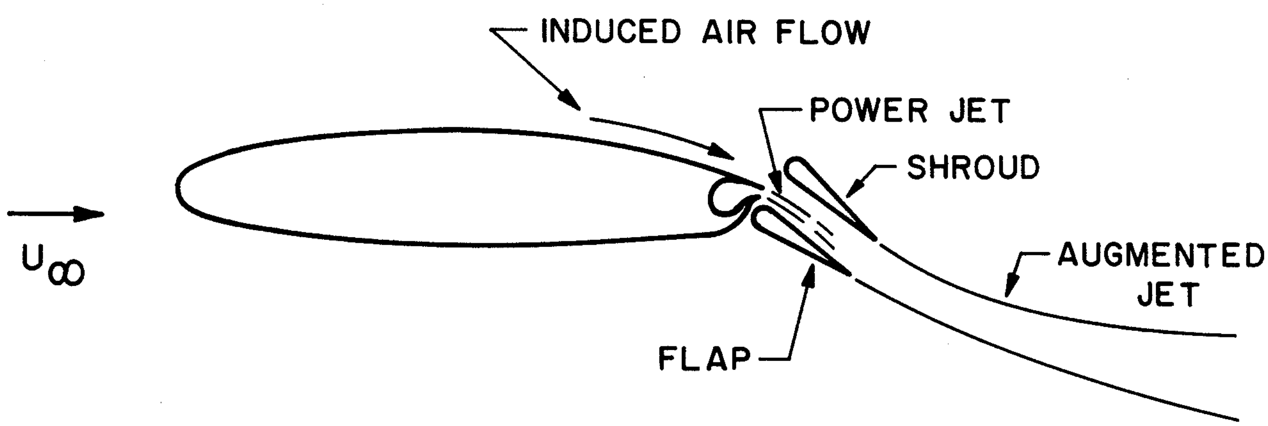

Fig. 4. Two Dimensional Augmentor Wing.

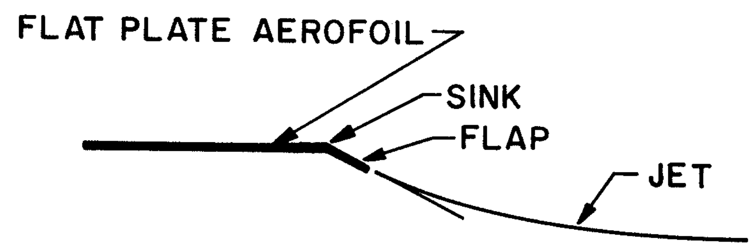

Fig. 5 . Chan's Model of the Augmentor Wing .

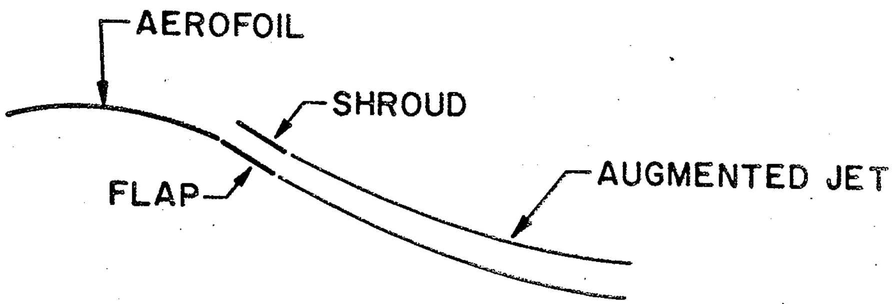

(a) Simplified model of augmentor wing .

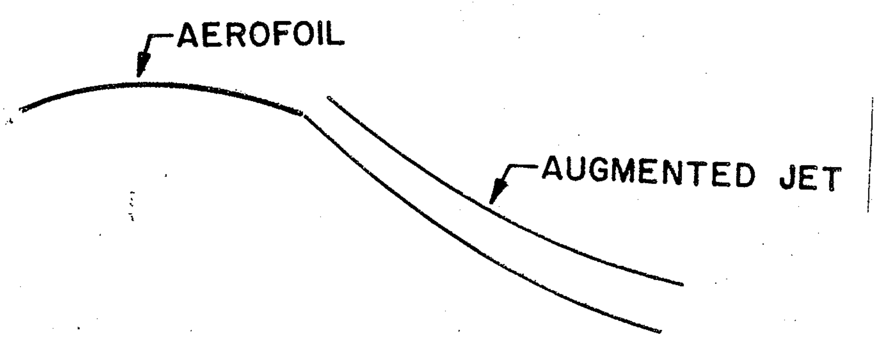

(b) Simplified Model of Augmentor Wing with Zero-Length Shroud and Flap

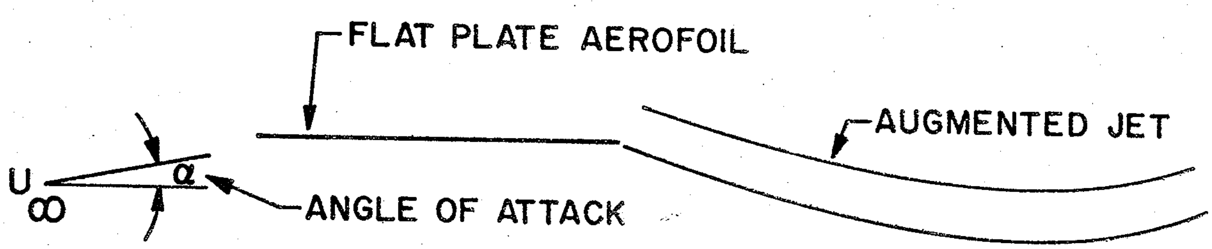

(c) Final model of augmentor wing .

Fig. 6 . Development of an Augmentor Wing Model .

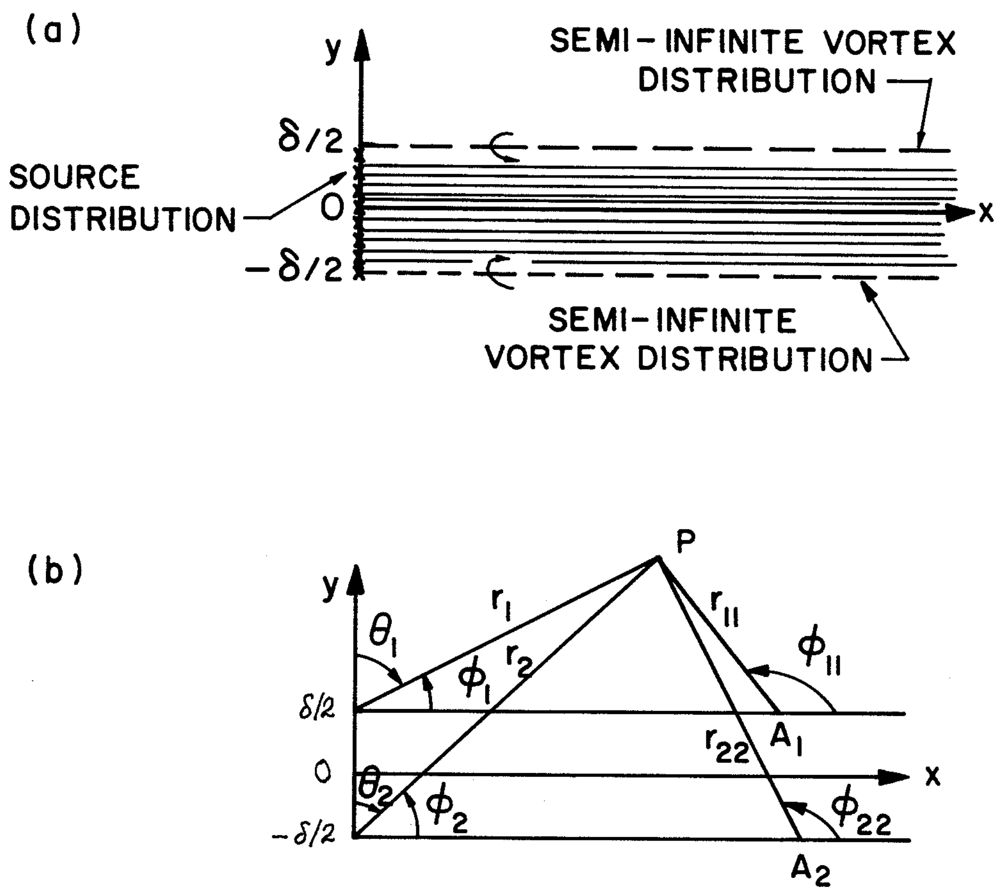

Fig. 7 . Straight Uniform Jet Represented by Source and Vortex Distributions .

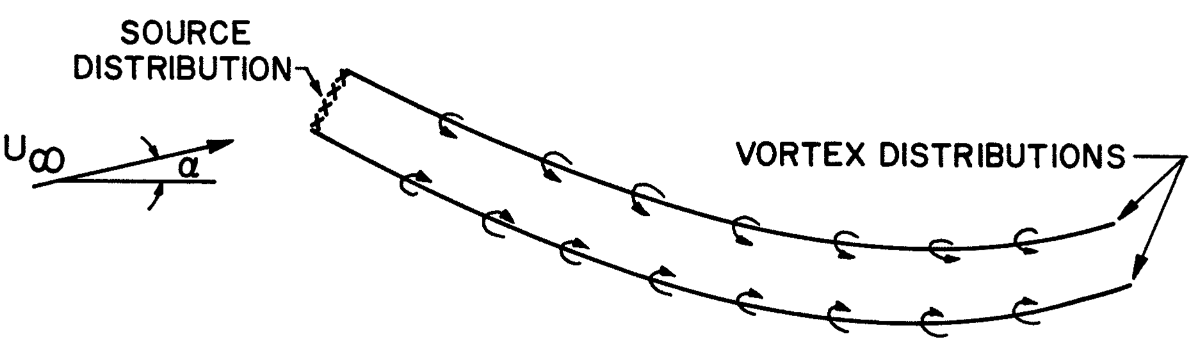

Fig. 8 . Representation of a Curved Thick Jet .

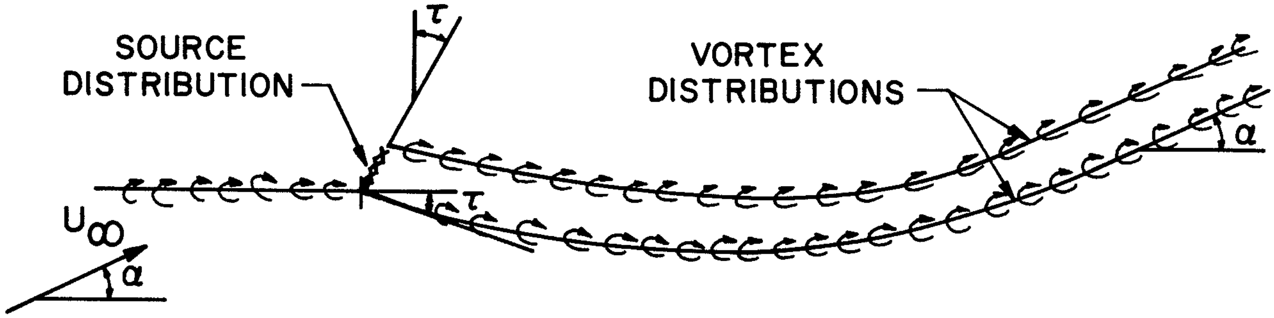

Fig. 9. Augmentor Wing Represented by Distributed Singularities.

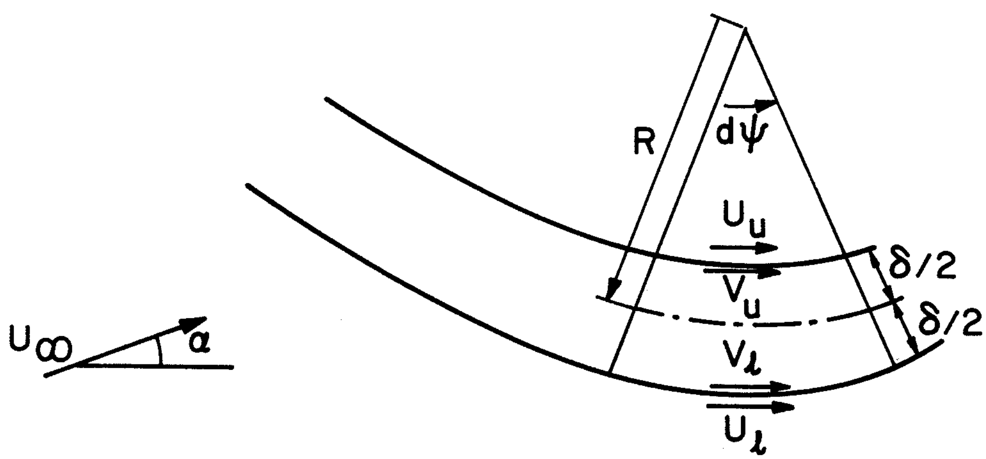

Fig. 10. A Polar Element of a Curved Jet.

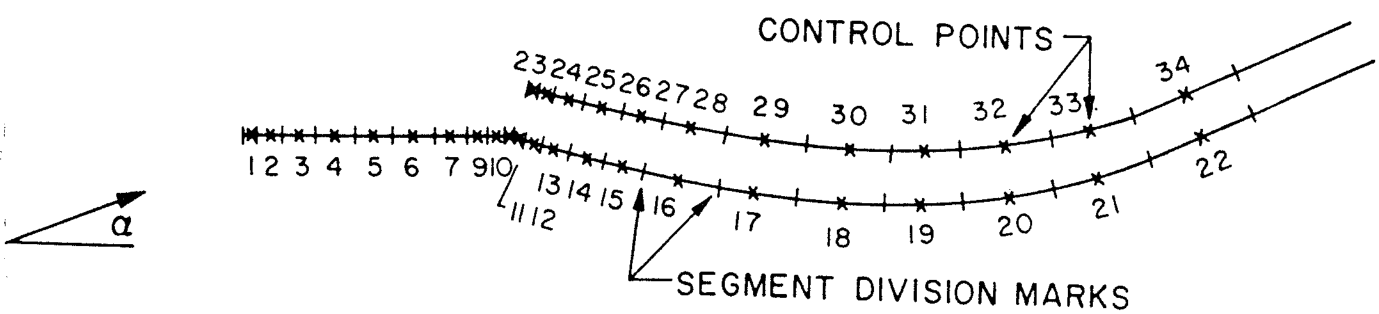

(a) Control points and distributed vortex segments.

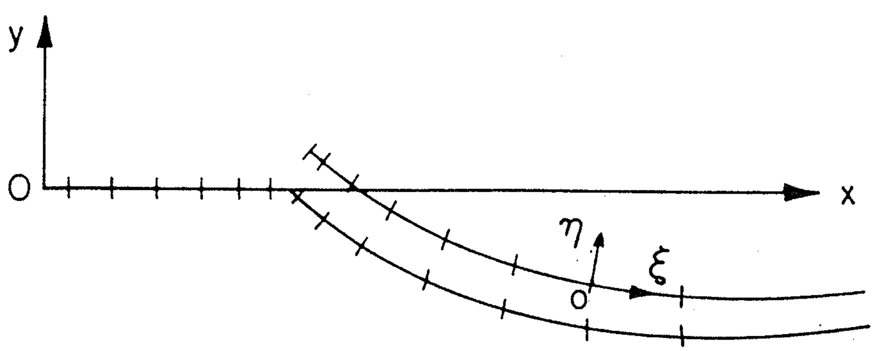

(b) Relationship of the coordinate systems.

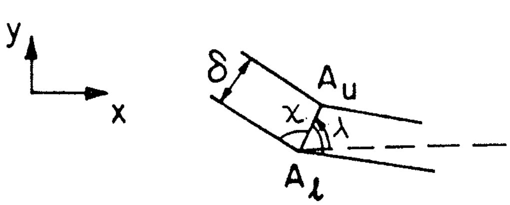

(c) Construction of the coordinates of a division point on the jet upper boundary.

Fig. 11. Locations of Elements and Control Points.

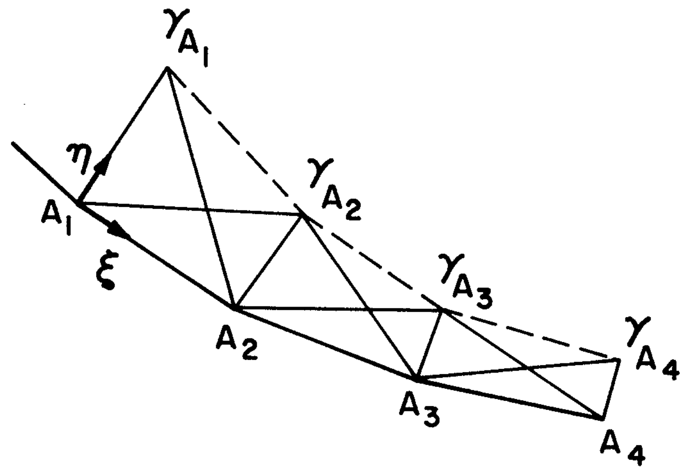

Fig. 12. Example of three consecutive vortex segments

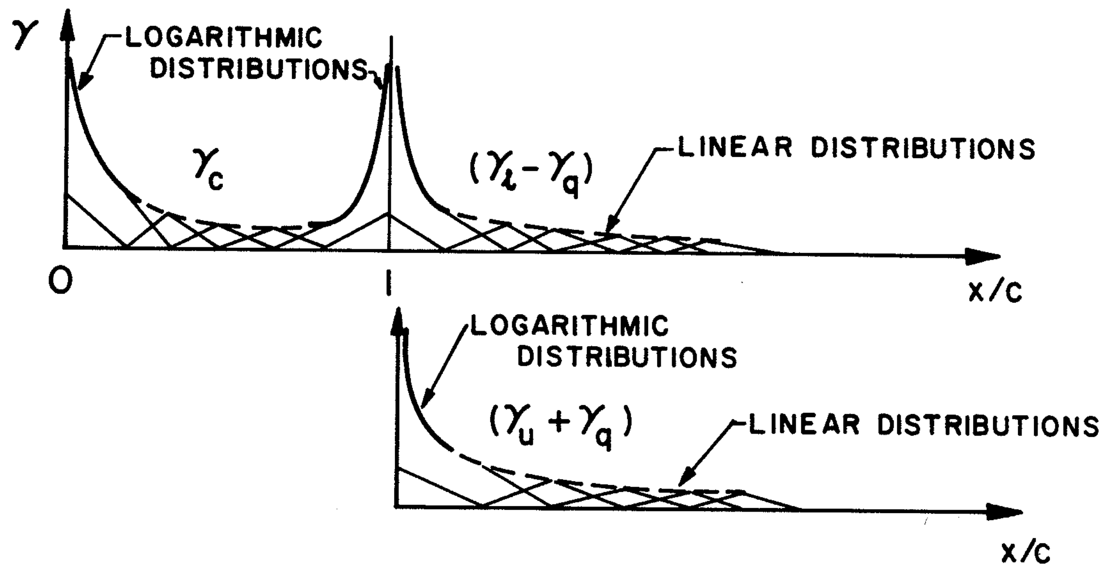

Fig. 13. Typical Logarithmic and Linear Vortex Strength Distributions.

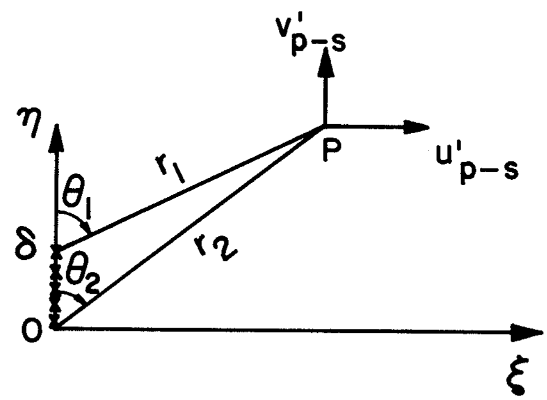

Fig. 14. A Distributed Source Segment and Induced Velocities.

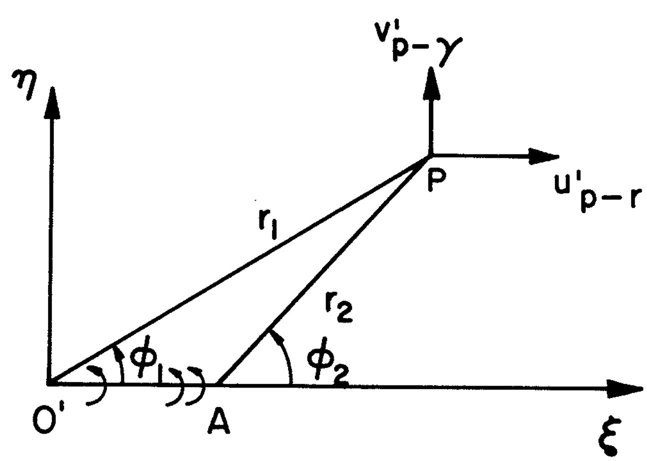

Fig. 15. A Distributed Vortex Segment and Induced Velocities.

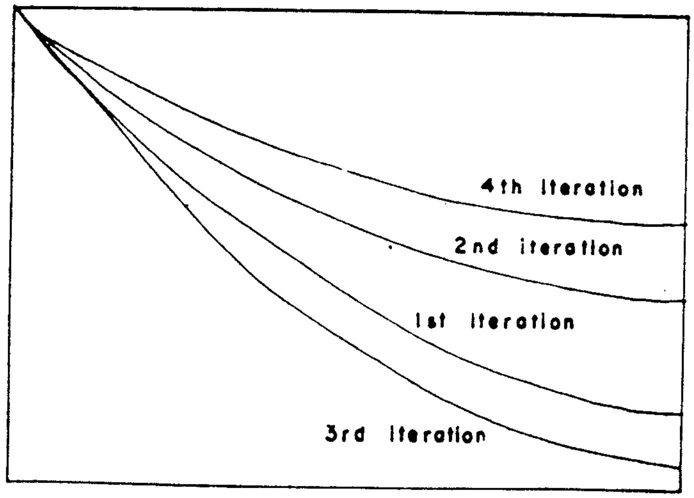

Fig. 16. Sketch of Jet Shapes After Four Normal Iterative Steps.

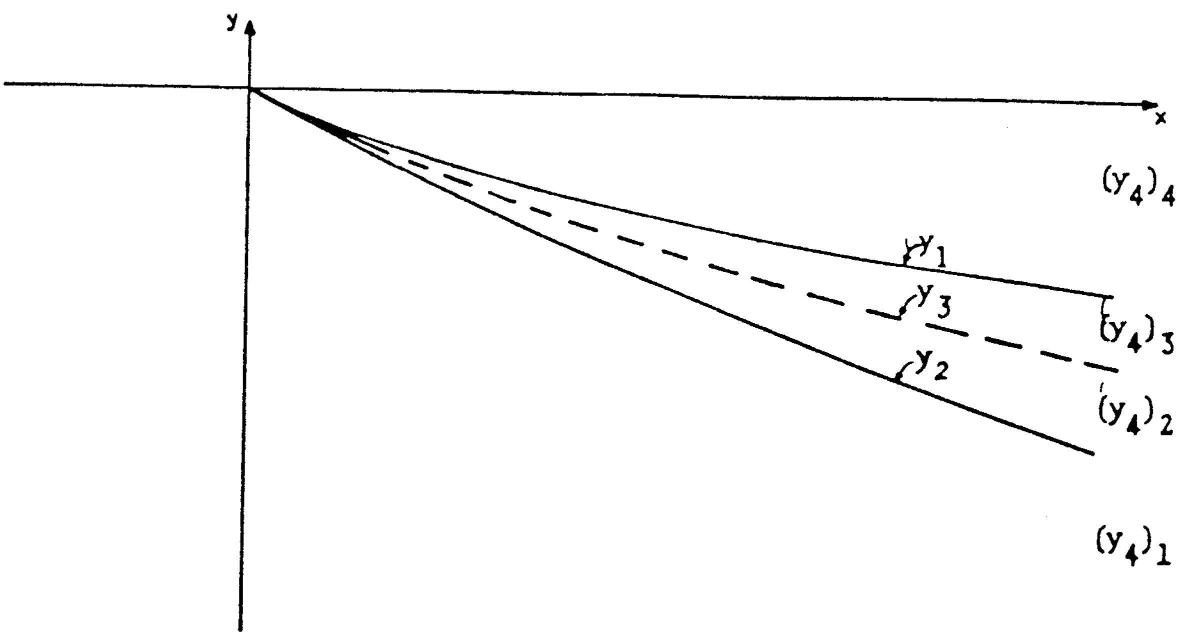

Fig. 17. Specified Regions of Jet Shapes.

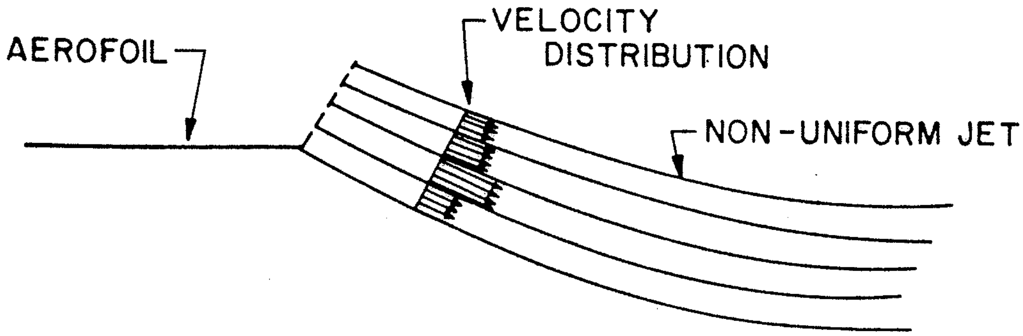

(a) An Augmentor Wing with a Non-uniform Jet.

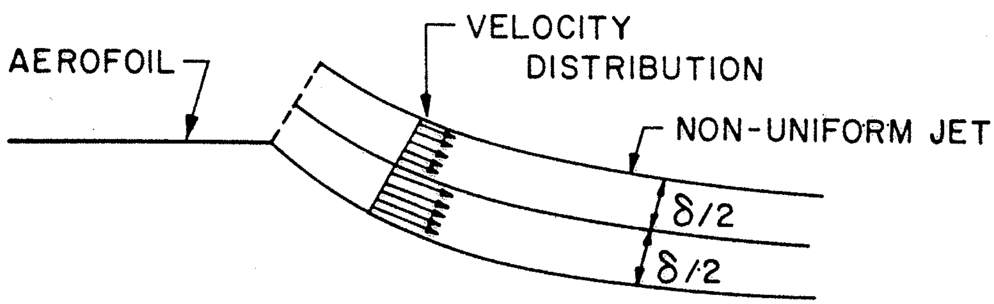

(b) An Augmentor Wing with a Simplified Non-uniform Jet

Fig. 18. Model of the Non-Uniform Jet Augmentor Wing.

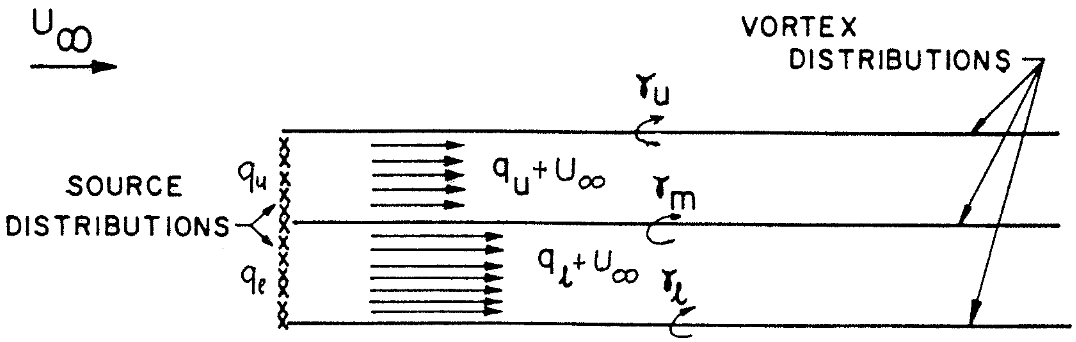

Fig. 19. Straight Non - uniform Jet .

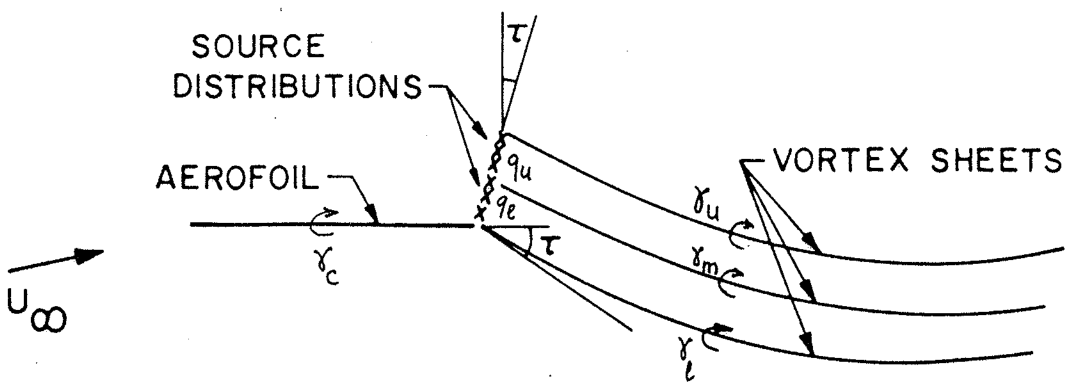

Fig. 20. Mathematical Model of the Non-Uniform

Jet Augmentor Wing

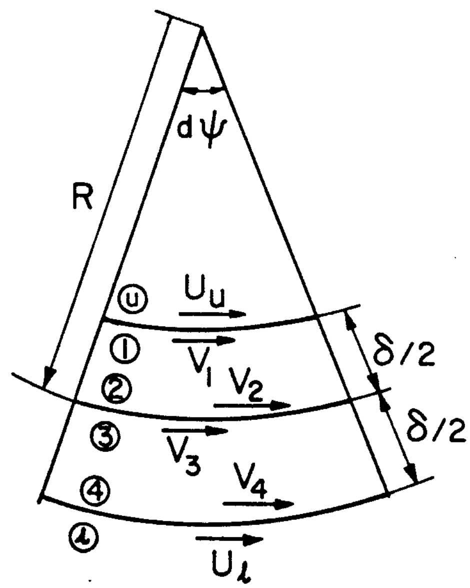

Fig. 21. An Element of the Non-Uniform Jet.

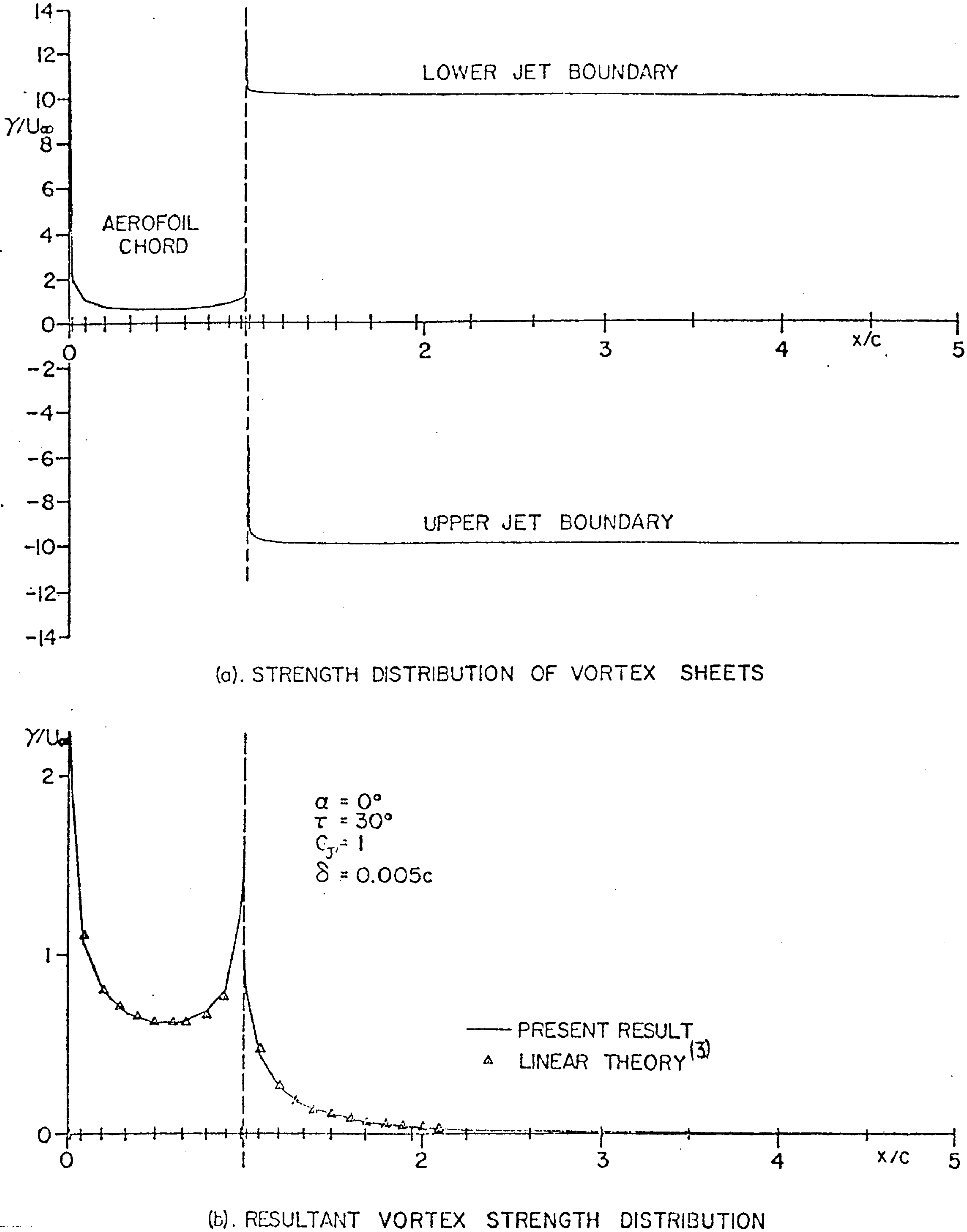

Fig. 22. Vortex Strength Distributions for a Thin Jet Augmentor Wing

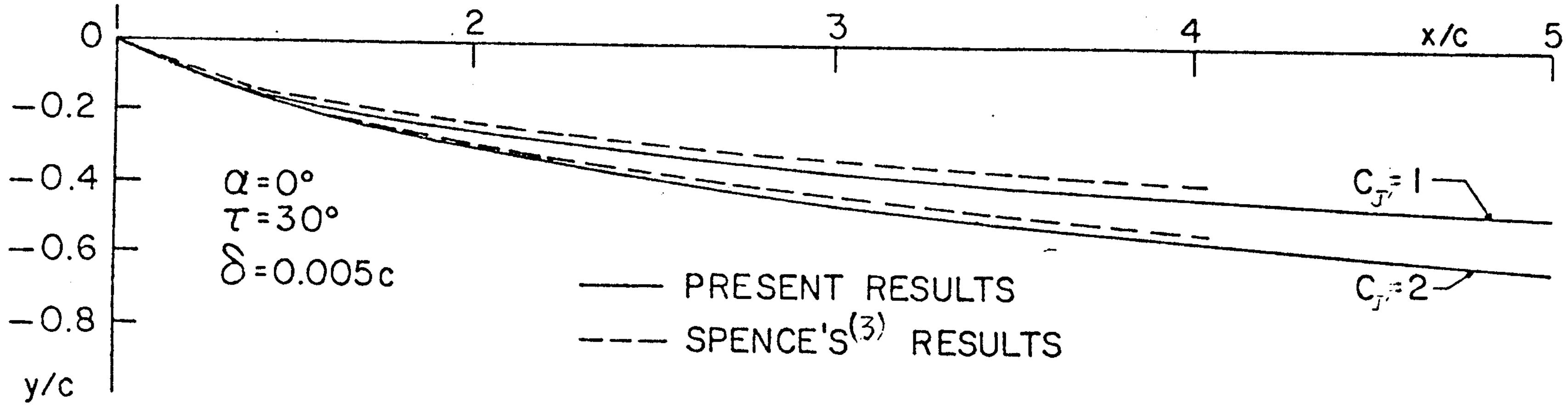

Fig. 23. Center Lines of Jet Trajectories.

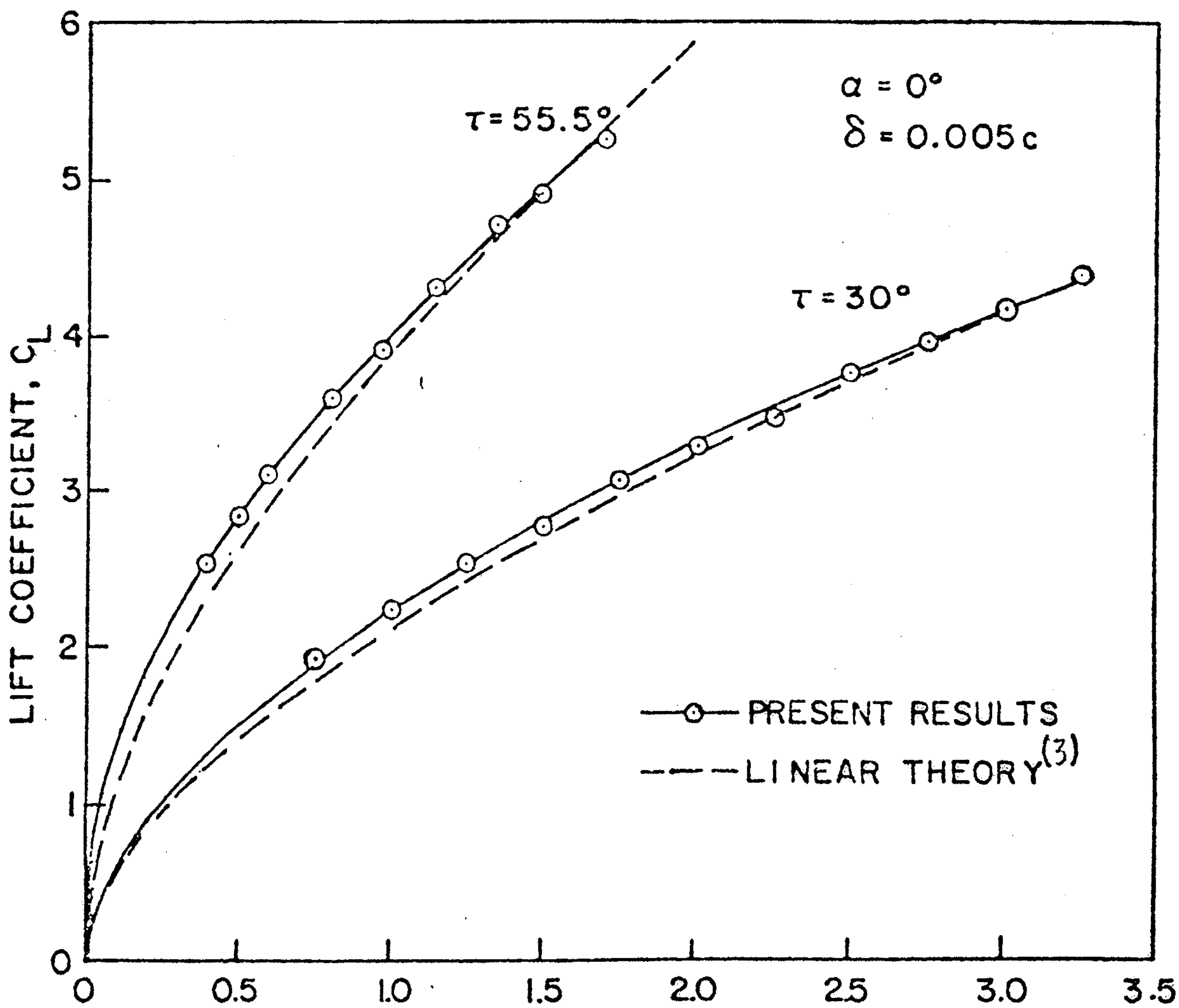

PRIMARY JET MOMENTUM COEFFICIENT, $C_{J'}$

Fig. 24. Predictions of effect of Primary Jet Momentum Coefficient on Lift When the Jet is Thin

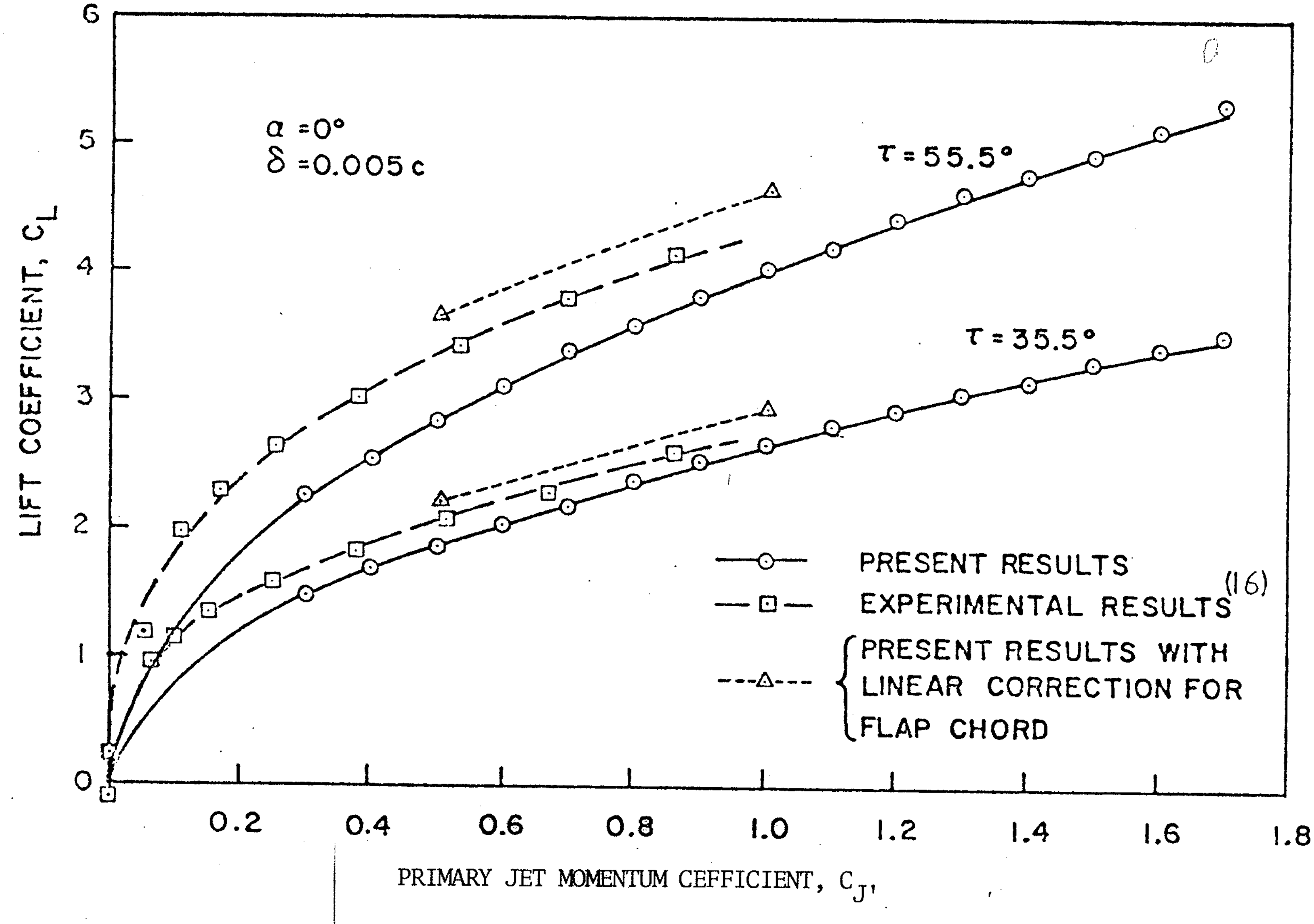

Fig. 25. Comparison of Present Theory with Experimental Results for the Effect of Primary Jet Momentum on Lift for a Thin Jet

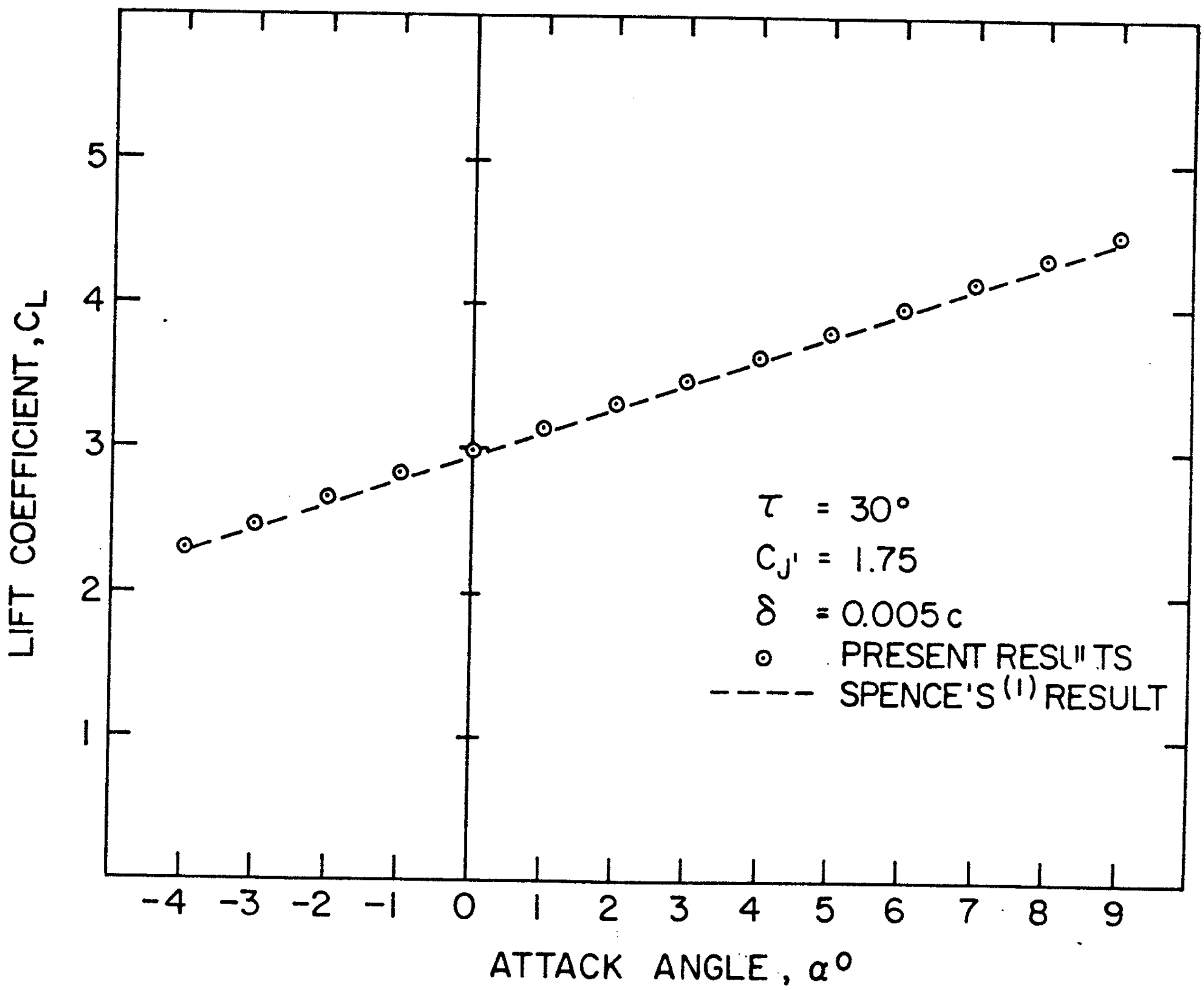

Fig. 26. Lift Coefficient Variation with Attack Angle for a Thin Jet Augmentor Wing.

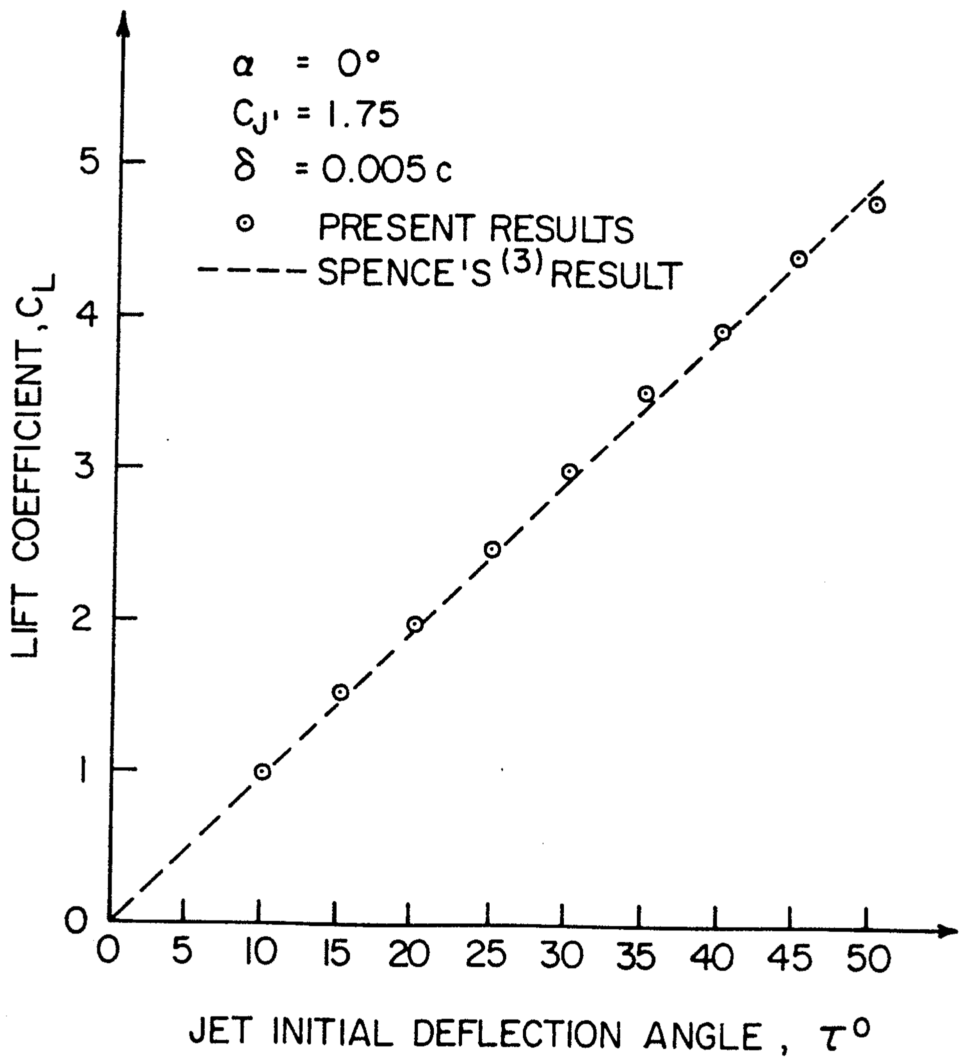

Fig. 27. Lift Coefficient Variation with Initial Jet Deflection Angle for a Thin Jet Augmentor Wing.

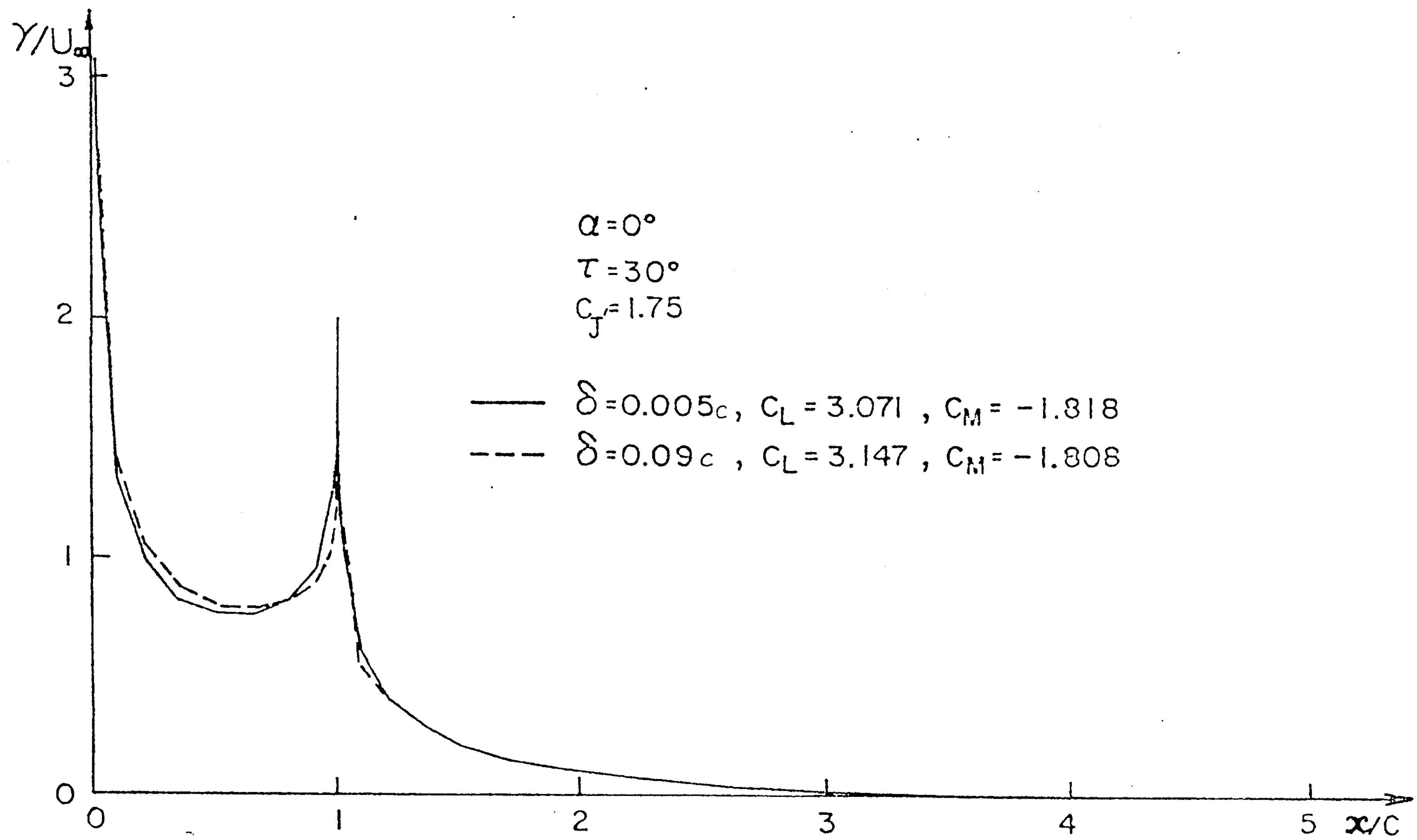

Fig. 28. Vortex Strength Distributions for a Thick Jet Augmentor Wing.

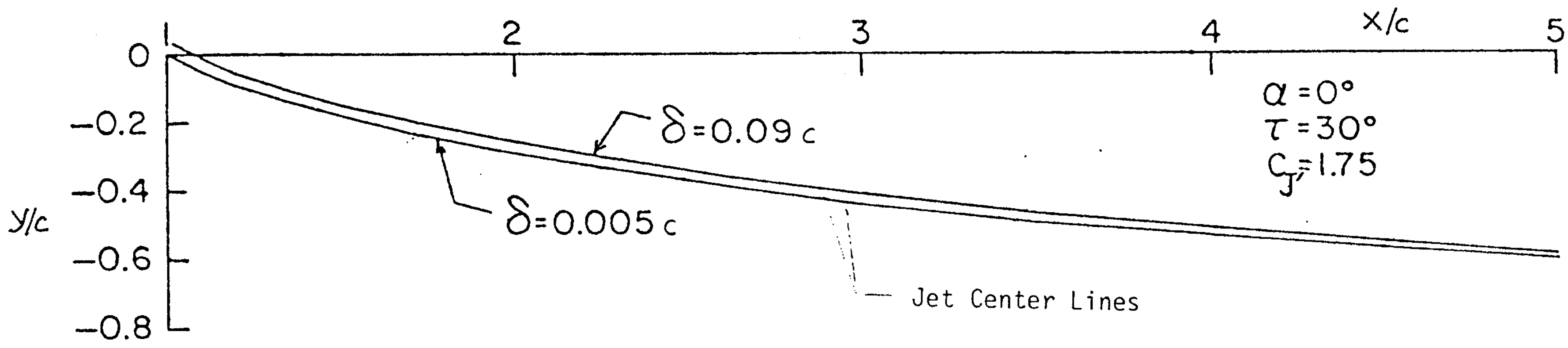

Fig. 29. Effect of Jet Thickness on Jet Trajectory.

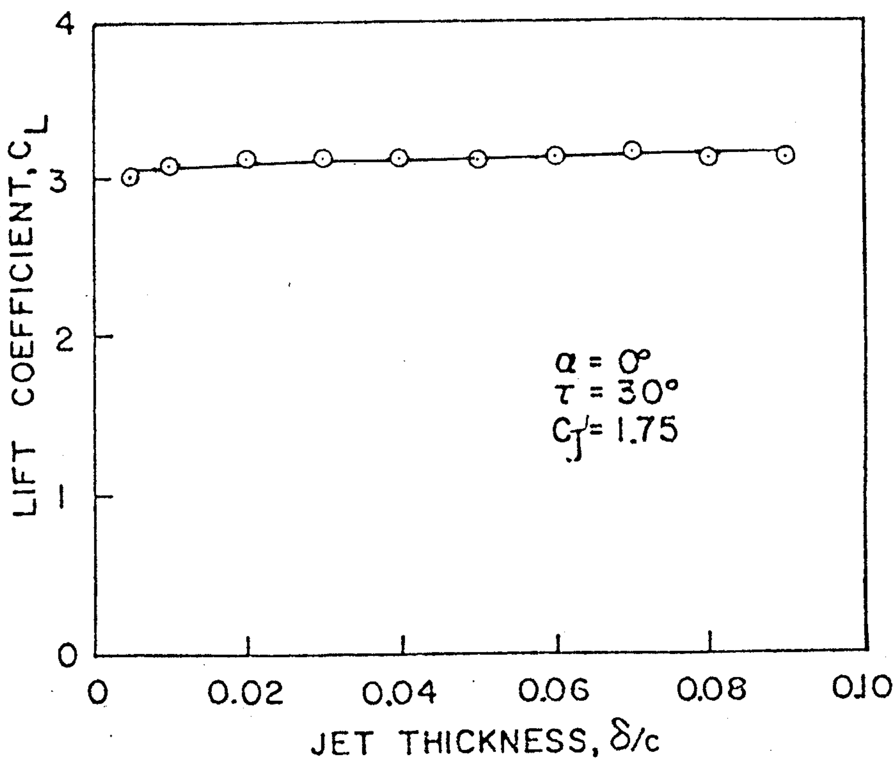

Fig. 30. Effect of Jet Thickness on Lift Coefficient.

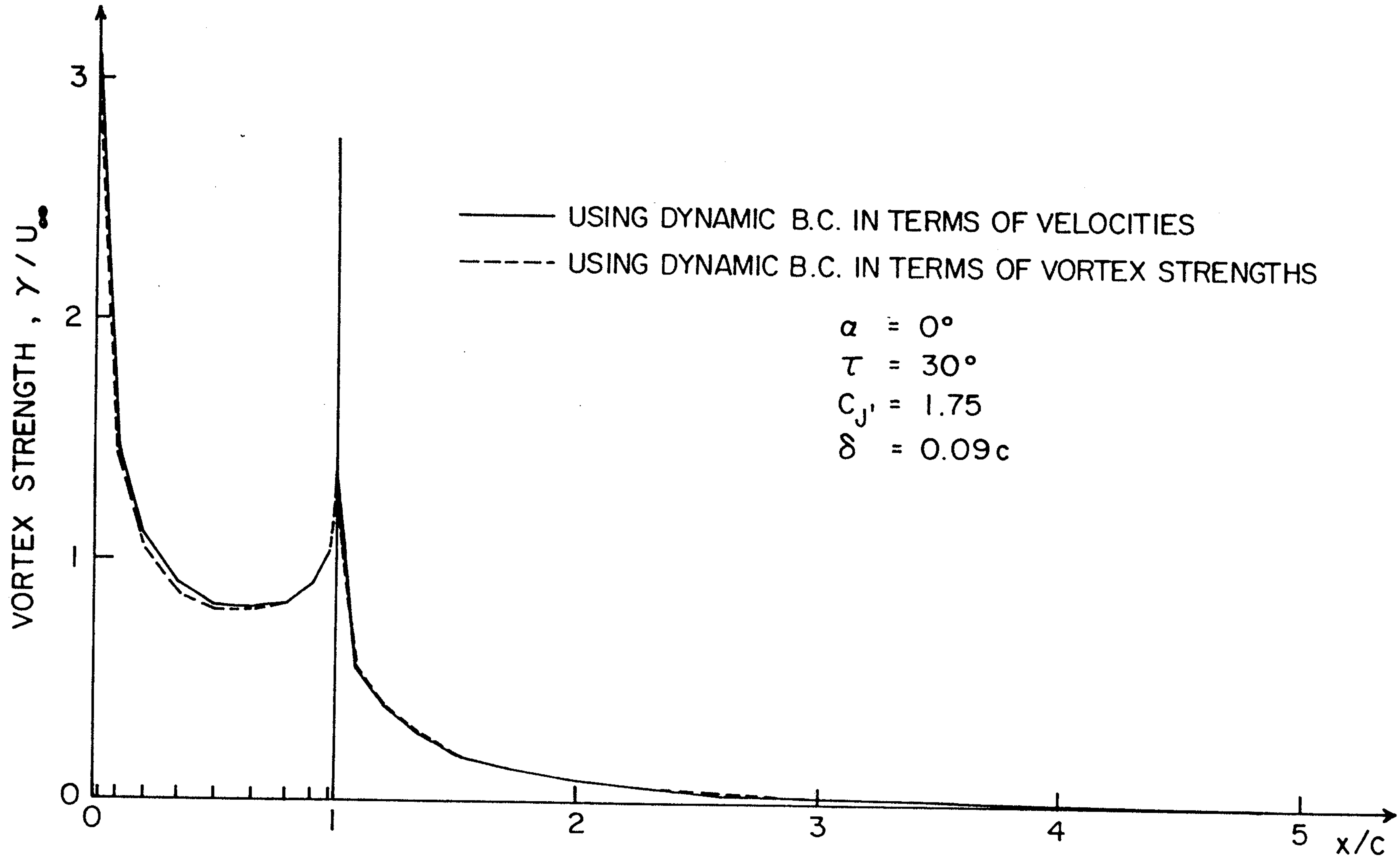

Fig. 31. Vortex Strength Distributions for Different Dynamic Boundary Conditions.

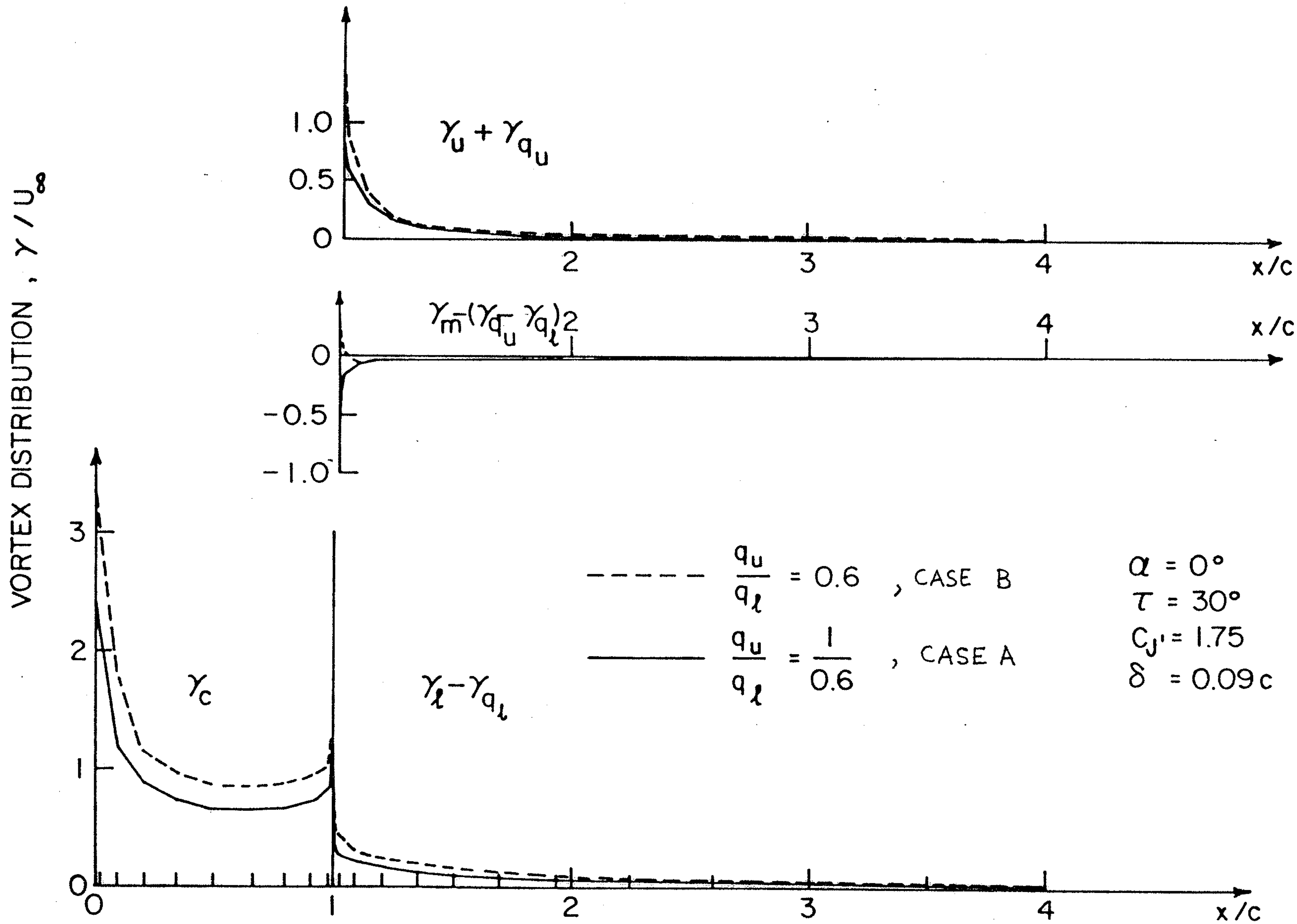

Fig. 32. Vortex Strength Distributions for Non-Uniform Jet.

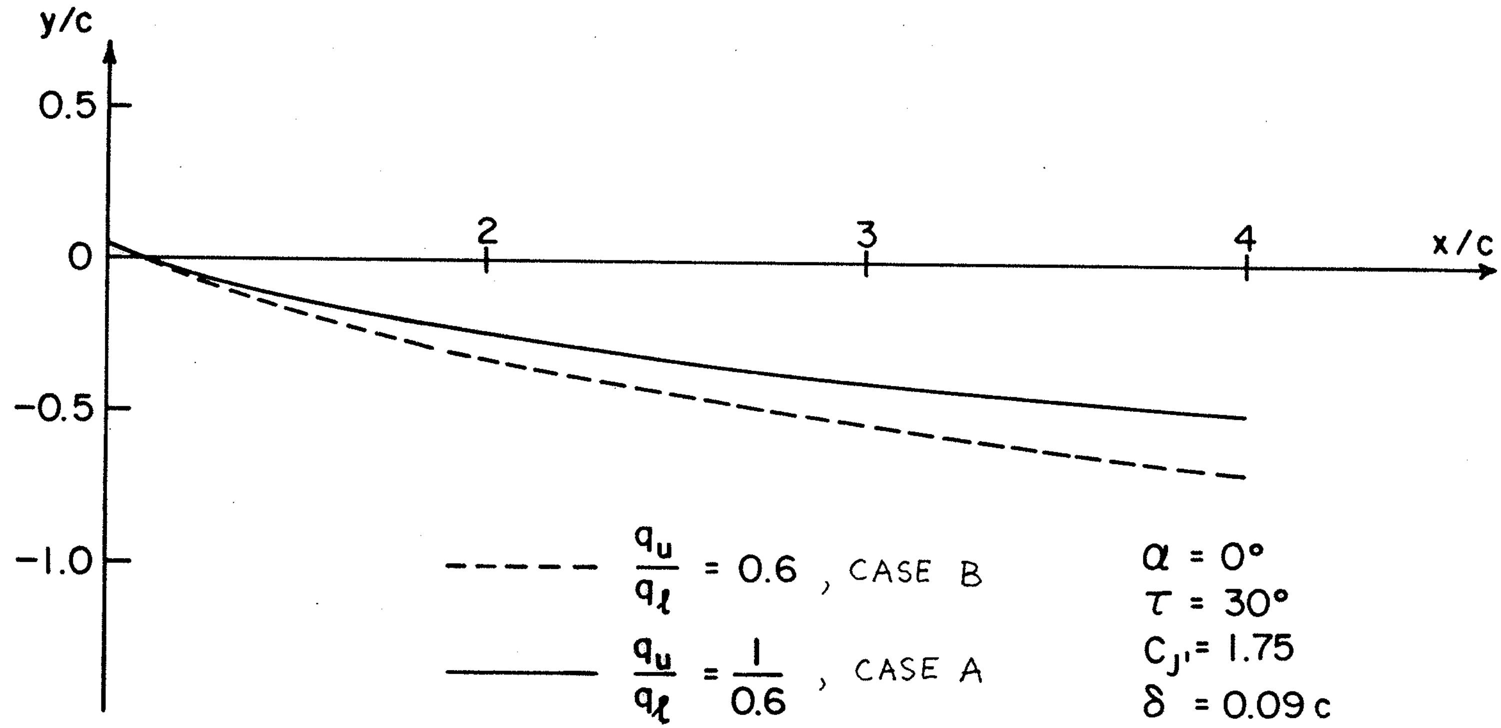

Fig. 33. Effect of velocity ratio on jet center lines.

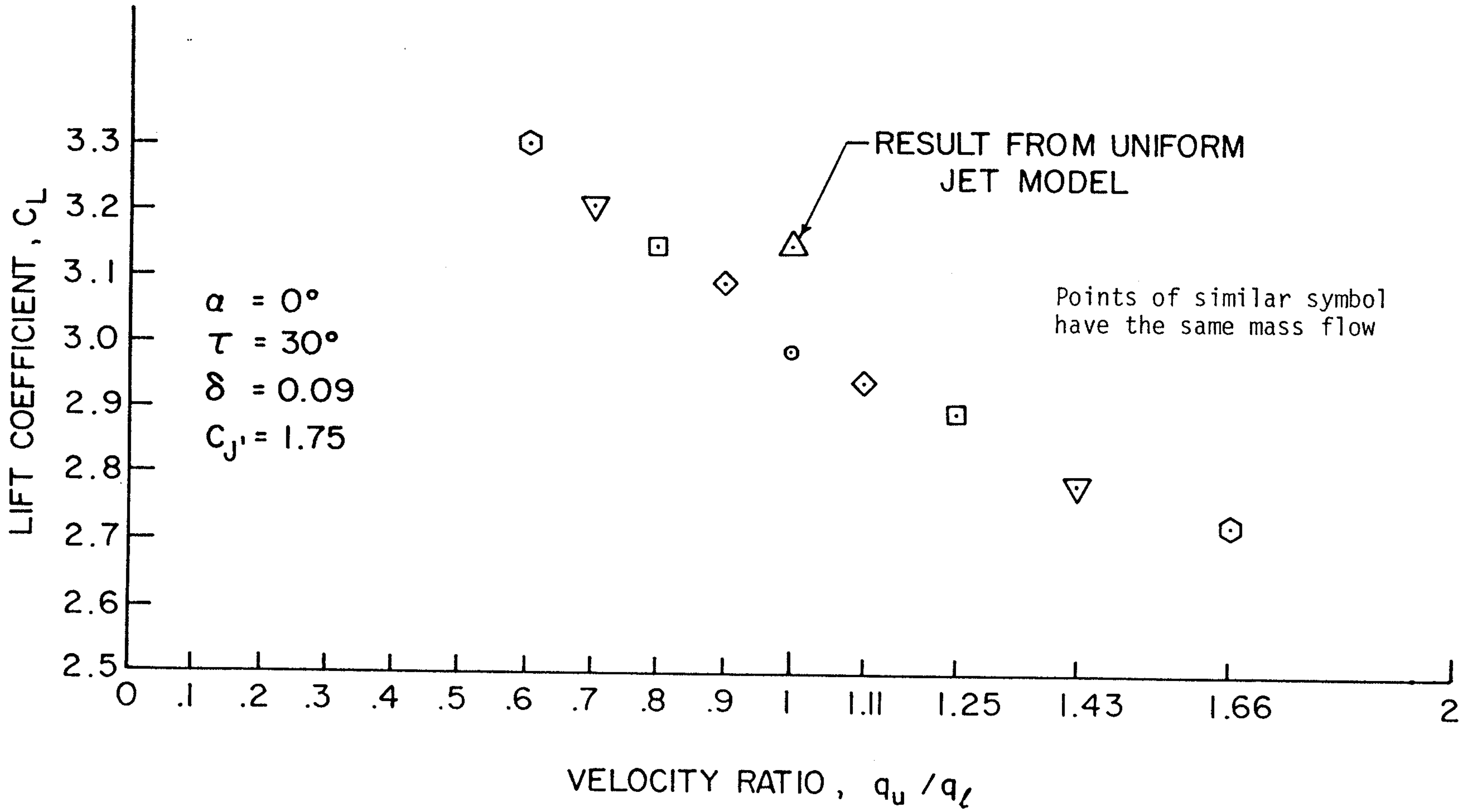

Fig. 34. Effect of Velocity Ratio on Lift Coefficient .

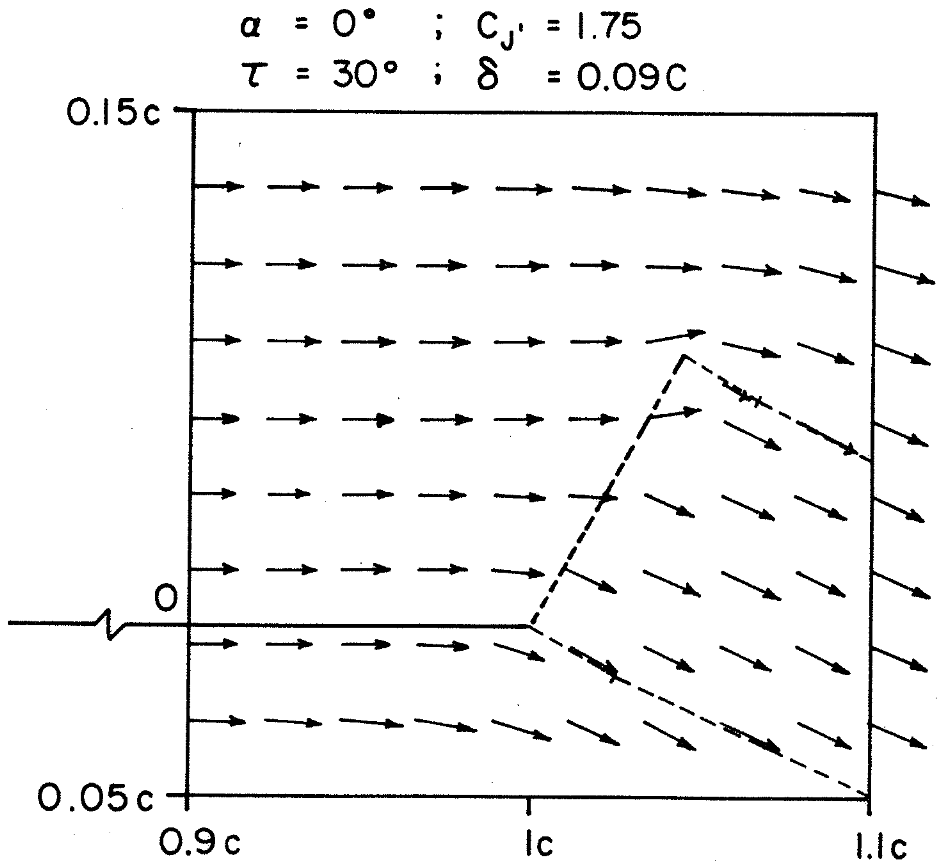

(a) Flow direction near the trailing edge.

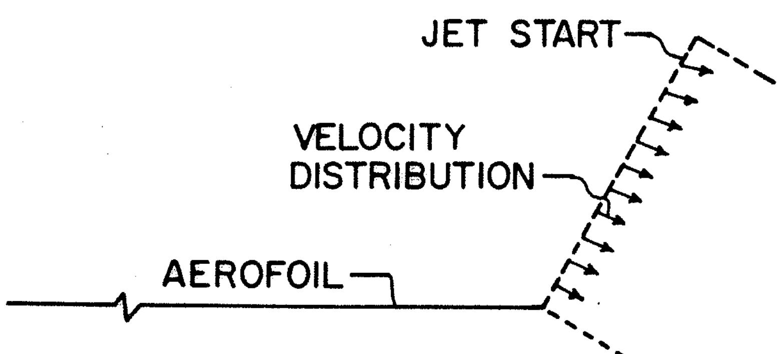

(b) Velocity distribution at the jet start.

Fig. 35. Flow Direction at and near the Jet Start (Uniform Jet)